Defense Threat Reduction Agency
8725 John J. Kingman Road, MS-6201
Fort Belvoir, VA 22060-6201

DTRA-TR-15-024

TECHNICAL REPORT

Models of Hematopoietic Dynamics Following Burn for Use in Combined Injury Simulations

April 2015

HDTRA1-14-D-0003; 0005

Prepared by:

Nuclear Survivability and Forensics Integrated Program Team

REPORT DOCUMENTATION PAGE

Form Approved
OMB No. 0704-0188

1. REPORT DATE *(DD-MM-YYYY)*	2. REPORT TYPE	3. DATES COVERED *(From - To)*
28/04/2015	Technical Report	

4. TITLE AND SUBTITLE
Models of Hematopoietic Dynamics Following Burn for Use in Combined Injury Simulations

5a. CONTRACT NUMBER
HDTRA1-14-D-0003

5b. GRANT NUMBER

5c. PROGRAM ELEMENT NUMBER

6. AUTHOR(S)
Jacqueline Wentz
Darren Oldson
Daniela Stricklin

5d. PROJECT NUMBER

5e. TASK NUMBER
0005

5f. WORK UNIT NUMBER

7. PERFORMING ORGANIZATION NAME(S) AND ADDRESS(ES)
Applied Research Associates, Inc.
801 N. Quincy Street, Suite 700
Arlington, VA 22203

8. PERFORMING ORGANIZATION REPORT NUMBER
DTRA-TR-15-024

9. SPONSORING/MONITORING AGENCY NAME(S) AND ADDRESS(ES)
Nuclear Technologies Directorate
Defense Threat Reduction Agency
8725 John J. Kingman Road, Mail Stop 6201
Fort Belvoir, VA 22060-6201

10. SPONSOR/MONITOR'S ACRONYM(S)
DTRA J9

11. SPONSOR/MONITOR'S REPORT NUMBER(S)

12. DISTRIBUTION/AVAILABILITY STATEMENT
Approved for public release; distribution is unlimited.

13. SUPPLEMENTARY NOTES

14. ABSTRACT

The effects of thermal injury were incorporated into previously developed models that simulate hematopoiesis in humans following acute radiation exposure. These include models of thrombopoiesis, granulopoiesis, and lymphopoiesis. In thrombopoiesis, burn leads to platelet consumption and an increase in circulating stimulatory mediators. In granulopoiesis, burn leads to an increased bone marrow release rate, granulocyte demargination, granulocyte uptake into the tissue, and an increased mitotic progenitor repopulation rate. In lymphopoiesis, burn increases the rate of lymphocyte clearance. The models were validated against human data from subjects with different burn sizes. Model outputs were compared to combined injury data from animals to verify that trends were accurately predicted. Outputs from these models will be correlated with mortality, and this information will assist in disaster preparedness and medical resource planning.

15. SUBJECT TERMS
Radiation, Combined Injury, Ordinary Differential Equation Model, Thrombopoiesis, Granulopoiesis, Lymphopoiesis

16. SECURITY CLASSIFICATION OF:			17. LIMITATION OF ABSTRACT	18. NUMBER OF PAGES	19a. NAME OF RESPONSIBLE PERSON
a. REPORT	b. ABSTRACT	c. THIS PAGE			Dr. Paul Blake
U	U	U	UU	86	19b. TELEPHONE NUMBER (Include area code) 703-767-3433

UNIT CONVERSION TABLE

U.S. customary units to and from international units of measurement*

U.S. Customary Units	Multiply by → / ← Divide by†		International Units
Length/Area/Volume			
inch (in)	2.54	$\times 10^{-2}$	meter (m)
foot (ft)	3.048	$\times 10^{-1}$	meter (m)
yard (yd)	9.144	$\times 10^{-1}$	meter (m)
mile (mi, international)	1.609 344	$\times 10^{3}$	meter (m)
mile (nmi, nautical, U.S.)	1.852	$\times 10^{3}$	meter (m)
barn (b)	1	$\times 10^{-28}$	square meter (m^2)
gallon (gal, U.S. liquid)	3.785 412	$\times 10^{-3}$	cubic meter (m^3)
cubic foot (ft^3)	2.831 685	$\times 10^{-2}$	cubic meter (m^3)
Mass/Density			
pound (lb)	4.535 924	$\times 10^{-1}$	kilogram (kg)
atomic mass unit (AMU)	1.660 539	$\times 10^{-27}$	kilogram (kg)
pound-mass per cubic foot (lb ft^{-3})	1.601 846	$\times 10^{1}$	kilogram per cubic meter (kg m^{-3})
Pound-force (lbf avoirdupois)	4.448 222		Newton (N)
Energy/Work/Power			
electron volt (eV)	1.602 177	$\times 10^{-19}$	joule (J)
erg	1	$\times 10^{-7}$	joule (J)
kiloton (kT) (TNT equivalent)	4.184	$\times 10^{12}$	joule (J)
British thermal unit (Btu) (thermochemical)	1.054 350	$\times 10^{3}$	joule (J)
foot-pound-force (ft lbf)	1.355 818		joule (J)
calorie (cal) (thermochemical)	4.184		joule (J)
Pressure			
atmosphere (atm)	1.013 250	$\times 10^{5}$	pascal (Pa)
pound force per square inch (psi)	6.984 757	$\times 10^{3}$	pascal (Pa)
Temperature			
degree Fahrenheit (^oF)	$[T(^oF) - 32]/1.8$		degree Celsius (^oC)
degree Fahrenheit (^oF)	$[T(^oF) + 459.67]/1.8$		kelvin (K)
Radiation			
activity of radionuclides [curie (Ci)]	3.7	$\times 10^{10}$	per second (s^{-1}‡)
air exposure [roentgen (R)]	2.579 760	$\times 10^{-4}$	coulomb per kilogram (C kg^{-1})
absorbed dose (rad)	1	$\times 10^{-2}$	joule per kilogram (J kg^{-1}§)
equivalent and effective dose (rem)	1	$\times 10^{-2}$	joule per kilogram (J kg^{-1}**)

*Specific details regarding the implementation of SI units may be viewed at http://www.bipm.org/en/si/.

†Multiply the U.S. customary unit by the factor to get the international unit. Divide the international unit by the factor to get the U.S. customary unit.

‡The special name for the SI unit of the activity of a radionuclide is the becquerel (Bq). (1 Bq = 1 s^{-1}).

§The special name for the SI unit of absorbed dose is the gray (Gy). (1 Gy = 1 J kg^{-1}).

**The special name for the SI unit of equivalent and effective dose is the sievert (Sv). (1 Sv = 1 J kg^{-1}).

Table of Contents

List of Figures

List of Tables

Acknowledgments

The authors gratefully acknowledge programmatic support provided by Dr. Paul Blake of DTRA/J9. We are also indebted to the previous work of Dr. Olga Smirnova and Dr. Shaowen Hu, whose models provided a foundation for the models developed in this study.

Executive Summary

Applied Research Associates, Inc. is developing a suite of biomathematical models that describe the health effects of nuclear and radiological environments for scenarios which include nuclear detonations. In such scenarios, many radiation injuries combined with acute injuries, such as trauma and thermal burns, are anticipated. Since radiation and burn have a significant effect on hematopoiesis, we have developed a set of models to predict the impact of these insults on hematopoietic cell kinetics. Modeling these essential biological processes will help improve casualty predictions and the evaluation of combined radiation and burn injury.

In this study, we incorporate the effects of thermal injury into existing radiation models of hematopoiesis. Models that describe the effects of acute radiation exposure on thrombopoiesis, granulopoiesis, and lymphopoiesis were detailed in a previous report (Wentz et al. 2014a). Experimental data in rodents and observational data in humans were analyzed to determine the specific biological processes affected by burn. Based on this data, we hypothesize the following hematopoietic effects of thermal injury:

- thrombopoiesis: decreased platelet lifespan, increased levels of circulating stimulatory mediators which lead to an increased rate of platelet progenitor repopulation, and increased maturation rate of immature megakaryocytes.
- granulopoiesis: increased release rate of granulocytes from the bone marrow, demargination of granulocytes in the blood, increased uptake rate of granulocytes into the tissues, and increased rate of granulocyte progenitor repopulation.
- lymphopoiesis: decreased lymphocyte lifespan.

These effects, quantified as functions of burn size, were incorporated into the radiation injury models to create biomathematical models of radiation combined injury. The models accurately describe blood cell kinetics following thermal injury and provide predictions of blood cell kinetics following combined injury. Compared to their predictions for single injury types (radiation alone or thermal injury alone), the models predict that, in some cases, combined injury leads to lower cell count nadirs and longer recovery times. These models aid in casualty predictions and provide insight into the time-course of injury and recovery, medical resource planning, and disaster preparedness.

1 Introduction

1.1 Biomathematical Modeling to Support DTRA Mission

Applied Research Associates, Inc. (ARA) has been tasked by the Defense Threat Reduction Agency (DTRA) to support its mission to safeguard the United States against weapons of mass destruction. ARA supports this effort by developing state–of–the–art mathematical models that predict medical and performance effects of radiation and burn injuries, thereby enhancing our understanding of the potential impact of a nuclear detonation. We are developing mechanistic, biologically-motivated models that describe the link between insults and the probability of mortality.

1.2 Modeling Hematopoietic Cell Kinetics

Radiation and burn injury lead to significant alterations in hematopoiesis. Cytopenias and cytoses, states of decreased and increased blood cell concentrations, respectively, have been associated with increased mortality risk (Mirsaeidi et al. 2010). Thus, understanding progenitor and blood cell kinetics following radiation and burn can be useful for predicting outcomes. We have developed a set of mechanistic models to simulate how these combined insults lead to alterations in blood cell kinetics. Models that describe the effects of acute radiation exposure on thrombopoiesis, granulopoiesis, and lymphopoiesis were presented in a previous report (Wentz et al. 2014a). In the present report, we incorporate the hematopoietic effects of thermal injury into the previously developed radiation models by mathematically interpreting burn-dependent mechanisms and developing new model parameters. The resulting models predict the effects of radiation and burn combined injury.

Experimental data in rodents and observational data in humans were analyzed to determine the specific biological processes affected by burn. Based on this data, we hypothesize the following hematopoietic effects of thermal injury:

- thrombopoiesis: decreased platelet lifespan, increased levels of circulating stimulatory mediators which lead to an increased rate of platelet progenitor repopulation, and increased maturation rate of immature megakaryocytes (MKs).
- granulopoiesis: increased release rate of granulocytes from the bone marrow, demargination of granulocytes in the blood, increased uptake rate of granulocytes into the tissues, and increased rate of granulocyte progenitor repopulation.
- lymphopoiesis: decreased lymphocyte lifespan.

These effects, quantified as functions of burn size, were incorporated into the radiation injury models to create mechanistic models of radiation and burn combined injury. To our knowledge, these are the first mathematical models describing the effects of burn on hematopoiesis. This report presents an updated version of ARA's thrombopoiesis model that was previously published (Wentz et al. 2014b).

One of the most important advantages of these biomathematical models is that they provide information that aids in predicting time-dependent casualty streams and medical resource requirements over time. Through the development of mechanistic combined injury

models, we can gain insight into the underlying pathophysiology of combined injury, predict potentially synergistic effects, and investigate the effects of countermeasures. In contrast, probit models do not permit this type of exploration.

1.3 Implementation of Models

The models described in this report have been implemented in Health Effects from Nuclear and Radiation Environments (HENRE), a user–friendly software platform with which one can (1) define an insult, (2) run models to predict health effects of that insult, and (3) analyze model output. Eventually HENRE will be integrated with DTRA's Hazard Prediction and Assessment Capability (HPAC), a modeling platform that predicts nuclear environment information such as radiation dose and thermal fluence at specific locations. The environment parameters obtained from HPAC can be mapped to the environment parameters that drive the combined injury models described in this report. A future goal will be to predict the effect of these environments on heterogeneous populations.

2 Methods

2.1 Model Parameterization

To optimize parameters, quantify parameter uncertainty, and assess model identifiability we used nonlinear least squares curve fitting and Markov Chain Monte Carlo (MCMC) sampling. All ordinary differential equation (ODE) simulations, optimization procedures, and parameter confidence interval calculations were performed using the statistical computing environment R (v3.0.0, R Core Team 2013).

Parameter estimation can be formulated as a nonlinear least squares optimization problem, and the structure of the least squares objective function can be leveraged to create alternatives to Newton's method, such as the Levenberg–Marquardt Method (Moré 1978). The Levenberg–Marquardt Method, which can be viewed as a combination of the Gauss–Newton Method and the Steepest Descent Method, provides a robust and efficient way to locate optimum parameter values. An optimized parameter set $\vec{\xi}_{LM}$ was obtained using the Levenberg-Marquardt algorithm implemented in the modCost and modFit tools from the Flexible Modeling Environment (FME) package (Soetaert et al. 2010a). As part of this process, solution curves for the hematopoiesis model equations (see Appendix A) were calculated using the "ode" function from the deSolve package (Soetaert et al. 2010b).

ModFit performs constrained fitting of a model to data using input including (1) a function to be minimized, (2) initial parameter values, (3) the lower and upper bounds to be used for each parameter, and (4) the optimization method. The objective function f we provided to modFit() maps a given parameter vector $\vec{\xi}_k$ to a residual. This mapping includes the following steps:

1. the ODE simulation is performed for each radiation dose and burn size combination;

2. the output of each ODE simulation and the observed data are used as input for modCost, which calculates and returns the residuals;

3. the residuals from each simulation are combined and returned.

modFit uses $f(\vec{\xi}_k)$ and the Levenberg–Marquardt Method to generate the next approximate parameter vector $\vec{\xi}_{k+1}$. These steps are then repeated to generate additional approximate solutions $\vec{\xi}_{k+2}$, $\vec{\xi}_{k+3}, \ldots$ until a convergence test is passed. Finally, we note that the optimizations were performed on normalized data in which each data value was divided by a baseline value. This allows for comparison of residuals between datasets without inadvertently weighting one dataset more than another.

Next, using the parameter set $\vec{\xi}_{LM}$ to initialize a Markov Chain, the MCMC method with the adaptive Metropolis algorithm was used to estimate confidence intervals for parameters (Laine 2008; Haario et al. 2001). The MCMC sampling procedure included the following steps: (1) given an initial parameter vector $\vec{\xi}_j$, an estimate for the parameter covariance matrix, and the same function f as described above, the parameter space was randomly sampled to generate a new parameter vector $\vec{\xi}_{j+1}$; (2) the likelihood L of the new parameter vector $\vec{\xi}_{j+1}$ was determined, and if $L(\vec{\xi}_{j+1}) \geq L(\vec{\xi}_j)$, $\vec{\xi}_{j+1}$ was chosen; (3) if $L(\vec{\xi}_{j+1}) < L(\vec{\xi}_j)$, $\vec{\xi}_{j+1}$ was selected with probability α, where $\alpha = P(\vec{\xi}_{j+1})/P(\vec{\xi}_j)$ and P is the probability

of a given parameter vector. These calculations were performed in R using modMCMC, a function in the FME library.

2.2 Optimization and Validation Data

To model the effects of thermal injury on blood cell populations, human and murine data were collected from published literature. Data on the time-course of blood cell concentrations following thermal injury were digitized and reviewed (Marck et al. 2013; Baxter 1974; Pavić et al. 2007; Simon et al. 1977; Peterson et al. 1983; Vindenes et al. 1995; Nijsten et al. 1991; Balch 1963; D'Arpa et al. 2009; Kagan et al. 1989; Neilan et al. 1977). In some cases, the data available for a particular cell line was limited, leading to broader inclusion criteria. Data not included in the optimization were used to validate the resulting models. During the optimization procedure, data was divided by predetermined baseline cell concentrations, specific to each cohort of subjects. The comparison of data to the dimensionless form of the model allows for differences between the data and the model to be comparable across studies.

2.3 Comparisons of Models with Data

Comparisons of model simulations with human data are challenging due to the sources of variability within a population. In the literature, blood cell kinetic data is usually provided as averaged values across a group containing individuals with different burn sizes and different baseline blood cell concentrations. Rather than provide burn sizes for each individual, studies provide the mean, median, or range of percent total body surface area affected by burn (%TBSA). In the models presented, burn depth is not currently accounted for. However, it likely influences the hematopoietic response, leading to variability between patients with the same burn size. For mathematical purposes the burn size is denoted as S in the equations and figures of this report. S represents the burn size fraction and ranges between 0 and 1, where $S = 1$ corresponds to 100% TBSA. Baseline values for subjects in human case studies are not available and must be assumed based on distributions in the general population. To understand the effect of the variability of burn size and blood cell concentration, multiple model outputs are compared to the data using a range of inputs.

3 Thrombopoiesis Model

Burn-dependent parameters were developed and integrated into our previously developed mathematical model of thrombopoiesis. The previous model developed by ARA simulates the effects of acute radiation exposure (Wentz et al. 2014a). Briefly, the existing thrombopoiesis model consists of three compartments containing mitotic progenitors in the bone marrow, post-mitotic progenitors in the bone marrow, and platelets in circulation. These compartments are regulated through feedback mechanisms. Acute radiation exposure leads to damage and the eventual death of a dose-dependent proportion of radiosensitive cells. A structural diagram of the thrombopoiesis model with the effects of burn is given in Figure 3.1.

3.1 Modeling the Effect of Burn

The effects of burn on thrombopoiesis were incorporated into the model through the analysis of observational and experimental data in rodents and humans. To improve the model-selection process, a model was first developed for rodents and then translated to humans. After thermal injury, rodents and humans exhibit an immediate thrombocytopenia followed by recovery and sustained thrombocytosis (Kalmaz et al. 1991; Marck et al. 2013). The likely mechanisms for the observed trends are discussed and incorporated into the mathematical

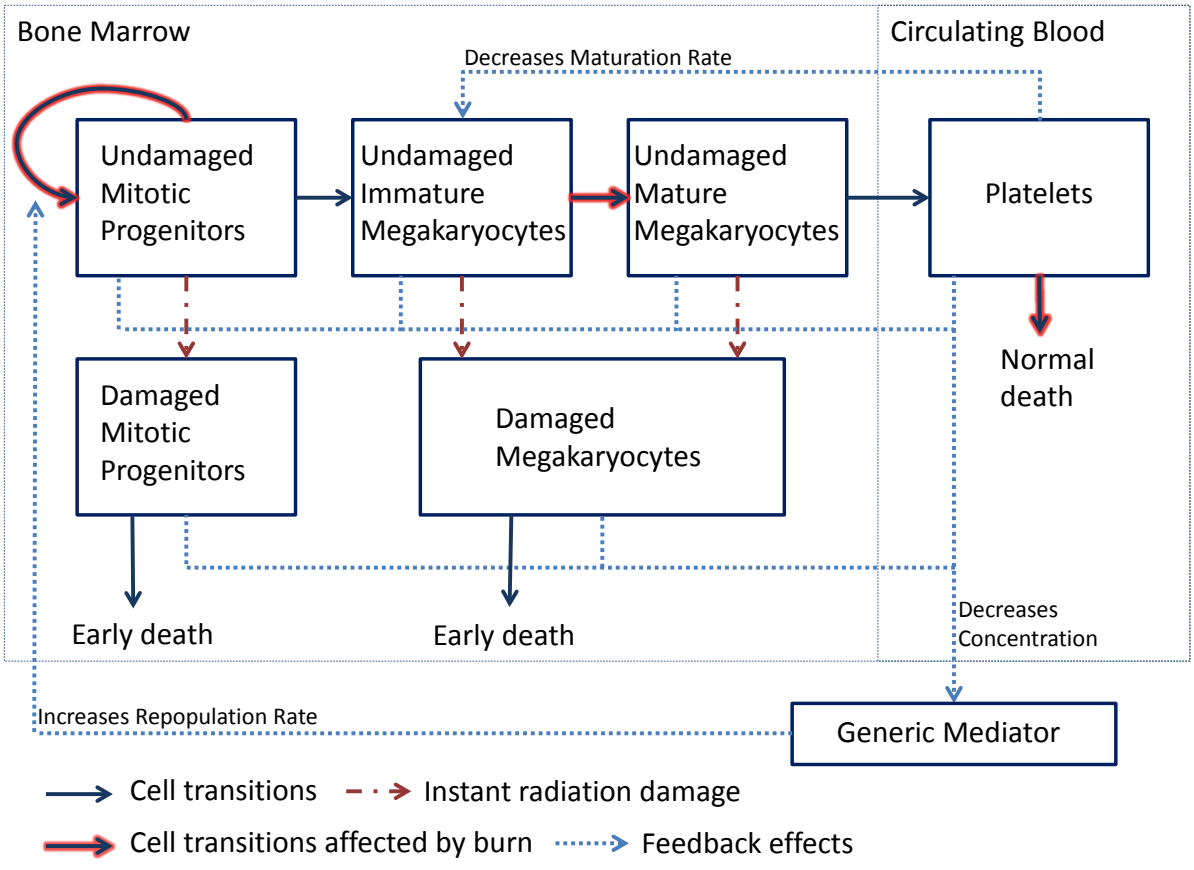

Figure 3.1: Thrombopoiesis model diagram (adapted from Figure 4.1, Wentz et al. 2014a).

model of thrombopoiesis. These mechanisms include both a decreased platelet lifespan and an increased mitotic progenitor cell repopulation rate. The equations for the mathematical model for thrombopoiesis with radiation and burn effects are given in Appendix A.1.

3.1.1 Reduction in Platelet Lifespan

Several mechanisms could cause the immediate thrombocytopenia observed following burn. Various burn treatments are known to cause thrombocytopenia, but burn-induced thrombocytopenia is also observed in controlled murine experiments in which treatment is not administered (Kalmaz et al. 1991; Fujimi et al. 2006; Davis et al. 1955). A decreased production rate of platelets could cause thrombocytopenia; however, an increased rate of platelet production as well as an increased MK count were observed in the early postburn period in rodents (Wallner et al. 1984; Eurenius et al. 1972). This evidence implies that the observed thrombocytopenia following burn is not due to bone marrow deficiency or treatment.

Experimental and observational studies have shown that thermal injury decreases the lifespan of circulating platelets in rodents (Eurenius et al. 1972) and humans (Simon et al. 1977). The mechanism of platelet clearance from the blood in rodents at 1 hour postburn was determined to be extrinsic; factors in the serum led to the removal of platelets from circulation (Eurenius et al. 1972). In this same study, the fractional proportion of platelets at the burn-wound site increased compared with controls, while there was no fractional change in the percent of platelets in the spleen, liver, kidney, or lung. Taken together, this evidence suggests that the burn-induced thrombocytopenia is caused by the activation of platelets and subsequent coagulation cascade at the burn-wound site. Thus, in our model, consumption of platelets is assumed to be the sole mechanism of thrombocytopenia.

To incorporate this biological effect into the mathematical model of thrombopoiesis, the rate of platelet consumption is determined as a function of burn size and time postburn. The burn insult initially leads to an increased rate of platelet decay. However, as the time postburn increases, the platelet decay rate gradually returns to the baseline value. In reality, burn leads to tissue damage resulting in a complex inflammation response involving platelet activation (Van Hinsbergh 2012). Once activated, platelets release the contents of granules into the serum which, through a positive feedback mechanism, lead to the activation of more platelets. Rather than attempting to model this entire cascade of events, the system is simplified, and the rate of platelet clearance is directly related to burn size and time postburn.

To determine the dependency of the platelet decay rate ψ on burn size S and time postburn t, we (1) define an expected platelet lifespan function $T_{plt}(S,t)$ using data from the literature, and then (2) relate $T_{plt}(S,t)$ to platelet decay rate by implementing a transit compartment model ($\psi = 1/T_{plt}(S,t)$).

To determined $T_{plt}(S,t)$, we first examined how burn size S affected platelet lifespan at a constant time postburn t. Data on platelet lifespan changes in humans as a function of burn size at $t = 1$ (i.e., the survival time of platelets radio-labeled at $t = 1$; Simon et al. 1977) were fit to linear, exponential, and Hill decay (Hill coefficient=1) functions (Figure 3.2). The functions implemented all contained two parameters; thus, least squares curve fitting was used to determine which function best described the data (see Figure 3.2; SSR=sum of squared residuals).

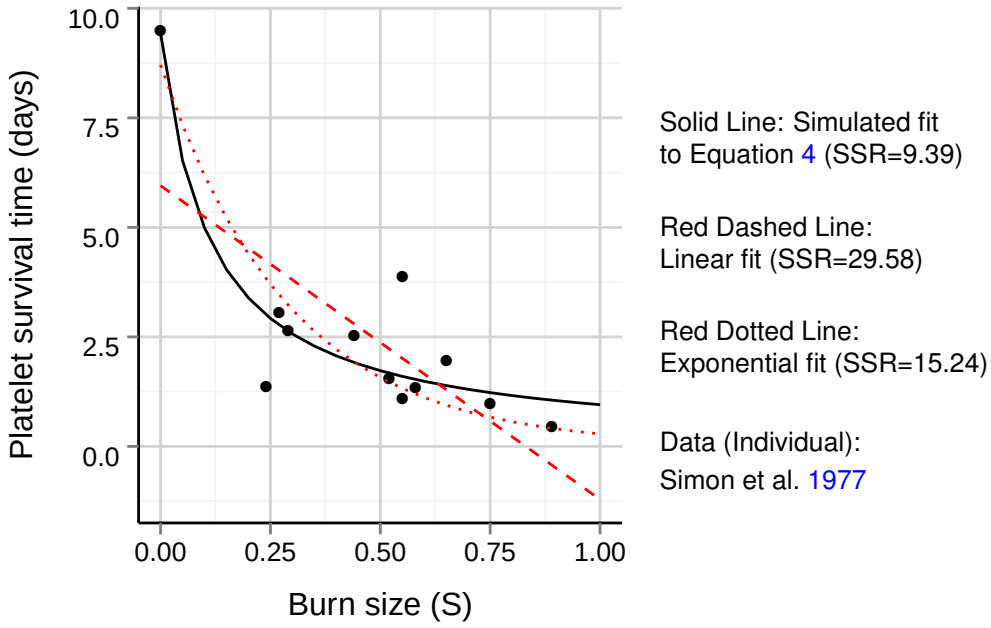

Figure 3.2: Platelet survival time as a function of burn size.

The data was best described by the following function:

$$T_{plt}(S,1) = \frac{1}{\psi_0} \cdot \frac{1}{1+\frac{S}{K_S}} \tag{1}$$

where $\psi_0 = 0.106\,\mathrm{d}^{-1}$ and $K_S = 0.112$. Note that ψ_0 is the rate of platelet consumption under healthy conditions, and K_S determines the burn fraction at which T_{plt} is half the normal value ($T_{plt}(K_S,1) = 1/2\psi_0 = T_{plt}(0,1)/2$).

Next, to add time dependence to our platelet lifespan model, we assume the rate of recovery does not depend on S and let K_S depend on time:

$$T_{plt}(S,t) = \frac{1}{\psi_0} \cdot \frac{1}{1+\frac{S}{K_S(t)}} \tag{2}$$

Assuming platelet lifespan is minimal immediately following burn and that platelet lifespan gradually returns to normal levels, the function $K_S(t)$ should have a minimum at $t = 0$ and K_S should be defined so that $\lim_{t\to\infty} K_S(t) = \infty$. We therefore define

$$K_S(t) = d_0 + d_1 t \tag{3}$$

so

$$T_{plt}(S,t) = \frac{1}{\psi_0} \cdot \frac{1}{1+\frac{S}{d_0+d_1 t}} \tag{4}$$

Since $K_S(1) = 0.112$, $d_0 = 0.112 - d_1$; to estimate d_1, we used data obtained by Simon on the temporal effects of burn on platelet lifespan (Simon et al. 1977; see Fig. 3.3). Five of the patients examined 1 day postburn were also examined 3 and 5 weeks following burn.

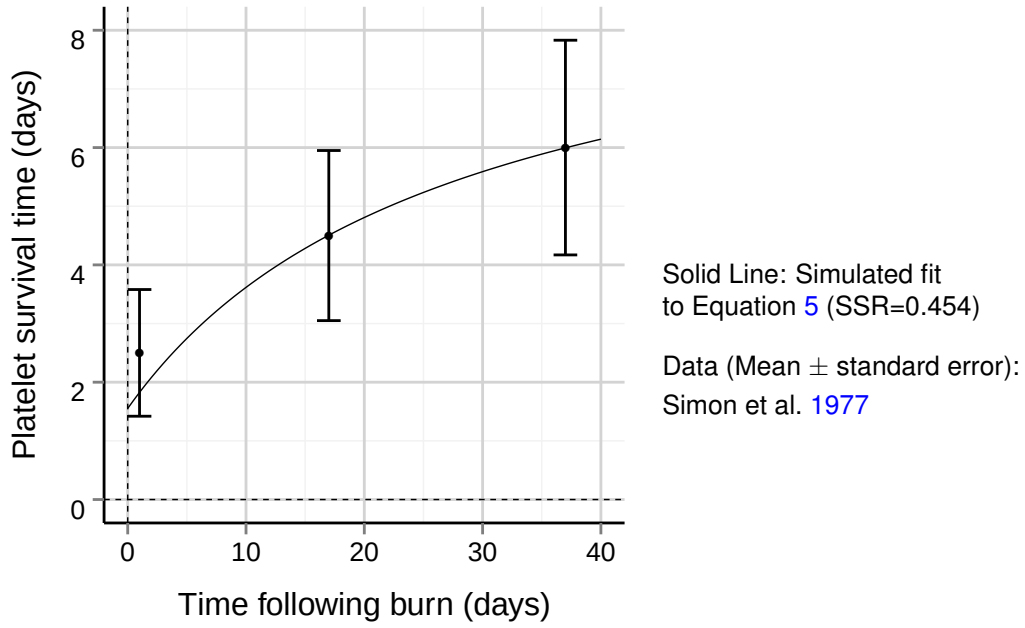

Figure 3.3: Mean platelet survival time as a function of time postburn.

However, each of these patients had different burn sizes, and only the mean platelet lifespan for the group was provided at each time point. The mean platelet lifespan for the 5 subjects, each with a specified burn size, at time t is given by

$$\bar{T}_{plt}(t) = \frac{1}{5\psi_0}\sum_{i=1}^{5}\frac{1}{1+\frac{S_i}{d_0+d_1 t}} = \frac{1}{5\psi_0}\sum_{i=1}^{5}\frac{1}{1+\frac{S_i}{(0.112-d_1)+d_1 t}} \tag{5}$$

where S_i is the fraction of surface area burned for subject $i = 1, 2, ..., 5$. Figure 3.3 shows the result of fitting Equation 5 to the mean platelet survival time for the patient group. The solid line in Figure 3.3 is a plot of $\bar{T}_{plt}(t)$ using $d_1 = 0.0202$.

Thus, we have defined an expected lifespan function $T_{plt}(S, t)$, given by Eq. 4. Motivated by the study by Simon (Simon et al. 1977), in which platelet survival time was determined by fitting gamma distributions to data on radio-labeled platelet concentrations, we relate $T_{plt}(S, t)$ to platelet decay rate by dividing the platelet compartment into subcompartments. Specifically, in our model, we divide the platelet compartment into m subcompartments, and the transition rate between subcompartments is $m\psi$, where

$$\psi(S, t) = \frac{1}{T_{plt}(S, t)}.$$

This model structure yields platelet compartment transit times that are approximately gamma distributed (if ψ is constant, the transit time has a gamma distribution).

3.1.2 Increased Mitotic Progenitor Repopulation Rate

The sustained thrombocytosis following burn suggests that burn increases the rate of stem cell repopulation. One could argue that this effect is simply the system's homeostatic re-

sponse to thrombocytopenia: when platelet levels drop, negative feedback increases the stem cell repopulation rate, and overcompensation leads to thrombocytosis. However, the thrombocytosis would be transient; that is, by a similar argument, platelet concentration would drop again, overcompensation would lead to thrombocytopenia, and the cycle would continue as the system oscillates around equilibrium and then returns to a steady state. Sustained thrombocytosis is therefore not consistent with negative feedback driven by platelet concentration per se. We therefore hypothesize that the thrombocytosis following burn is due to a burn–induced surge of a stimulatory mediator, of which one consequence is an increase in early progenitor cell repopulation rate.

The principle mediator of thrombopoiesis is thrombopoietin (TPO). TPO acts as a thrombopoietic stimulator while platelets and MKs provide a negative feedback mechanism by receptor-mediated uptake and destruction of TPO (for a review of TPO regulation see Kaushansky 2005). Interleukin 6 (IL-6) stimulates thrombopoiesis *in vivo* in mice and monkeys by increasing TPO transcription in the liver (Ishibashi et al. 1989; Asano et al. 1990; Kaser et al. 2001). Following a dosing regimen of IL-6 in mice, platelet counts increased significantly by day 4 in a dose–dependent fashion (Ishibashi et al. 1989). In monkeys, platelet counts increased significantly on day 7 of IL-6 treatment (Asano et al. 1990). This delay between treatment and effect suggests IL–6–induced TPO is likely acting on early thrombopoietic progenitors.

Increased levels of IL-6 have been observed within the first few hours following burn in humans (Carsin et al. 1997; Drost et al. 1993; Schluter et al. 1991) and remain detectable through at least 5 weeks postburn (Drost et al. 1993). The increase in IL-6 levels has been correlated with burn size (Schluter et al. 1991; Kowal-Vern et al. 1994), although one study saw no relationship between burn size and IL-6 levels (Drost et al. 1993). Increased levels of circulating TPO have also been observed in burn patients both with and without sepsis (Lupia et al. 2009). Although elevated TPO levels could be caused by a thrombocytopenic state, no difference in platelet counts between subject groups was observed by Lupia et al. 2009. Lupia et al. 2009 quantified levels of TPO in burn subjects at an unspecified time following burn. In burn patients, the average TPO concentration was 153.79 ± 33.07 pg mL^{-1}, and in septic burned patients, it was 374.93 ± 62.41 pg mL^{-1}. These values are compared with control subject values of 68.90 ± 17.16 pg mL^{-1}. In burn patients, TPO values were increased by 123%, demonstrating TPO concentrations can greatly fluctuate following burn. Collectively, this evidence suggests that burn leads to an IL-6-dependent increase in circulating TPO levels, resulting in an increased hematopoietic stem cell repopulation rate.

To model this effect of burn, the baseline rate of mediator production G is multiplied by the factor $1 + b_0 S^{c_0} e^{-a_0 t}$ so that the mediator production rate increases immediately after burn and gradually returns to normal (b_0 describes the magnitude of the effect, a_0 describes the duration of the effect, and c_0 describes the effect's dependence on burn size).

The rate of change of mediator concentration is thus

$$\frac{dI}{dt} = G(1 + b_0 S^{c_0} e^{-a_0 t}) - H(x_1^{ud} + x_1^d + \theta_2(x_2^{ud} + x_2^d) + \theta_3 x_3)I \tag{6}$$

where S is the fraction of skin surface area burned. Using a quasi–steady–state approxima-

tion for I, we can solve Equation 6 for I and express the repopulation rate B as

$$B = \frac{\alpha}{1 + \beta \left(x_1^{ud} + x_1^d + \theta_2(x_2^{ud} + x_2^d) + \theta_3 x_3\right) / (1 + b_0 S^{c_0} e^{-a_0 t})} \tag{7}$$

Note that including the effect of burn on the mediator production rate has not altered the maximum rate of mitotic progenitor repopulation, α.

3.1.3 Increased Immature MK Maturation Rate

The two thrombopoietic effects of burn modeled so far, reduction in platelet lifespan and increased repopulation rate, allow one to describe the initial thrombocytopenia and the subsequent sustained thrombocytosis. However, without further modification the model does not accurately predict the time at which the system transitions from a state of thrombocytopenia to a state of thrombocytosis. The issue is the MK maturation time in the model: data show that platelet levels start increasing within 5 days after burn, though MKs in the model require more than 5 days to mature. We therefore hypothesize that burn also affects the maturation rate of MKs. This is supported by data that show that TPO, in addition to increasing repopulation rate, also affects the maturation of MKs (Kaushansky 2005).

For these reasons, an effect of burn is incorporated into our model of the maturation rate of immature MKs. Specifically, burn leads to an increased transit rate through the immature MK subcompartments. In the model we developed for thrombopoiesis following acute radiation exposure (Wentz et al. 2014a), the transition rate between immature MK subcompartments is $n\delta$, where n is the total number of MK subcompartments (both immature and mature MKs) and

$$\delta = \frac{1}{2} Z(2\delta_0, \frac{\delta_{min}}{1 - \frac{\delta_{min}}{2\delta_0}}, \frac{\delta_{max}}{1 - \frac{\delta_{max}}{2\delta_0}}) \tag{8}$$

$$Z(x, x_{min}, x_{max}) = x_{min} + (x_{max} - x_{min})^{1 - \left(\frac{x_3}{\bar{x}_3}\right)^\lambda} (x - x_{min})^{\left(\frac{x_3}{\bar{x}_3}\right)^\lambda} \tag{9}$$

where $\bar{x}_3$ is the platelet concentration at equilibrium (see Eq. 25–26, 35–36 in Wentz et al. 2014a). Equations 8 and 9 describe a negative feedback mechanism in which platelet concentration regulates immature MK maturation rate. To describe burn's effect on the maturation rate as an effect driven by mediator concentration (as opposed to platelet concentration per se), we multiply δ in Eq. 8 by a factor that is independent of x_3:

$$\delta = \frac{1}{2} Z(2\delta_0, \frac{\delta_{min}}{1 - \frac{\delta_{min}}{2\delta_0}}, \frac{\delta_{max}}{1 - \frac{\delta_{max}}{2\delta_0}})(1 + b_f S^{c_f} e^{-a_f t}) \tag{10}$$

Similar to the parameters that describe the effect of burn on repopulation rate, b_f describes the magnitude of burn's effect on MK maturation rate, a_f describes the duration of the effect, and c_f describes the effect's dependence on burn size.

3.2 Results and Discussion

In this section, we present optimization and validation results for our model of the effect of burn on thrombopoiesis.

Table 3.1: Thrombopoiesis model optimization and validation data.

Reference	Burn Size (S)*	Number of Subjects**	Use
Marck et al. 2013	0.0825 (0.015-0.15)	84	Optimization
Marck et al. 2013	0.225 (0.15-0.30)	96	Optimization
Marck et al. 2013	0.6 (0.30-0.90)	64	Optimization
Baxter 1974	0.20 (0-0.40)	NA	Validation
Baxter 1974	0.55 (0.40-0.70)	NA	Validation
Baxter 1974	0.85 (0.70-1.0)	NA	Validation
Pavić et al. 2007	0.05 (0-0.10)	32	Validation
Pavić et al. 2007	0.55 (0.10-1)	36	Validation
Simon et al. 1977	0.57 (0.24-0.89)	10	Validation

* Represents the fraction of surface area burned (i.e., S=0.50 corresponds to 50% of the surface area burned). Data is given as median (min-max).
** Represents number of subjects at beginning of study. For later blood cell kinetic data, this number is likely decreased due to mortality and shorter hospital stays.
NA = not available

3.2.1 Parameter Optimization

Values of b_0, a_0, c_0, b_f, a_f, and c_f in humans were determined using the optimization procedure described in Section 2.1 and data on platelet concentrations in humans following burn (Marck et al. 2013). Details about the study done by Marck et al. are provided in Table 3.1. When optimizing and comparing the model output to the data, the median burn size was used as input into the model. The data from Marck et al. data was used for parameter optimization because of the large study size, temporal resolution of the platelet data (in particular for small t), long duration of study, and detailed information for three separate groups based on burn size. Because the initial platelet concentration was recorded soon after the burn incident, and all three burn size groups had average initial platelet counts within the normal platelet concentration range for humans (140–440 x $10^3/\mu L$; Valentin 2002), the initial platelet count was used as the baseline level when optimizing (i.e., the first recorded platelet count was used as the model's equilibrium platelet level). If significant decreases in platelet count occurred before the first recorded value, the model would underestimate the platelet counts.

In the optimization data, the group with the largest burn size showed the lowest nadir while the group with the smallest burn size had the lowest peak in the thrombocytosis period. The goal of our parameterization was thus to reproduce these trends as well as approximately match the observed nadirs, slopes of recovery, and thrombocytosis peaks. Not as much emphasis was put on matching data 25 days after burn, because this data was obtained from subjects with longer hospital stays with potential complications resulting in treatment and surgery.

Table 3.2 gives the parameter values for the entire human thrombopoiesis model. Figure 3.4 shows the model overlaid on the optimization data. The depth of the nadir as well as the subsequent rate of recovery are accurately predicted by the thrombopoiesis model. In subjects with smaller burns ($0.015 < S < 0.15$), the subsequent thrombocytosis and ensuing

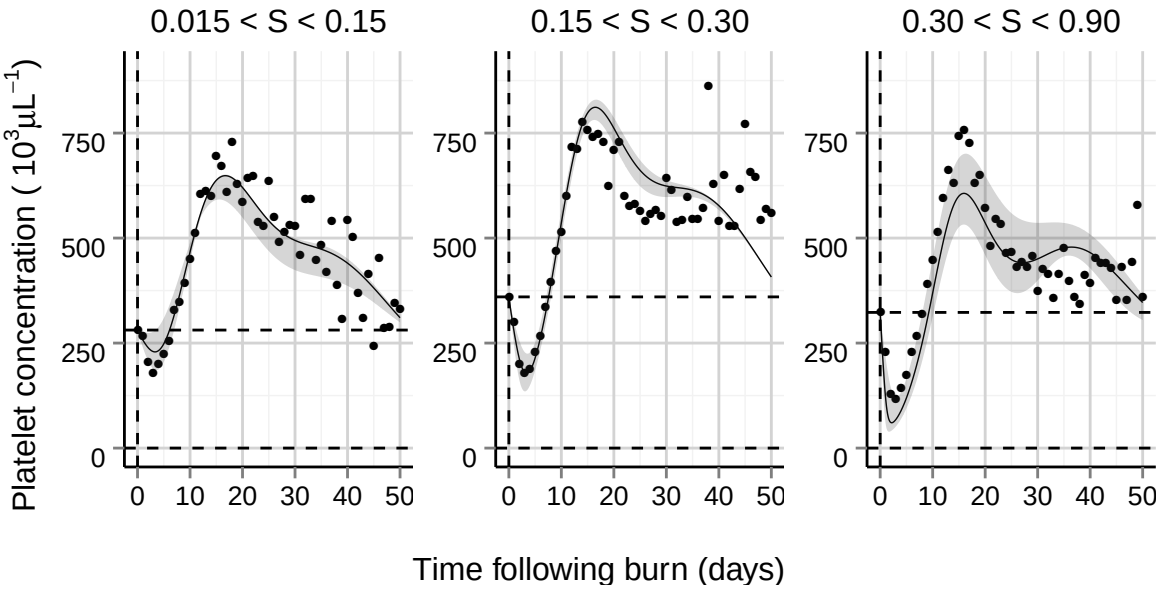

Figure 3.4: Human thrombopoiesis model compared with optimization data.

return to a normal platelet concentration is also accurately predicted. For the case of larger burns ($S > 0.15$), the data from Marck et al. study did not include the return to normal platelet levels. However, in those cases, it is possible that complications leading to longer hospital stays led to an increased platelet concentration. Thus, the recovery times predicted by our model for $S > 0.15$ may not be unrealistic.

The optimized parameters suggest that the effect of burn on mediator concentrations is more sustained than the effect on the immature MK maturation rate (i.e., $a_0 < a_f$). Specifically, approximately 4 days are required for the burn effect on the mediator concentrations to be reduced by half, while 2 days are required for the effect on the MK maturation rate to be reduced by half. Also, the value of the parameter b_f, which determines the magnitude of the effect of burn on the immature MK maturation rate, approached the upper bound imposed during the optimization, 50. This implies the immature MK maturation time in the model (i.e., the time spent in the X_{2I} compartment) is very small right after burn injury. Although biologically this is unrealistic, the model also includes a fixed maturation time in the X_{2M} compartment (see Fig. 4.2 in (Wentz et al. 2014a)). This result suggests that burn may be affecting more than just the first half the of MK maturation time.

Simulated platelet trajectories for a range of burn sizes are shown in Figure 3.5. For burn sizes ranging from 10% to 100% TBSA, as burn size increases, the nadir and subsequent thrombocytosis are decreased (see Figure 3.5, left panel). For each burn size group there are similar peak values during the thrombocytosis period, suggesting at burn sizes greater than 15%, the effect of increasing burn size is minimal. This suggests that c_0 should be less than 1 (i.e., the marginal effect of burn size is decreased as the burn size increases. A small value of c_0 causes small burns to result in a large, perhaps unrealistic, thrombocytosis in

Table 3.2: Biological parameter values for human thrombopoiesis.

Parameter	Biological Meaning	Value
α	Maximum rate of mitotic progenitor repopulation	2.0 d^{-1}
γ	Rate of mitotic progenitor maturation	0.26 d^{-1}
δ_0	Rate of MK maturation at equilibrium	0.06 d^{-1}
ψ_0	Rate of platelet decay at equilibrium	0.11 d^{-1}
μ	Rate of damaged cell death	1 d^{-1}
θ_2	Decay rate of mediator due to x_2 cells relative to x_1 cells	0.006
θ_3	Decay rate of mediator due to x_3 cells relative to x_1 cells	0.00018
λ	Strength of feedback from platelets on MK maturation	3.5
σ	Number of platelets produced per MK	3000
δ_{min}	Minimum rate of MK maturation	0.048 d^{-1}
δ_{max}	Maximum rate of MK maturation	0.08 d^{-1}
n	Number of MK subcompartments	10
m	Number of platelet subcompartments	9
D_1^0	Determines fraction of damaged x_1 cells	0.79 Gy
n_1	Number of targets per x_1 cell	1
D_2^0	Determines fraction of damaged x_2 cells	2.77 Gy
n_2	Number of targets per x_2 cell	4
μ	Rate of damaged cell death	1 d^{-1}
b_0	Determines max burn effect on repopulation rate	9.38
a_0	Determines duration of burn effect on repopulation rate	0.17 d^{-1}
c_0	Determines how burn size affects repopulation rate change	0.20
b_f	Determines max burn effect on MK maturation	49.85
a_f	Determines duration of burn effect on MK maturation	0.31 d^{-1}
c_f	Determines how burn size affects MK maturation rate change	0.10
d_0	Determines max effect of burn on platelet decay	0.092
d_1	Determines duration of effect of burn on platelet decay	0.0202 d^{-1}

Values for b_0, a_0, c_0, b_f, a_f, and c_f were determined through optimization (see Section 2.1).
Values for d_0 and d_1 are discussed in Section 3.1.1.
See Wentz et al. 2014a for source of all other parameter values.

burn sizes of less than 1% as illustrated in Figure 3.5 (right panel).

We acknowledge that our parameter optimization was based on a retrospective study (Marck et al. 2013) and, while platelet consumption is known to occur after burn, other factors may influence the observed thrombocytopenia. The initial decline in platelet concentration could be caused by the administration of resuscitation fluids or by drugs known to cause thrombocytopenia, such as silver sulphadiazine, heparin, morphine, and paracetamol (Marck et al. 2013). Heparin–induced thrombocytopenia is known to occur, however the thrombocytopenia following burn typically is much shorter than that caused by heparin. Finally, the thrombocytosis period could be artificially caused as well by the administration of transfusions, but typically transfusions are only advised when the nadir is below $50 \cdot 10^3$ platelets per μL, a condition that was not observed the Marck et al. study.

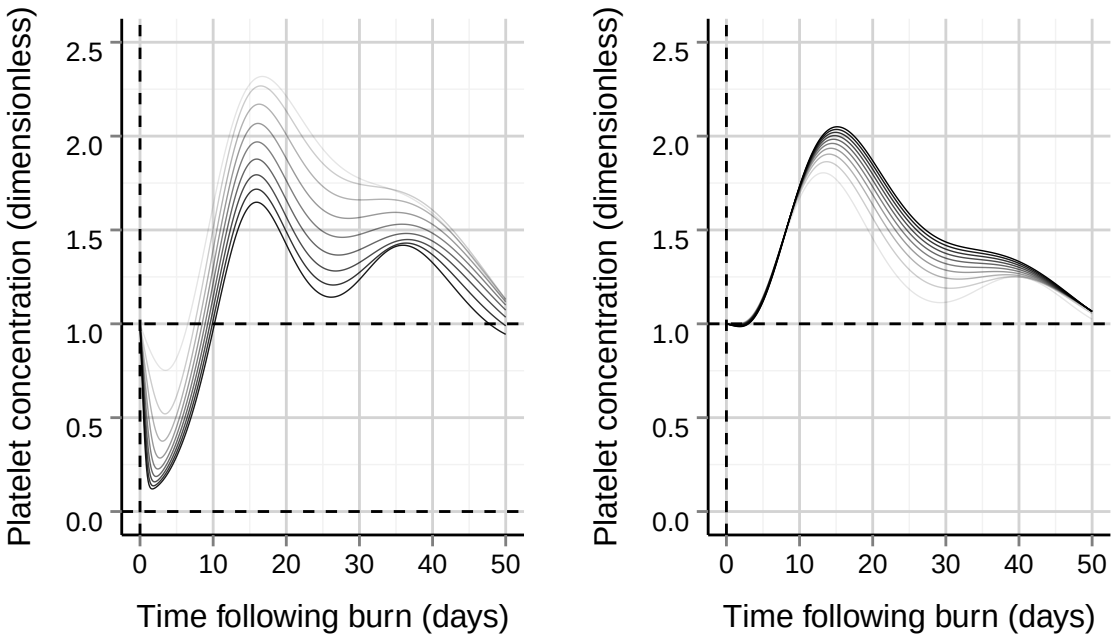

Left Panel: Model output with S ranging from 0.1 to 1 (darker lines for larger S).
Right Panel: Model output with S ranging from 0.001 to 0.01 (darker lines for larger S).

Figure 3.5: Optimized model simulations at increasing burn size.

3.2.2 Model Validation

Validation of the thrombopoiesis model was performed by comparing model outputs to platelet data that was not used to optimize model parameters. For validations, we used the baseline platelet count mean and range ($250 \cdot 10^3$ and $140 \cdot 10^3$-$440 \cdot 10^3$ cells per μL, respectively) observed in healthy humans (Valentin 2002). Information on validation data is provided in Table 3.1, and Figure 3.6 shows the validation results. This validation provides evidence that the model is able to match trends observed in platelet concentration following burn. In the burn studies from Baxter 1974 (Figure 3.6, top row), the platelet concentration shows a faster rebound and greater thrombocytosis than predicted by the model. This recovery could be caused by the effects of treatment; however, the study does not provide information on treatment protocols for the subjects included. Also, the study only included patients who survived, leading to the removal of subjects who likely had lower platelet counts. Thus, the discrepancy between the data and the model may be due to selection bias. The comparisons shown in the bottom row of Figure 3.6 show general agreement between the data and simulations, despite the large burn size ranges and lack of error estimates for the data.

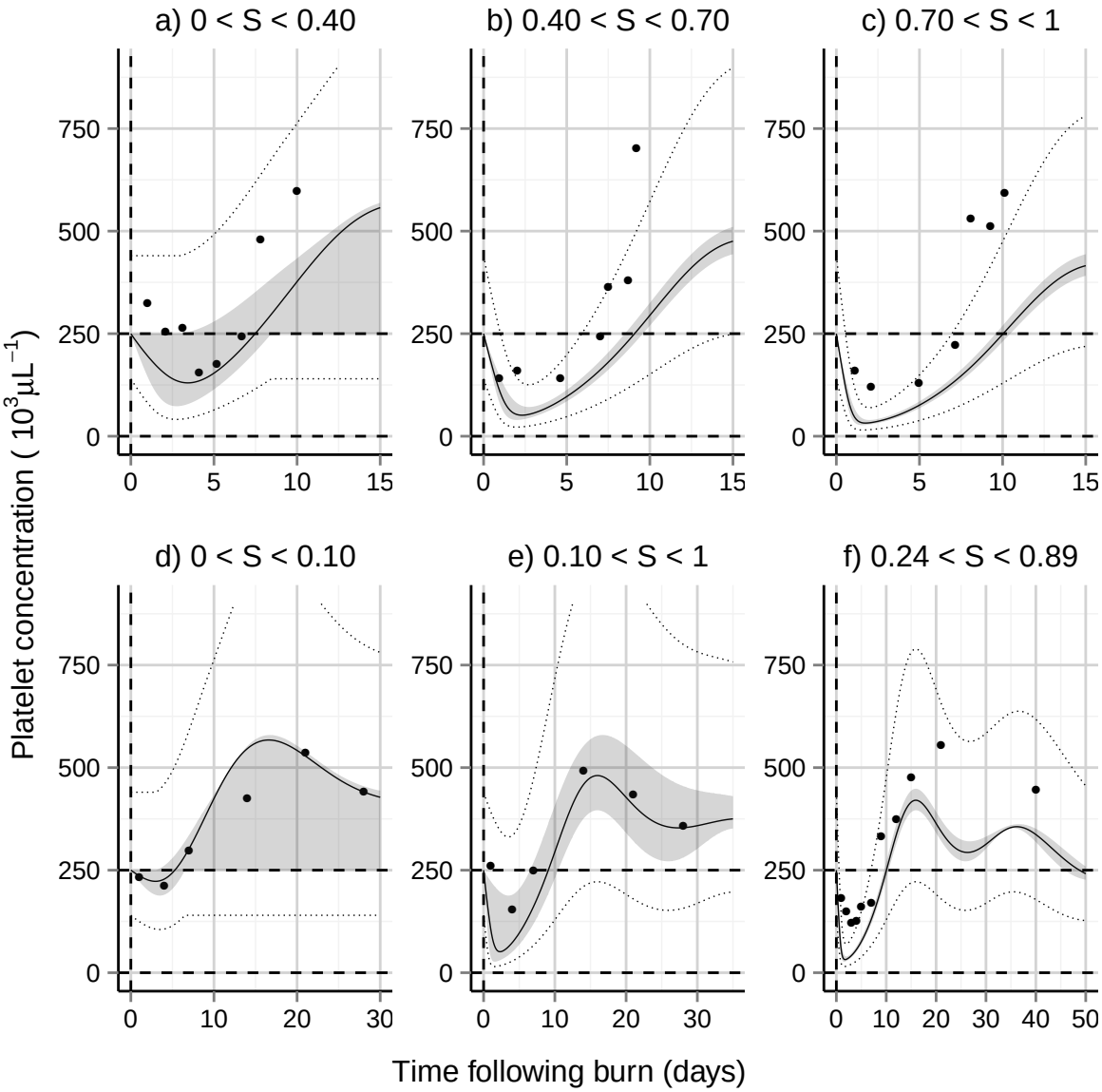

Solid Line: Model output using median of S and $250 \cdot 10^3 \mu L^{-1}$ as baseline
Shaded Region: Possible model output for range of S, using $250 \cdot 10^3 \mu L^{-1}$ as baseline
Dotted Lines: Bounds on model output for range of S and baseline values $(140 - 440 \cdot 10^3 \mu L^{-1})$
Data (Mean): Baxter 1974 (a,b,c); Pavić et al. 2007 (d,e); Simon et al. 1977 (f)

Figure 3.6: Human thrombopoiesis model compared with validation data.

4 Granulopoiesis Model

Burn-dependent parameters were determined and integrated into our previously developed mathematical model of granulopoiesis. The previous model, developed by ARA, simulates the effects of acute radiation exposure (Wentz et al. 2014a). Briefly, the granulopoiesis model consists of four compartments containing mitotic progenitors in the bone marrow, post-mitotic progenitors in the bone marrow, granulocytes in circulation, and granulocytes in the tissues. These compartments are regulated through multiple feedback mechanisms. Acute radiation exposure leads to damage and the eventual death of a dose-dependent proportion of radiosensitive cells. A structural diagram of the granulopoiesis model, including burn effects, is given in Figure 4.1.

4.1 Modeling the Effect of Burn

The effects of burn on granulopoiesis were incorporated into the model through the analysis of observational and experimental data in rodents and humans. To help guide development of the human model, the effects of burn on granulopoiesis were first simulated in rodents. Murine data is more readily available and can be obtained from controlled environments

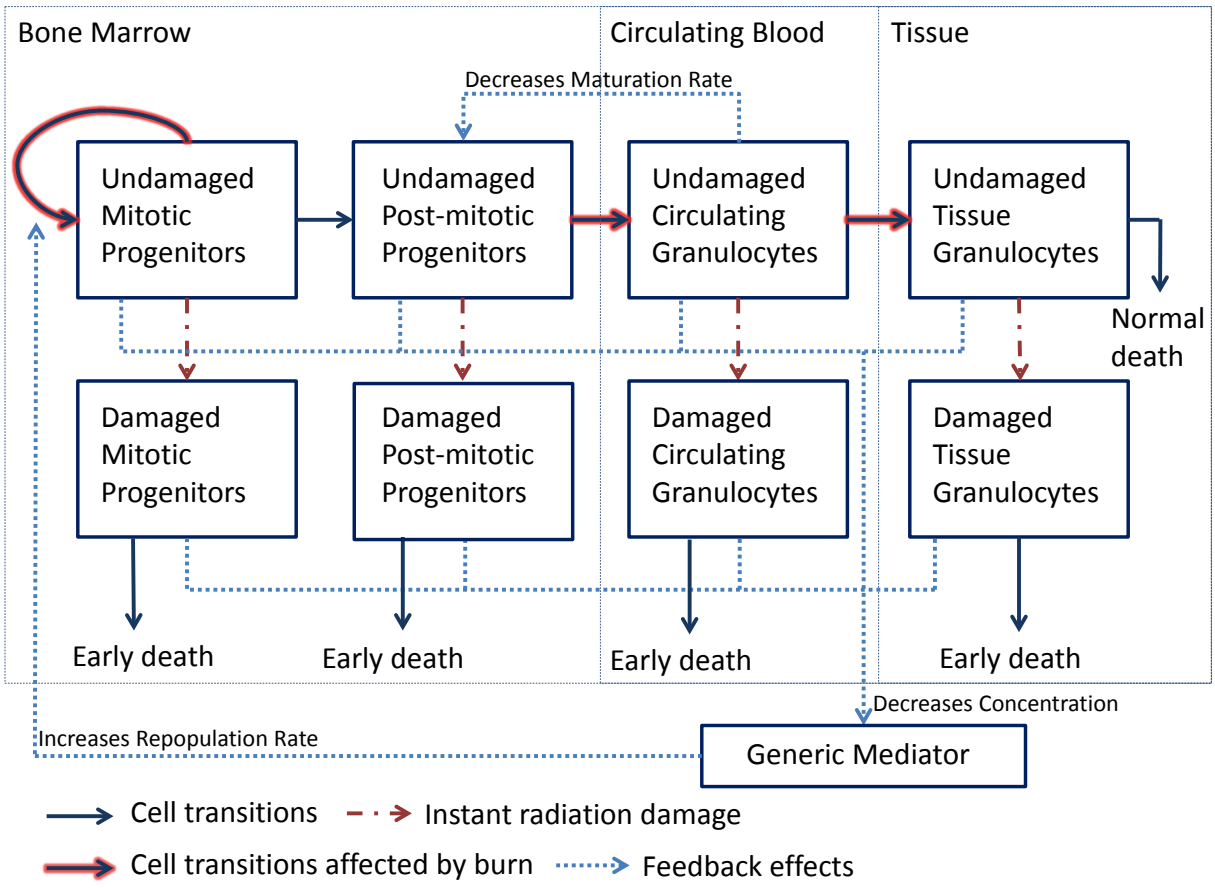

Figure 4.1: Granulopoiesis model diagram (adapted from Figure 5.1, Wentz et al. 2014a).

which greatly facilitates the identification of true effects. Once developed, the structure of the model was conserved across species, but the model was re-parameterized with human data.

Following burn there is a bimodal granulocytosis in both rodents and humans (Palmer et al. 2011; Wallner et al. 1984; McManus 1983; Peterson et al. 1983; Vindenes et al. 1995). Granulocyte levels rapidly increase but then quickly decline and approach normal concentrations observed in healthy humans. There is a second granulocytosis that, although not as strong as the first, is more sustained. The mechanisms behind these responses and the corresponding adjustments to the mathematical model are described here. The equations for the mathematical model for granulopoiesis after radiation and burn are given in Appendix A.2.

4.1.1 Increased Granulocyte Demargination

Following burn, in both rodents and humans there is a brief, yet rapid, increase in peripheral granulocytes in the blood. Granulocytes become marginated when they attach to the epithelial lining of blood vessels, and demargination occurs when the granulocytes detach from the epithelium and begin circulating in the blood once more (Summers et al. 2010). Epinephrine studies have shown that thermally injured rats have a reduced proportion of marginated granulocytes and an increased total number of peripheral granulocytes when compared with controls (McManus 1983). This suggests the observed granulocytosis is due, in part, to granulocyte demargination.

The compartment for granulocytes in the blood, X_3, represents both freely circulating granulocytes and marginated granulocytes. Thus, the concentration of granulocytes in the blood x_3 can be represented as follows:

$$x_3 = x_{3,c} + x_{3,m} \tag{11}$$

where $x_{3,c}$ represents granulocytes in the freely circulating pool and $x_{3,m}$ represents granulocytes in the marginated pool. Epinephrine studies have shown in mice approximately 1/4 of granulocytes in the blood are in the freely circulating pool while 3/4 are in the marginated pool (Johnson et al. 1995; Van Furth et al. 1986). Thus, at equilibrium $\bar{x}_{3,c} = \frac{1}{3}\bar{x}_{3,m}$. In humans the ratio of marginated to freely circulating granulocytes at equilibrium is closer to 1, and, thus, $\bar{x}_{3,c} = \bar{x}_{3,m}$ (Summers et al. 2010).

To simulate the initial granulocytosis following burn, we include a burn-dependent effect on the proportion of marginated granulocytes. This change, however, does not affect the total blood granulocyte concentration. Moreover, in our granulopoiesis model we assume that the transition rates among compartments X_i, $i = 1, 2, 3, 4$, depend only on the total blood granulocyte concentration x_3 and not on how the blood granulocytes are partitioned, at any given time point, into circulating and marginated pools. $x_{3,c}$ therefore does not appear explicitly in our differential equations (see Appendix A.2). However, $x_{3,c}$ is the quantity that is measured in experiments.

Let $r(t)$ denote the circulating fraction at time t, so that

$$x_{3,c}(t) = r(t)x_3(t) \tag{12}$$

and, in terms of normalized model variables,

$$\widetilde{x}_{3,c}(t) = \frac{x_{3,c}(t)}{\bar{x}_3 \bar{r}} = \widetilde{x}_3(t)\frac{r(t)}{\bar{r}}$$

where $\bar{r}$ is the circulating fraction at equilibrium. To compare model output to normalized peripheral granulocyte concentration data, we therefore multiply $\widetilde{x}_3(t)$ by the factor $r(t)/\bar{r}$. As $r(t)$ increases, a larger proportion of granulocytes is in circulation, and $\widetilde{x}_{3,c}(t)$ increases. For example, for the case of complete demargination ($r = 1$) in humans ($\bar{r} = 0.5$), we multiply $\widetilde{x}_3$ by 2 to estimate the normalized peripheral granulocyte concentration.

To model the circulating fraction at time t, we want to choose $r(t)$ so that

- $r(t)$ is maximized immediately following burn,
- $r(t)$ gradually returns to normal levels,
- $\bar{r} \leq r(t) \leq 1$

We therefore define

$$r(t) = \bar{r}(1 + f_r(S)e^{-a_r t}), \tag{13}$$

where S is the fraction of skin surface area affected by burn ($0 \leq S \leq 1$) and burn occurs at $t = 0$. Note that the constant a_r determines the duration of the effect and the function $f_r(S)$ determines the magnitude of the effect. Also, the maximum value of $r(t)$ should be 1 (i.e., $r(0) \leq 1$), so we must have that

$$f_r(S) \leq \frac{1}{\bar{r}} - 1 \tag{14}$$

Thus, if $\bar{r} = 0.5$, $f_r(S) \leq 1$. The complete form of $f_r(S)$ is given in Equation 18 and Appendix A.2. In summary, the non-dimensional model output $\widetilde{x}_3(t)$ is multiplied by $1 + f_r(S)e^{-a_r t}$ prior to comparison to normalized peripheral granulocyte data.

4.1.2 Increased Rate of Bone Marrow Release

The other hypothesized mechanism contributing to the immediate granulocytosis following burn is an early bone marrow release of granulocytes (Asko-Seljavaara 1974; Eurenius et al. 1973). In humans, the proportion of immature cells in the blood increases following burn, meaning the transit time through the post-mitotic compartment is temporarily decreased (Volenec et al. 1979). To represent this change in the model, the rate of granulocyte release from the bone marrow, δ, is given by

$$\delta(t) = \delta_0 \frac{1 + M(x_3^{ud} + x_3^{wd} + x_3^d)^2}{1 + L(x_3^{ud} + x_3^{wd} + x_3^d)^2} \cdot (1 + f_2(S)e^{-a_2 t}) \tag{15}$$

where δ_0 is the maximum release rate in the absence of thermal injury, S is the fraction of skin surface area affected by burn ($0 \leq S \leq 1$), and burn occurs at $t = 0$. a_2 determines the duration of the effect, and $f_2(S)$ determines the magnitude of the effect. Thus, thermal injury leads to an increase in the bone marrow release rate by a factor of $1 + f_2(S)e^{-a_2 t}$.

4.1.3 Increased Rate of Entry into the Tissues

Thermal injury in rats leads to an increased granulocyte influx into the tissues, presumably due to an increased rate of transition from the serum to the tissues (Hansbrough et al. 1996). Another potential mechanism for the increased granulocyte counts in the tissue is a burn-induced inhibition in granulocyte apoptosis (Chitnis et al. 1996). However, this effect was mediated by factors in the serum rather than intrinsically, suggesting a slower rate of apoptosis would not be observed in the tissues. Also, in the bimodal granulocyte response following burn there is a sharp decline after the first increase in granulocyte count. This steep decline suggests an increased rate of transition from serum to tissues is occurring rather than a decreased apoptosis rate. Also, granulocytes could become demarginated to travel to other sites in the body for entry into the tissues.

In our mathematical model of granulopoiesis, the rate of entry into the tissue, κ, is adjusted to include this effect as follows:

$$\kappa(t) = \kappa_0(1 + f_3(S)e^{-a_3 t}) \tag{16}$$

where κ_0 is the rate of transition in the absence of thermal injury, S is the fraction of skin surface affected by burn ($0 \leq S \leq 1$), and burn occurs at $t = 0$. κ increases immediately following burn and then returns to normal levels at a rate determined by a_3. The function $f_3(S)$ determines the magnitude of the effect.

4.1.4 Increased Mitotic Progenitor Repopulation Rate

Following thermal injury in rodents, granulocyte colony stimulating factor (G-CSF) levels increased 3.5 fold 1 to 2 days postburn (Shoup et al. 1998) and granulocyte progenitors increased 82% 1 day postburn (Noel et al. 2002). Although this evidence comes from rodent studies, we assume similar trends exist in humans. Therefore, we hypothesize the granulocytosis occurring 5-10 days postburn in humans is due to an increased production rate of granulocytes. These biological effects were implemented in the model by altering the rate of X_1 repopulation, B, as follows:

$$B(t) = \frac{\alpha}{1 + \frac{HK}{G}(\theta_1 x_1^{ud} + \theta_2 x_2^{ud} + \theta_3 x_3^{ud})} + f_0(S)e^{-a_0 t} \tag{17}$$

where S is the fraction of skin surface area affected by burn, burn occurs at $t = 0$, a_0 determines the duration of the effect, and the function $f_0(S)$ determines the magnitude of the effect. Note that Equation 17 describes the repopulation rate in the absence of radiation damage. An expression for $B(t)$ that includes the effects of radiation exposure is given in Appendix A.2.

The alteration to the repopulation rate in the granulopoiesis model given in Equation 17 is different than the effect of burn on the repopulation rate in the thrombopoiesis model (see Equation 7). In the thrombopoiesis model, by having burn act on the mediator production rate, the maximum possible mitotic cell repopulation rate is not altered. However, in the granulopoiesis model, thermal injury causes an increase in the maximum mitotic repopulation rate. During the granulopoiesis model development, adding an effect of burn on only the mediator production rate was also examined, and it was found that this resulted in similar

model outputs as the effect given in Equation 17. Thus, these two mechanisms could both explain the observed granulocyte kinetics following thermal injury. Both mechanisms are also biologically feasible. The maximum mitotic repopulation rate could appear to increase due to burn-dependent increase in cells transitioning into the granulopoietic lineage. Burn could also cause a faster repopulation of mitotic cells already in the granulopoietic lineage. Both of these mechanisms would be mediated by cytokines such as G-CSF. Ultimately, the chosen mechanism was somewhat arbitrary. Thus, during future model development, an effect of burn on the mediator production rate should also be considered.

4.1.5 Mapping Burn Size to Magnitude of Effect

To describe the effect of thermal injury on granulopoiesis we have implemented four modifications to our previously developed radiation injury model: increased demargination, increased maximum rate of bone marrow release, increased rate of entry into tissues, and increased rate of mitotic progenitor repopulation. The magnitudes of these effects f_i are assumed to depend on the fraction of skin surface area affected, S. Specifically, we assume that

$$f_i(S) = b_i \frac{(A+1)S^k}{A+S^k} \tag{18}$$

where $i = r, 0, 2, 3$. These functions represent the magnitude of the burn effect on margination $f_r(S)$, the mitotic progenitor repopulation rate $f_0(S)$, the bone marrow release rate $f_2(S)$, and tissue entry rate $f_3(S)$. b_r, b_0, b_2, and b_3 are constant parameters representing the maximum possible effect. A and k are also constant parameters which determine the dose-response curve.

As shown in Figure 4.2, Equation 18 can describe a variety of responses. First, if $k = 0$ or $A = 0$, $f_i(S) = b_i$ (the magnitude of effect f_i is independent of the size of the burn). If $k = 1$ and $A \to \infty$, f_i is approximately a linear function of S. For larger values of k, f_i is more clearly sigmoidal. Finally, in all cases $f_i(0) = 0$ and $f_i(1) = b_i$. Values for A, k, and b_i were determined through optimization. Note that the four functions $f_i(S)$, $i = r, 0, 2, 3$, differ only in the value of b_i; that is, we used the same "shape parameters" A and k for the four thermal injury response functions.

4.2 Results and Discussion

In this section the optimization and validation results for the burn parameters of the granulopoiesis model are presented.

4.2.1 Parameter Optimization

To determine values for parameters A, k, a_r, b_0, a_0, b_2, a_2, b_3, and a_3, the granulopoiesis model was optimized to data on granulocyte concentrations in humans following burn. b_r was set to 1 because at most 100% of granulocytes in the blood can become demarginated. For optimization and subsequent comparisons, the baseline granulocyte count was the mean value in healthy humans ($4.102 \cdot 10^3$ cells per μL; Valentin 2002). The model was optimized using several studies (Table 4.1). Due to the limited number of studies that provided quantitative

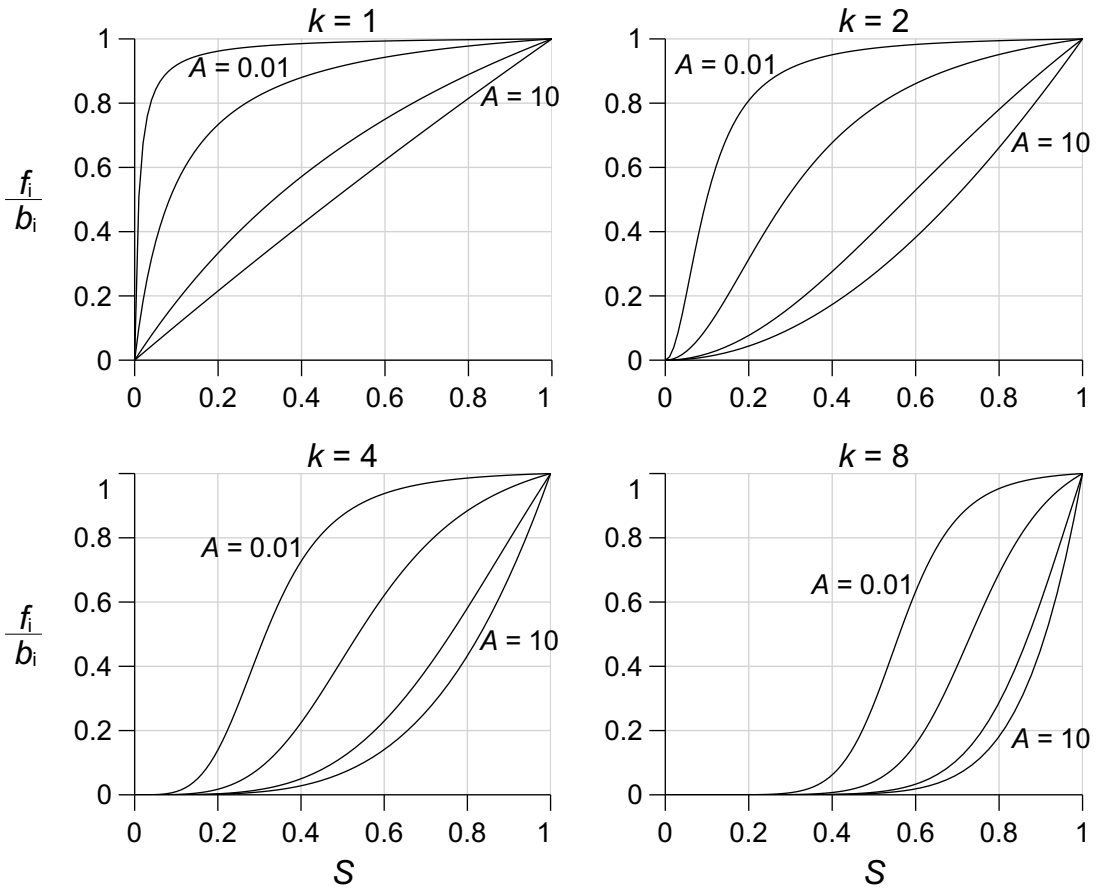

Figure 4.2: Possible functions defining the effect of burn size on the magnitude of effects (see Equation 18).

Table 4.1: Granulopoiesis model optimization and validation data.

Reference	Burn Size (S)*	Group	Number	Use
Peterson et al. 1983	0.36 (0.30-0.50)	Survivors	16	Optimization
Peterson et al. 1983	0.58 (0.43-0.75)	Non-Survivors	6	Optimization
Vindenes et al. 1995	0.547 (0.21-0.95)		27	Optimization
Nijsten et al. 1991	0.38 (0.17-0.56)		13	Optimization
Balch 1963	0.40**		1	Validation

*Represents the fraction of surface area burned (i.e., S=0.50 corresponds to 50% of the surface area burned). Data is given as mean (min-max).
**No range provided because data was obtained from an individual.

data on granulocyte concentrations following burn in humans, four of the five studies listed in Table 4.1 were used to optimize parameters.

Figure 4.3 shows model simulations compared with data used for optimization. Table 4.2 gives the parameter values for the entire human granulopoiesis model. In the granulopoiesis model, we are able to simulate the bimodal granulocytosis observed in peripheral granulocyte

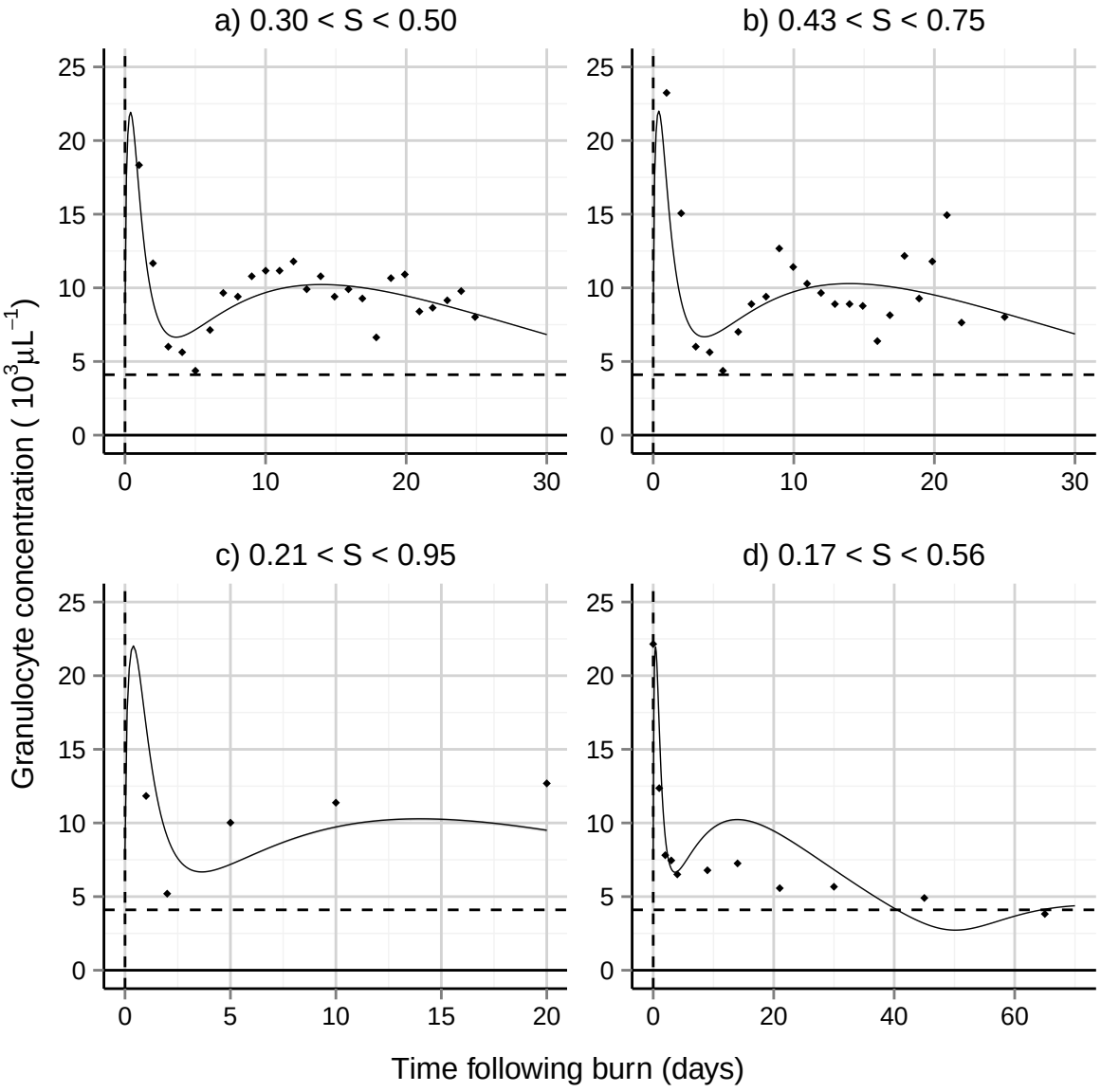

Solid Line: Model output using mean of S and $4.102 \cdot 10^3 \mu L^{-1}$ as baseline
Shaded Region: Model output for range of S using $4.102 \cdot 10^3 \mu L^{-1}$ as baseline
Data (Mean): Peterson et al. 1983 (a,b); Vindenes et al. 1995 (c); Nijsten et al. 1991 (d)

Figure 4.3: Human granulopoiesis model simulations compared with optimization data.

data from burn subjects. Based on the optimized parameter values, the effects of burn on the marginated granulocyte pool and on the hematopoietic stem cell repopulation rate have similar durations taking approximately 1.4 d for the burn-induced change to be reduced by half. The change in the bone marrow release rate and transition to tissue rate are more transient, taking 0.5 and 0.1 days, respectively, to be reduced by half.

Although the general trends in the granulocyte response are matched, there are some discrepancies between the data and the model simulation. The data from Vindenes et al. 1995 demonstrates a somewhat larger second granulocytosis than the model predicts (Figure

Table 4.2: Biological parameter values for human granulopoiesis.

Parameter	Biological Meaning	Value
α	Maximum rate of mitotic progenitor repopulation	2.0 d^{-1}
γ	Rate of mitotic progenitor maturation	0.17 d^{-1}
δ_0	Determines post-mitotic maturation rate	0.34 d^{-1}
m	Determines post-mitotic maturation rate	0.27
l	Determines post-mitotic maturation rate	1.69
κ_0	Normal rate of transition from blood to tissue	1.60 d^{-1}
ψ	Rate of granulocyte decay from tissue	1.05 d^{-1}
θ_2	Decay rate of mediator due to x_2 cells relative to x_1 cells	2.24
θ_3	Decay rate of mediator due to x_3 cells relative to x_1 cells	8.45
θ_4	Decay rate of mediator due to x_4 cells relative to x_1 cells	8.45
D_1^0	Determines fraction of damaged x_1 cells	0.46 Gy
D_1^{000}	Determines ratio of weakly damaged to damaged x_1 cells	2.46 Gy
D_2^0	Determines fraction of damaged x_2 cells	45.76 Gy
D_3^0	Determines fraction of damaged x_3 cells	45.76 Gy
D_4^0	Determines fraction of damaged x_4 cells	45.76 Gy
n_i	Number of targets per cell x_i (i=1,2,3,4)	1
μ	Rate of damaged cell death	1.0 d^{-1}
η	Rate of weakly damaged cell death (when $t > \Delta t_{ae}$)	0.08 d^{-1}
τ	Determines time of abortive rise: $\Delta t_{ae} = \tau - vD$	22.70 d
v	Determines time of abortive rise: $\Delta t_{ae} = \tau - vD$	1.25 d/Gy
$\bar{r}$	Fraction of x_3 that freely circulates at equilibrium	0.50
A	Determines how changing burn size affects the system	0.11
k	Determines how changing burn size affects the system	0.11
b_r	Determines max burn effect on marginated ratio	1
a_r	Determines duration of burn effect on marginated ratio	0.50 d^{-1}
b_0	Determines max burn effect on repopulation rate	1.13 d^{-1}
a_0	Determines duration of burn effect on repopulation rate	0.49 d^{-1}
b_2	Max relative burn effect on bone marrow release	20.00
a_2	Determines duration of burn effect on bone marrow release	1.36 d^{-1}
b_3	Max relative burn effect on transition to tissue	2.10
a_3	Determines duration of burn effect on transition to tissue	7.67 d^{-1}

Values for A, k, a_r, b_0, a_0, b_2, a_2, b_3 and a_3 were determined through optimization (see Section 2.1).
The value for b_r was set to 1 (at most 100% of granulocytes can be demarginated).
See Wentz et al. 2014a for source of all other parameter values.

4.3c) while the data from Nijsten et al. 1991 shows a smaller granulocytosis than the model predicts (Figure 4.3d). While these observations contradict each other to some extent, they highlight the variability observed in human data and emphasize the quantitative limitations of this modeling effort. In the Nijsten et al. 1991 study, other features, such as the first decline in granulocyte concentration, are accurately matched.

One challenge with the human granulopoiesis optimization is the lack of information on

the dose-dependency of the rate changes. Based on the optimized parameter values for A and k, burn size has practically no effect on the model output. This is not likely the case in reality, but is rather a consequence of the available data used to optimize the models. All the data were obtained from groups with a large range of burn sizes. Based on the data from Peterson et al. 1983, there is not a significant difference in granulocyte concentrations following burn between survivors (30-50% TBSA burned) and non-survivors (43-75% TBSA burned). The surviving group from the Peterson et al. 1983 study represents the group with the lowest mean burn size (S=0.36) used for optimization. The possibility exists that a maximal effect on granulopoiesis is reached at a certain TBSA, and above that TBSA, no greater effect is observed. However, in order to understand the response at lower burn sizes, data from individuals with burn sizes that are less than 30% TBSA would be needed. Without such data, our model predicts that even very minor thermal injury causes large changes in the rates discussed in Section 4.1. One way to manually resolve this issue would be to specify in the optimization a burn size greater than zero at which no effect is expected.

4.2.2 Model Validation

Validation of the granulopoiesis model was performed by comparing model output to granulocyte data not used during optimization. Table 4.1 provides information on the validation data used, and Figure 4.4 shows the validation results using data from an individual case study of a 40% TBSA burn exposure. Here, the model output is shown both using the mean granulocyte concentration observed in healthy humans ($4.102 \cdot 10^3$ cells per μL; Valentin 2002) as well as the range of granulocyte concentrations observed in healthy humans ($2.104 \cdot 10^3 - 7.510 \cdot 10^3$ cells per μL; Valentin 2002). In this validation, the model is able to predict the granulocytosis events; however, the second granulocytosis period in the data

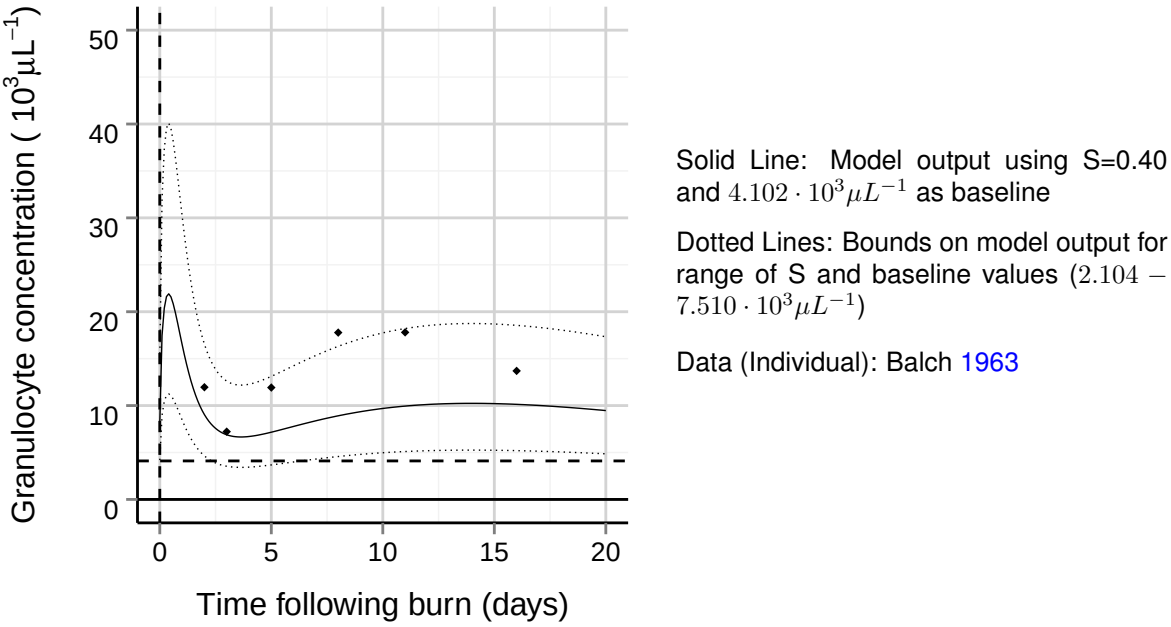

Figure 4.4: Human granulopoiesis model compared with validation data.

is more significant than the model predicts. This could be caused by a variety of factors including errors in the model's structure or the effect of factors associated with human data such as treatment. The patient received antibiotics including penicillin, streptomycin, and tetracyclin. Chloromycetin was given for a short time period when *Aerobacter aerogenes* was found in the blood stream on postburn day 8.

Infection alone can lead to a state of granulocytosis (Summers et al. 2010). Thus, the granulocytosis observed in burn subjects could be, in part, due to an ensuing infection. In one study on burn victims used for model optimization, the non-survivors all developed sepsis, while only 2 of the 16 survivors developed sepsis (Peterson et al. 1983). However, between these two groups, no significant difference in the granulocyte count was observed. This suggests that the effects of infection on the granulocyte concentration, in the case of burn injury, are minimal.

5 Lymphopoiesis Model

Burn-dependent parameters were developed and integrated into our previously developed mathematical model of lymphopoiesis. The previous model, developed by ARA, simulates the effects of acute radiation exposure (Wentz et al. 2014a). Briefly, the lymphopoiesis model consists of three compartments containing mitotic progenitors in the bone marrow, post-mitotic progenitors in the bone marrow, and lymphocytes in circulation. These compartments are regulated through various feedback mechanisms. Acute radiation exposure leads to damage and the eventual death of a dose-dependent proportion of radiosensitive cells. This model is an extreme simplification of the actual lymphopoiesis process. In reality lymphopoiesis leads to the production of many different types of lymphocytes which have different dynamic properties. A structural diagram of the lymphopoiesis model, including burn effects, is given in Figure 5.1.

5.1 Modeling the Effect of Burn

The effects of burn on lymphopoiesis were incorporated into the model through the analysis of observational and experimental data in rodents and humans. Lymphocytopenia is commonly

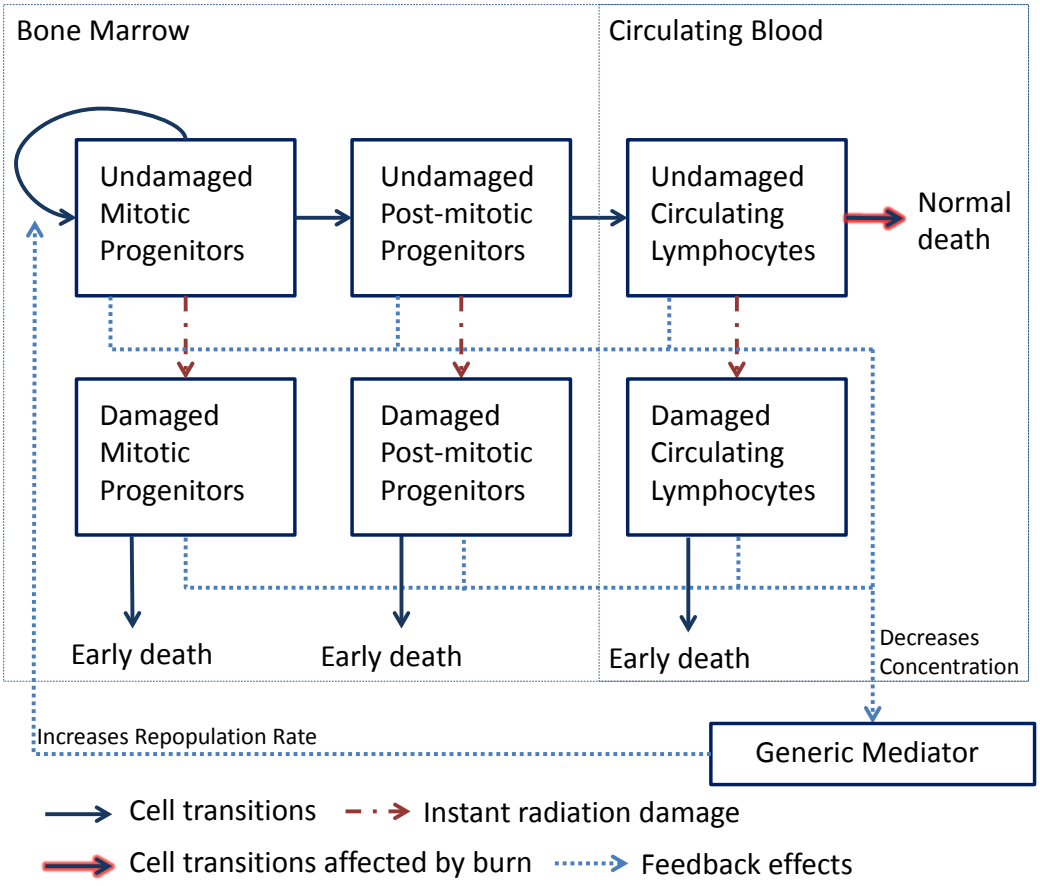

Figure 5.1: Lymphopoiesis model diagram (adapted from Figure 6.1, Wentz et al. 2014a).

observed in humans within the first few days following burn (Peterson et al. 1983; Nijsten et al. 1991; Neilan et al. 1977; Kagan et al. 1989; D'Arpa et al. 2009). The goal of our model development is to accurately predict this effect of burn. The equations for the mathematical model for lymphopoiesis after radiation and burn are given in Appendix A.3.

5.1.1 Increased Blood Lymphocyte Clearance Rate

Lymphocytopenia, or a net decrease in the population of lymphocytes, occurs after burn injury. However, both increases and decreases occur within lymphocyte subpopulations. Reductions in number of $CD3^+$, $CD4^+$, $CD8^+$ T lymphocyte levels and in the $CD4^+/CD8+$ ratio are observed after thermal injury, while the number of $CD19^+$ B cells and $CD16^+$ natural killer (NK) cells are increased (Entezami et al. 2010).

The decreased lymphocyte count is hypothesized to be the result of an increase in lymphocyte activation and clearance from the circulation. Adhesion and activation molecules on lymphocytes are up-regulated in humans following thermal injury (Maldonado et al. 1991). Up-regulation is likely caused by increased levels of circulating cytokines. For example, interleukin 1 (IL-1), which is known to increase the adhesiveness of lymphocytes to the endothelium (Cavender et al. 1986), is up-regulated following trauma (Dinarello 1984). Thus, the hypothesized mechanism causing lymphocytopenia, is a burn-induced increase in cytokine levels which in turn increases the rate of lymphocyte clearance from the blood. A second known outcome of lymphocyte activation is apoptosis or "activation-induced cell death" (Lebedev et al. 2003; Teodorczyk-Injeyan et al. 1995). In our model, increased lymphocyte clearance and lymphocyte apoptosis would lead to an alteration in the same parameter, ψ. The effect of burn on lymphocyte activation is potentially correlated with burn size. Lymphocyte subsets $CD25^+$, $CD71^+$, and $CD26^+$ decreased significantly in subjects with TBSA burn between 70 and 90%, while in subjects with TBSA burned between 30% and 70% the lymphocyte levels decreased but not significantly (Lebedev et al. 2003).

Although this hypothesized mechanism can explain the lymphocytopenia following burn, it does not take into account the increased numbers of B cells and NK cells observed following thermal injury (Entezami et al. 2010; Kagan et al. 1989). One hypothesized cause for the increase in B cells is burn-induced stress hormones leading to the release of B cells from storage sites (Kagan et al. 1989). However, because our model does not simulate lymphocyte subpopulations, our goal here is to capture the net effect. Thus, we simplify the system by not including this stimulatory effect of burn on lymphocyte subpopulations.

To model a burn-induced net decrease in peripheral lymphocytes, a burn-dependent change to the blood lymphocyte clearance rate ψ is added. The new equation describing the rate of lymphocyte clearance from the blood following a burn that covers $S \cdot 100\%$ of the body's surface area is

$$\psi(t) = \psi_0(1 + b_3 S^{c_3} e^{-a_3 t}) \tag{19}$$

where S is the fraction of surface area affected by burn, ψ_0 is the rate of lymphocyte clearance from the blood at equilibrium, and burn occurs at time $t = 0$. b_3 represents the maximum relative change of ψ which is assumed to occur immediately following burn. As t approaches infinity, $\psi(t)$ approaches ψ_0 and the system returns to equilibrium. The speed at which ψ returns to ψ_0 is determined by a_3. c_3 determines the shape of the burn response function.

Table 5.1: Lymphopoiesis model optimization and validation data.

Reference	Burn Size (S)*	Group	Number	Use
D'Arpa et al. 2009	0.187 ± 0.048	Non-septic	5	Optimization
	0.417 ± 0.09	Survivor septic	11	Optimization
	0.467 ± 0.25	Non-survivor septic	4	Optimization
Kagan et al. 1989	0.302 ± 0.044**	Survivor	6	Optimization
	0.623 ± 0.078**	Non-survivor	9	Optimization
Neilan et al. 1977	0.41 (0.15-0.90)		17	Optimization
Nijsten et al. 1991	0.38 (0.17-0.56)		13	Validation
Peterson et al. 1983	0.36 (0.30-0.50)	Survivor	16	Validation
	0.48 (0.43-0.75)	Non-survivor	6	Validation
Vindenes et al. 1995	0.547 (0.21-0.95)		27	Validation

*Data is given as mean ± SD or mean (min-max)
**Burn size given for multiple postburn periods. The value provided is from the earliest period.

When c_3 equals zero, the burn size has no effect. As c_3 increases, a larger burn size is required for a given effect to occur.

5.2 Results and Discussion

In this section, the optimization and validation results for the lymphopoiesis burn model are presented.

5.2.1 Parameter Optimization

To determine values for the new parameters b_3, a_3, and c_3, the lymphopoiesis model was optimized to data on lymphocyte count in humans following burn. The normal mean lymphocyte concentration in humans was used as the baseline value for the data ($2.45 \cdot 10^3 \mu L^{-1}$; Valentin 2002). For a summary of studies used in the optimization, see Table 5.1.

Figure 5.2 compares the model simulation with data used for the optimization, and Table 5.2 gives the parameter values for the model. The optimized value of b_3 is 120.55, which implies that a 100% TBSA burn would cause ψ to equal 1.22 d^{-1} immediately following burn. This leads to an expected lymphocyte transit time in the circulation of 0.82 days compared with 100 days at equilibrium. The optimized value of a_3 is 0.86 d^{-1}, meaning it takes 0.81 days for the change in the lymphocyte clearance rate to decrease by half.

Given available data and the structural constraints of the radiation-effects lymphopoiesis model, an effect of burn was added to the blood clearance rate of lymphocytes. In some case studies our optimization results match the data fairly well:

- Non-septic and survivor septic groups from D'Arpa et al. 2009 (Figure 5.2ab)
- Non-survivor group from Kagan et al. 1989 (Figure 5.2e)
- Data from Neilan et al. 1977 (Figure 5.2f)

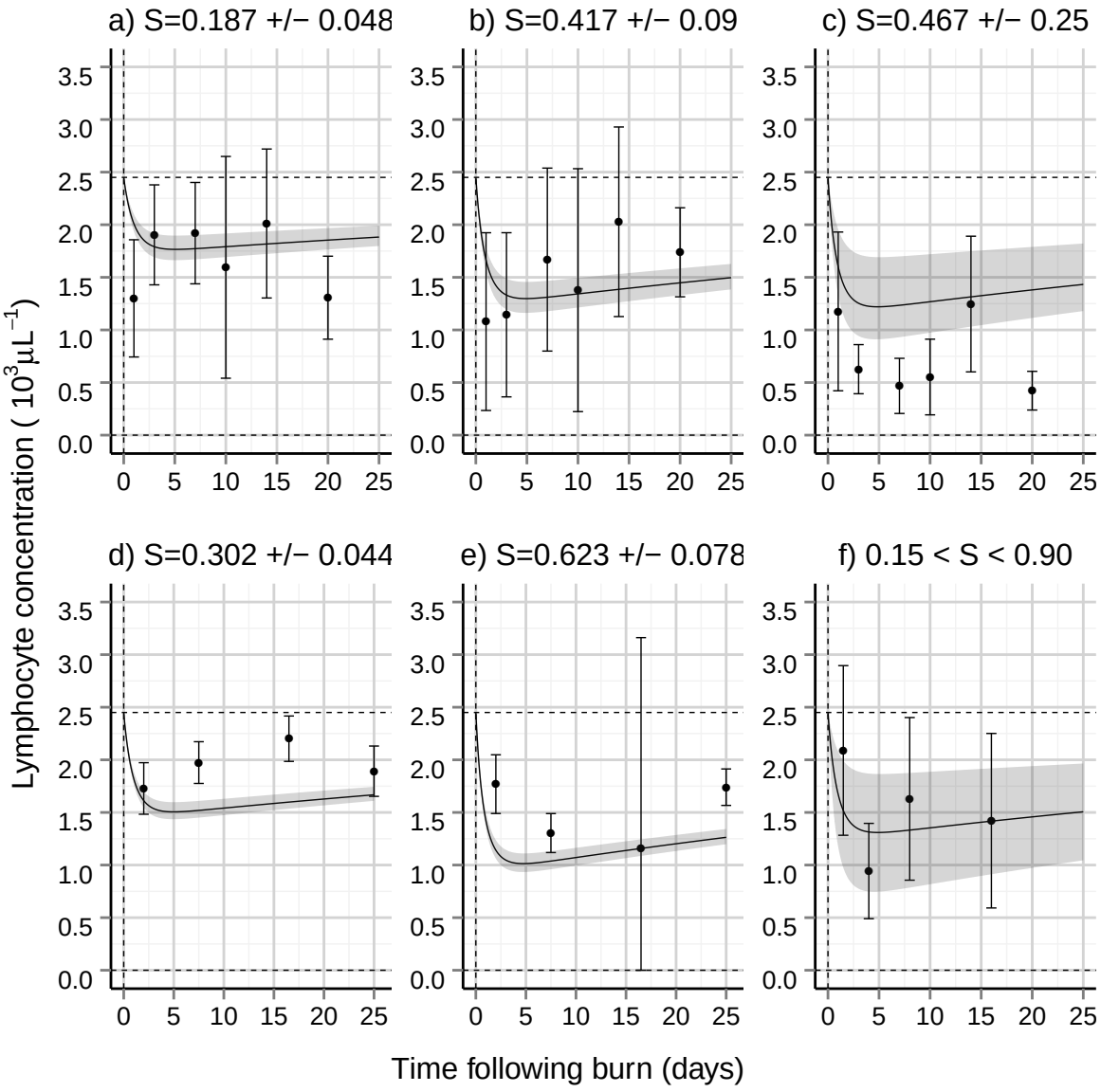

Solid Line: Model output using mean of S and $2.45 \cdot 10^3 \mu L^{-1}$ as baseline
Shaded Region: Model output for range of S and baseline values ($1.40 - 4.20 \cdot 10^3 \mu L^{-1}$)
Data (Mean ± SD): D'Arpa et al. 2009 (a,b,c); Kagan et al. 1989 (d,e); Neilan et al. 1977 (f)

Figure 5.2: Human lymphopoiesis model compared with optimization data.

In other cases the model does not capture the observed trends:

- Non-survivor septic group from D'Arpa et al. 2009 (Figure 5.2c)
- Survivor group from Kagan et al. 1989 (Figure 5.2d)

In the lymphocyte kinetic survivor data from Kagan et al. 1989, the recovery rate is faster than that predicted by the model (Figure 5.2d). This may be caused by selection bias in separating survivors from non-survivors with the same burn sizes. For the lymphocyte

Table 5.2: Biological parameter values for human lymphopoiesis.

Parameter	Biological Meaning	Value
α	Maximum rate of mitotic progenitor repopulation	2.0 d^{-1}
γ	Rate of mitotic progenitor maturation	0.06 d^{-1}
δ	Rate of post-mitotic progenitor maturation	0.001 d^{-1}
ψ_0	Normal rate of lymphocyte clearance from the blood	0.01 d^{-1}
θ_1	Mediator decay due to x_1 cells relative to decay due to x_1 cells	1
θ_2	Mediator decay due to x_2 cells relative to decay due to x_1 cells	2.67
θ_3	Mediator decay due to x_3 cells relative to decay due to x_1 cells	2.67
D_1^0	Determines fraction of damaged x_1 cells	3.98 Gy
n_1	Number of radiation targets per cell x_1	1
D_2^0	Determines fraction of damaged x_2 cells	3.98 Gy
n_2	Number of radiation targets per cell x_2	1
D_3^0	Determines fraction of damaged x_3 cells	6.22 Gy
n_3	Number of radiation targets per cell x_3	0.40
μ	Rate of damaged cell death	1 d^{-1}
b_3	Determines maximum effect of burn on blood clearance rate	120.55
a_3	Determines duration of effect of burn on blood clearance rate	0.86 d^{-1}
c_3	Determines how burn size affects rate changes	0.84

Values for b_3, a_3, and c_3 were determined through optimization (see Section 2.1).
See Wentz et al. 2014a for source of all other parameter values.

kinetic data from non-survivors who developed sepsis (Figure 5.2c; D'Arpa et al. 2009), the model predicts a less substantial nadir than that given by the data. The development of sepsis leads to an increase in lymphocyte apoptosis which ultimately leads to lymphocyte depletion (Hotchkiss et al. 2001). Thus, observing a lower nadir in the data is not unreasonable. The model optimization would benefit from the collection of more data on lymphocyte counts following burn so that septic patients are removed from the optimization, and ideally subjects would be grouped according to burn size rather than survival.

5.2.2 Model Validation

Validation of the lymphopoiesis model was performed by comparing model outputs to lymphocyte data that was not used in the optimization. For these comparisons, the mean and range of the lymphocyte concentration observed in healthy humans was used (2.45; $1.40 - 4.20 \cdot 10^3 \mu L^{-1}$; Valentin 2002). Table 5.1 provides a summary of the data used in validation, and Figure 5.3 shows the results of these comparisons. These data were reserved for validation as opposed to optimization due to the lack of error measurements on the lymphocyte concentration values. Without an estimate of the error, it is difficult to assess the predictive quality of our model. However, it is possible to assess the model's ability to match general trends. In all four studies used for validation, there is a decrease in lymphocyte values below the mean concentration observed in healthy human populations, which the model reliably predicts. However, in some cases, the model does not accurately predict the time

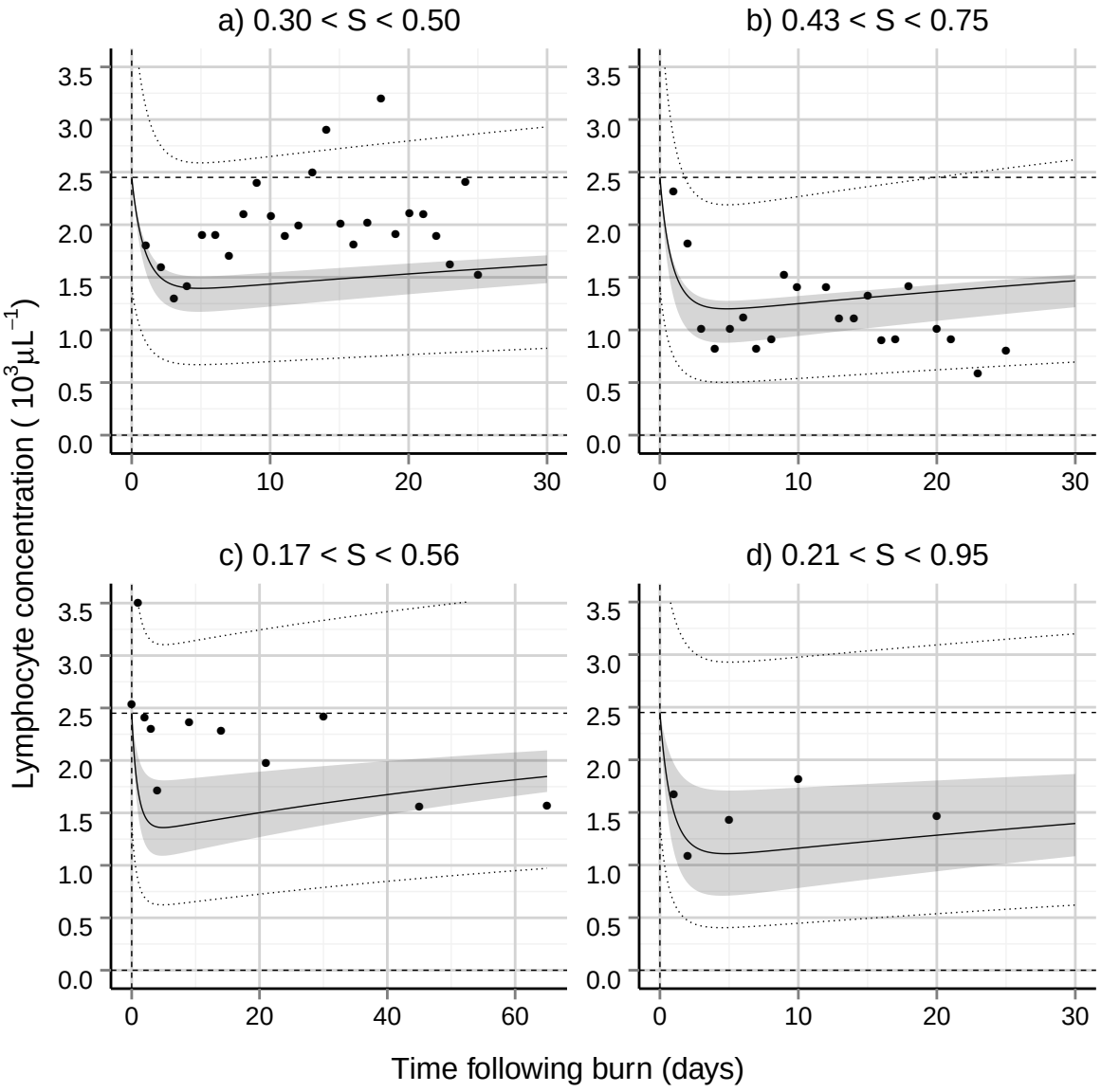

Solid Line: Model output using mean of S and $2.45 \cdot 10^3 \mu L^{-1}$ as baseline
Shaded Region: Model output for range of S using $2.45 \cdot 10^3 \mu L^{-1}$ as baseline
Dotted Lines: Bounds on model output for range of S and baseline values ($1.40 - 4.20 \cdot 10^3 \mu L^{-1}$)
Data (Mean): Peterson et al. 1983 (a,b); Nijsten et al. 1991 (c); Vindenes et al. 1995 (d)

Figure 5.3: Human lymphopoiesis model compared with validation data.

to recovery. Peterson et al. 1983 collected lymphocyte kinetic data from survivors and non-survivors (Figure 5.3a and 5.3b, respectively). Our model predicts a faster recovery for the non-survivors than that seen in the data and a slower recovery for the survivors than that seen in the data. This discrepancy may be again due to the grouping of patients into survivor and non-survivor groups since lymphocyte recovery seems to be correlated with survivability. The models developed here are intended to present the average response in humans after thermal injury, and therefore, it may not be possible to match outputs to stratified patient data. Furthermore, sepsis could be leading to a delayed recovery in the non-survivor group.

6 Combined Injury Model Analysis

Our aim in the current work is to develop computational models that predict hematopoietic responses of combined radiation and burn injury given the limited quantitative clinical data available of combined injury in humans. To predict blood and progenitor cell dynamics following combined radiation and burn injury, the effects of burn were integrated into previously developed hematopoietic models (Wentz et al. 2014a). These single injury models were validated using data from human patients who were accidentally irradiated or thermally injured. Due to a lack of data from patients with both radiation and burn injury, validation of the combined injury model using human data is not possible. However, to evaluate the credibility of the combined injury predictions, the structure of the combined injury model is validated by comparing murine data to murine versions of the models. In generating murine models, the model structure was conserved across species but was parameterized using only rodent data. Details of this parameterization for thrombopoiesis and granulopoiesis are provided in Appendix B. A murine model simulating the combined effects of burn and radiation on lymphopoiesis does not currently exist, and, therefore, we were unable to perform the comparisons between the murine combined injury data and the murine model output. Instead, for lymphopoiesis the murine combined injury data is compared to predictions given by the human model.

Blood cell concentrations following radiation only, burn only, and combined injury were obtained from studies in mice (Palmer et al. 2011; Boudagov et al. 2006; Tajima et al. 2013; Kiang et al. 2014), rats (Davis et al. 1955), and dogs (Reid et al. 1955). Since no canine models exist, the canine data was compared to human model outputs. The animal data were normalized using data from sham controls when available. Otherwise, the data were normalized using the control blood cell values prior to injury.

6.1 Platelets

Figure 6.1, 6.2, 6.3, and 6.4 compare radiation, burn, and combined injury platelet data in rodents to murine thrombopoiesis model predictions. In the data from rat experiments, shown in Figure 6.1 and 6.2, the combined injury and radiation alone data tend to follow similar trajectories. The data does suggest that following combined injury a faster recovery occurs than following only irradiation. This trend towards a faster recovery is predicted by the murine model. In the study done by Boudagov et al. 2006 in mice (Figure 6.3), relative comparisons between individual insults and combined injury effects are challenging because radiation and burn only data are not available past three days. During this first 3-day interval, the combined injury response appears worse than both the radiation and burn only response. Again, the early synergistic effect of burn and radiation is predicted by the model. An exacerbated early response is a reasonable prediction due to radiation-induced cell death and increased platelet consumption caused by the reaction to burn. However, a faster recovery is also predictable due to the stimulatory effect of burn on the early progenitors.

Kiang et al. 2014 quantified platelet cell counts at 30 days post 9.5 Gy and 15% TBSA burn combined injury in mice (Figure 6.4). The model is able to predict the relative difference in platelet concentration between injury types. However, compared with sham values platelet counts are decreased following any combinations of insults (Kiang et al. 2014 spec-

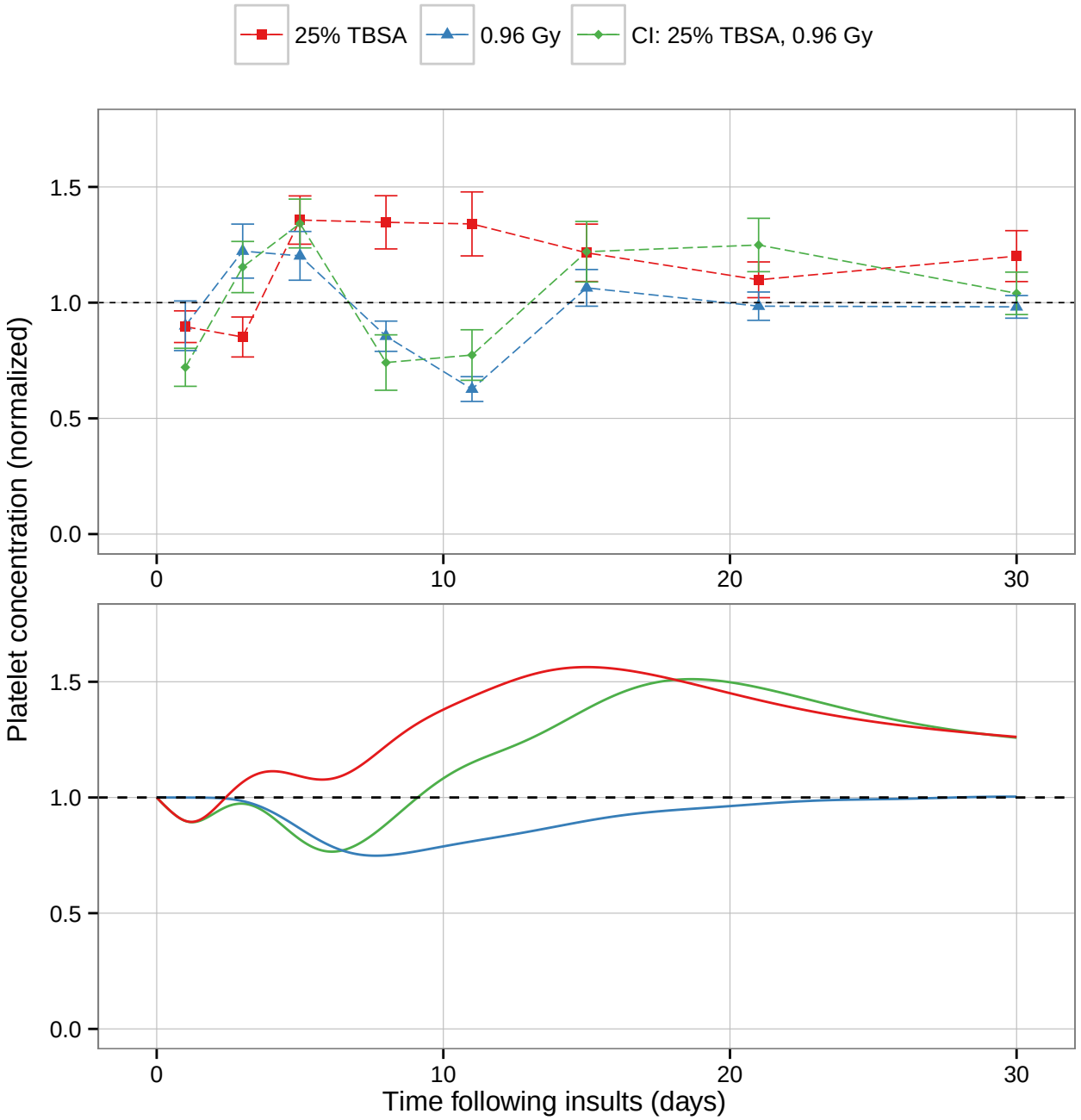

Figure 6.1: Platelet concentration following low radiation dose combined injury in rats (top; Davis et al. 1955) compared with murine model simulations (bottom).

ifies that only radiation alone and combined injury led to a significant decrease), while the model predicts platelet counts are close to normal for all three injury combinations. In developing the radiation only model for mice, the highest radiation dose used for optimization or validation was 7.68 Gy (see Figure B.1 and B.2). Thus, the model may not currently be able to capture the platelet response following 9.5 Gy. In the burn only optimization data,

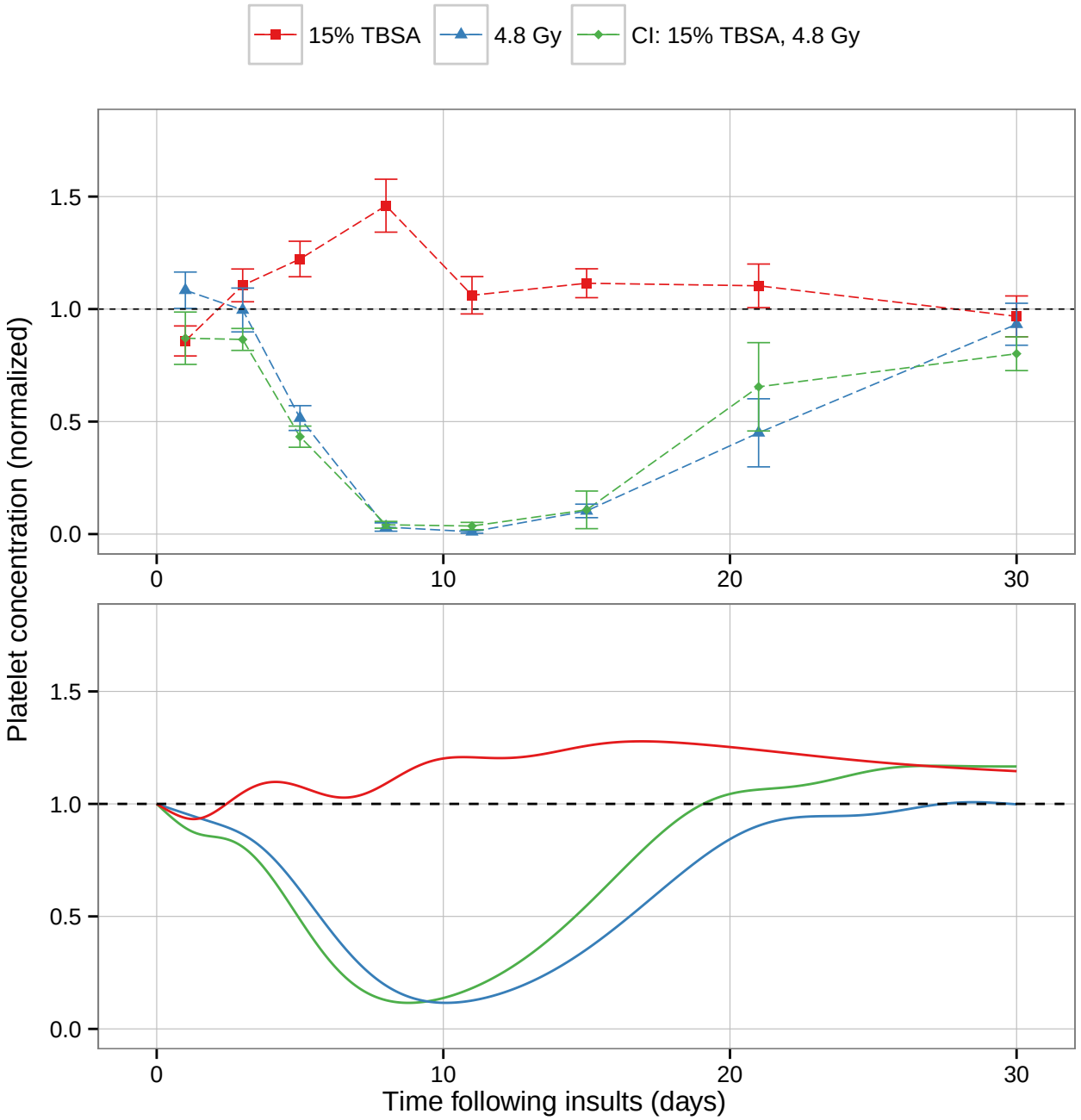

Figure 6.2: Platelet concentration following high radiation dose combined injury in rats (top; Davis et al. 1955) compared with murine model simulations (bottom).

platelet concentrations were either normal or higher than normal at close to 30 days postburn (Figure B.3). Thus, although Kiang et al. 2014 saw a trend towards a decreased platelet concentration following only burn, this is not a consistent observation across all combinations of insult ranges. The cause of the variability in platelet response between experiments may be due to differences in burn depth. This is not currently accounted for in the models.

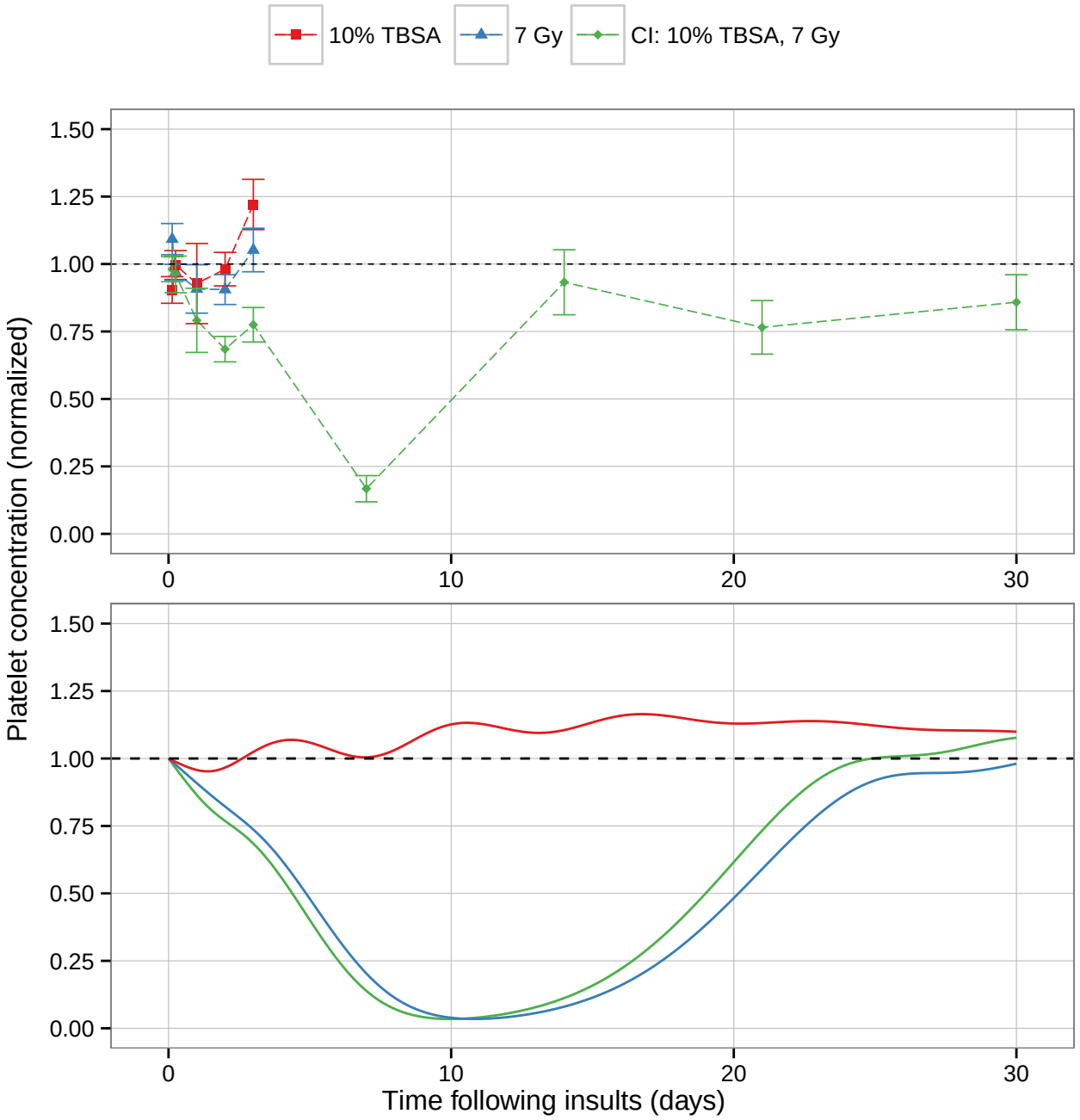

Figure 6.3: Platelet concentration following combined injury in mice (top; Boudagov et al. 2006) compared with murine model simulations (bottom).

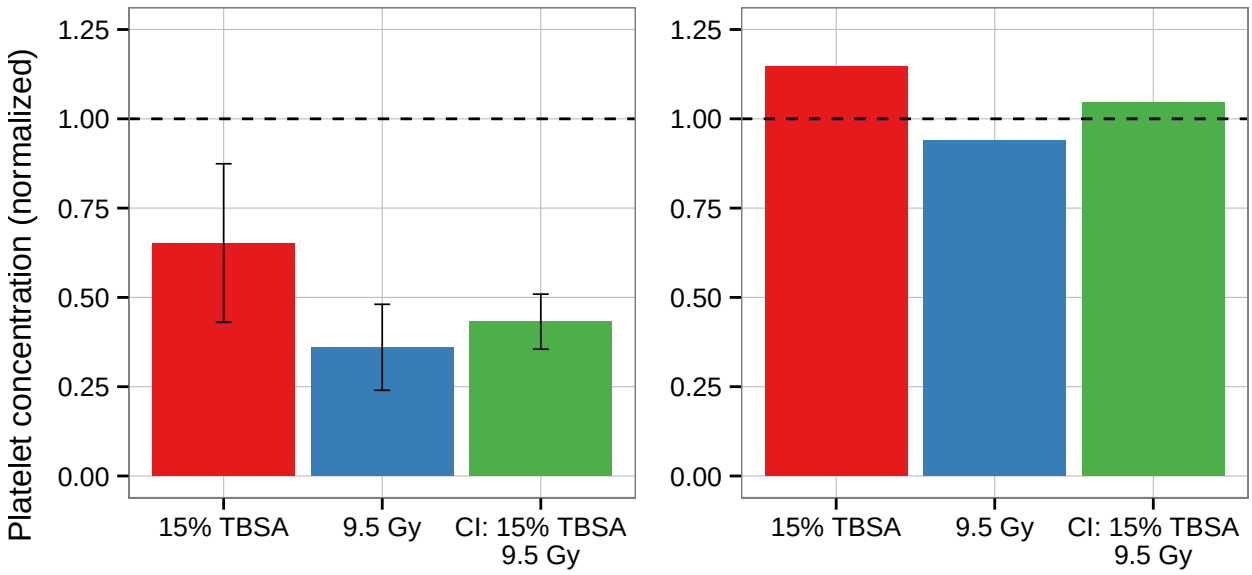

Figure 6.4: Concentration of platelets 30 days following combined injury. Data in mice (left; Kiang et al. 2014) compared with model predictions (right).

6.2 Granulocytes

Comparisons of granulopoiesis rodent data with murine model simulations are shown in Figure 6.5 and 6.6. Although there are deviations between the data and the model predictions, key trends are matched (Figure 6.5). Exposure to both radiation and burn leads to an ameliorated response compared with exposure to only radiation. Specifically, following

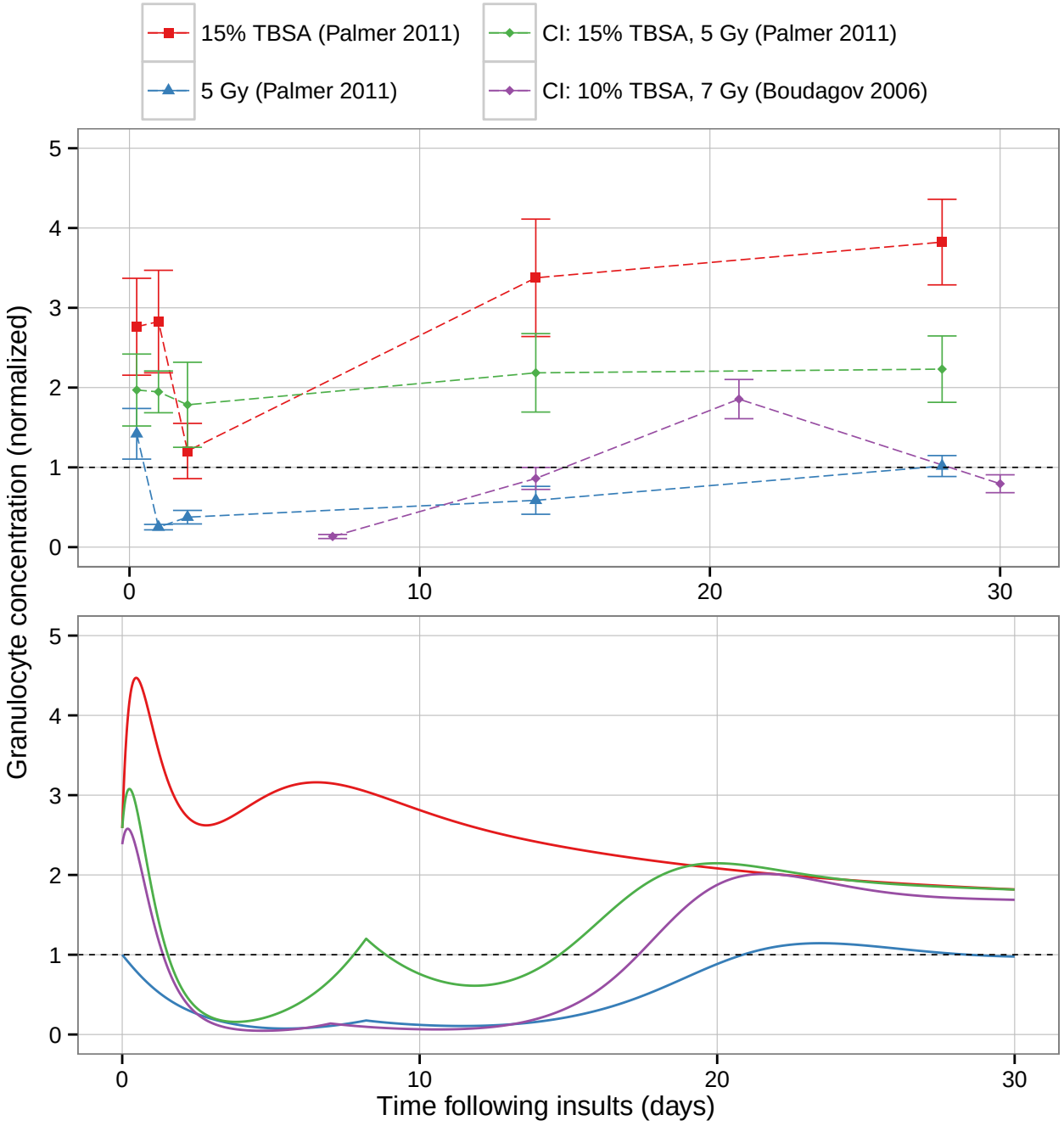

Figure 6.5: Granulocyte concentration following combined injury in mice (top) compared with murine model simulations (bottom).

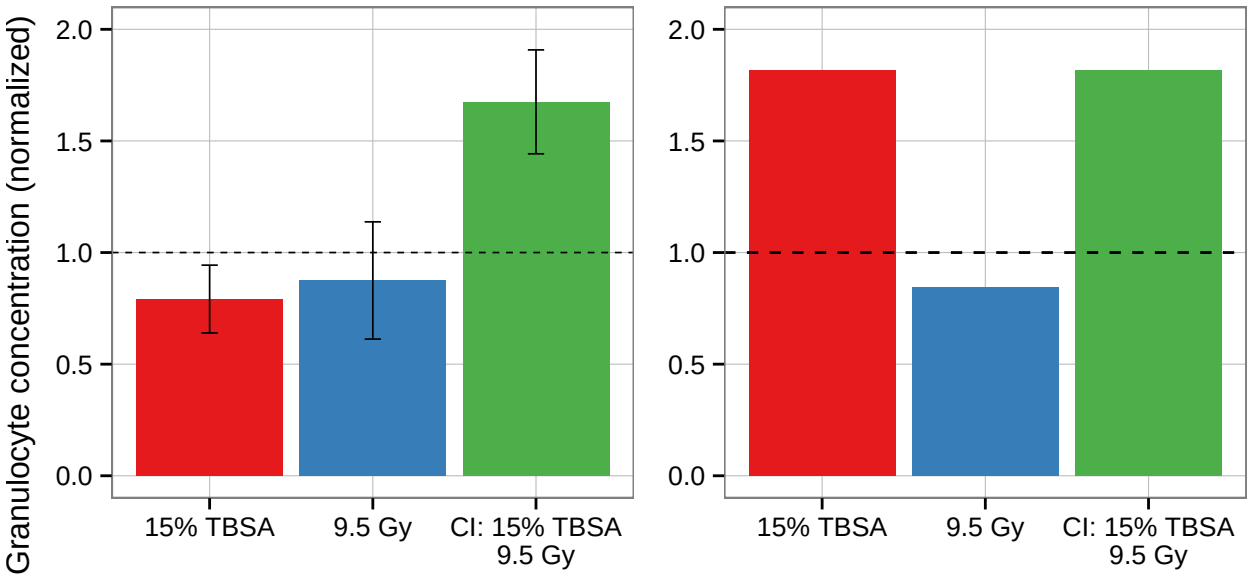

Figure 6.6: Concentration of granulocytes 30 days following combined injury. Data in mice (left; Kiang et al. 2014) compared with model predictions (right).

combined injury there is a less significant nadir and recovery occurs earlier than following only radiation. These effects are predicted by the murine model. Figure 6.5 also shows a comparison of two combined injury simulations with different insults. The model and the data both show that 10% TBSA burn and 7 Gy irradiation leads to a worse response than 15% TBSA burn and 5 Gy irradiation.

In a second comparison granulocyte concentrations at 30 days post insult are compared with model predictions (Figure 6.6). The radiation and combined injury model outputs match the data; however, following only burn granulocyte levels are close to normal while the model predicts that they are elevated. Other data obtained from mice with 15% TBSA burn shows the reverse trend in which the model is underpredicting the platelet response at 30 days postburn (Figure 6.5). This demonstrates that deviations from the model and the burn only data may be due to experimental variability (e.g., differences in burn depth/severity).

Additional combined injury data for granulopoiesis are shown in Figure 6.7. This second set of data comes from a flow cytometry analysis of neutrophils and other blood cells (Tajima et al. 2013). Information on the total cell population, as well as the relative proportion of each cell type in the population, was given. However, in some cases the total percentage was greater than 100%, suggesting the absolute values obtained using this data may be inaccurate. Thus, when examining this data we are mainly interested in the relative differences between combined injury, burn only, and radiation only exposure. Based on this data it is again clear that, as predicted by the murine model, adding burn to a radiation injury leads to a less severe granulocyte blood cell concentration nadir.

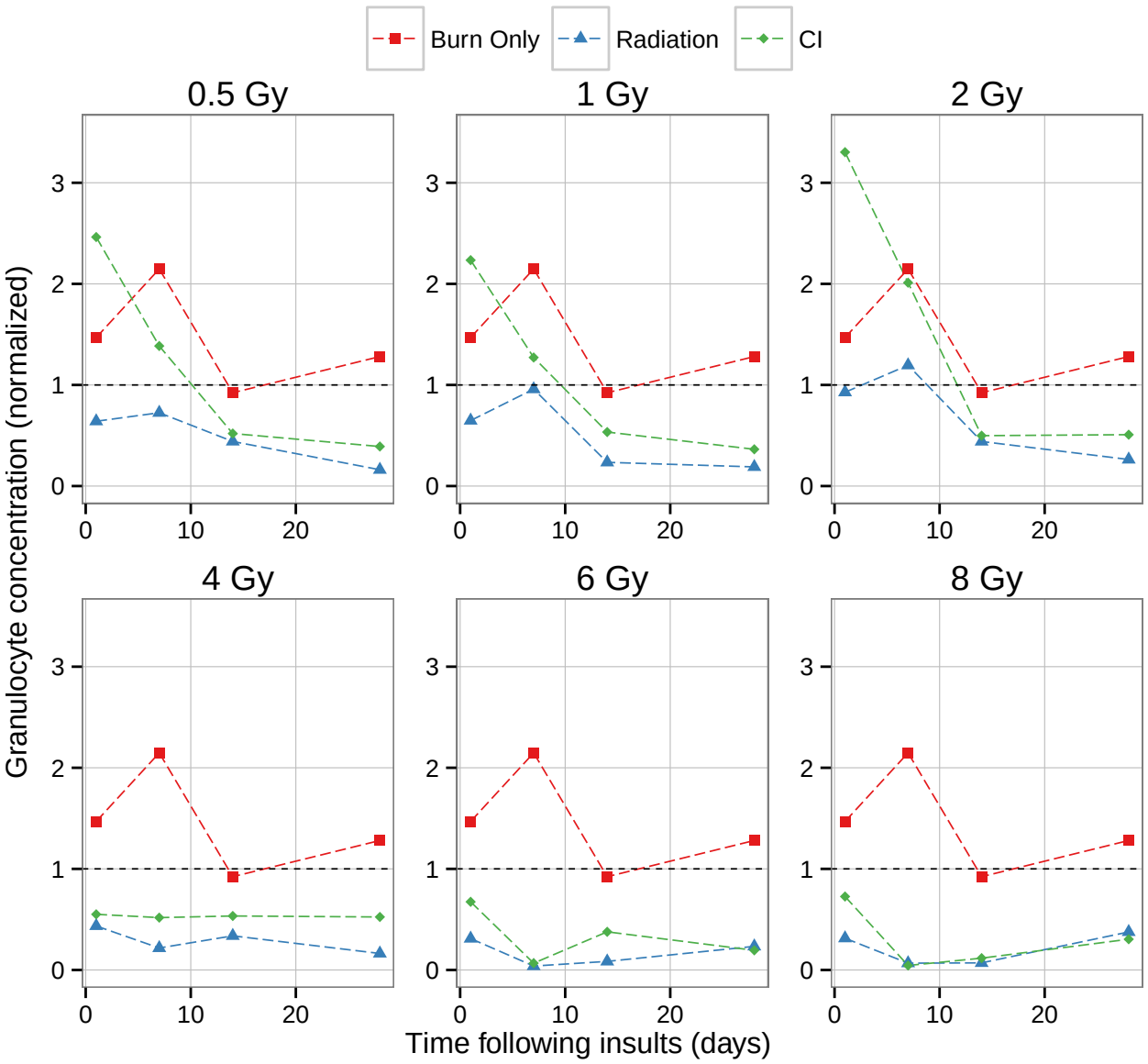

Figure 6.7: Granulocyte concentration following 25% TBSA burn and irradiation in mice (Tajima et al. 2013).

6.3 Lymphocytes

Figure 6.8 and 6.9 show comparisons of the human lymphopoiesis model with murine data. The lymphopoiesis model predicts that combined injury increases the lymphocyte depletion when compared with only radiation or burn injury (Figure 6.8). This effect is suggested by the murine data at later time points (i.e., 14 and 28 days after the insult). Furthermore, at 30 days post exposure, the model is able to match experimental predictions (Figure 6.9). However, at earlier time points (6 h, 24 h, 48 h), radiation resulted in a more significant nadir than combined injury (Figure 6.8). Following only burn, the data shows an initial brief increase in lymphocyte concentration, which the model does not predict. The lymphopoiesis model is an extremely simplified version of the biological reality. Lymphocytes represent

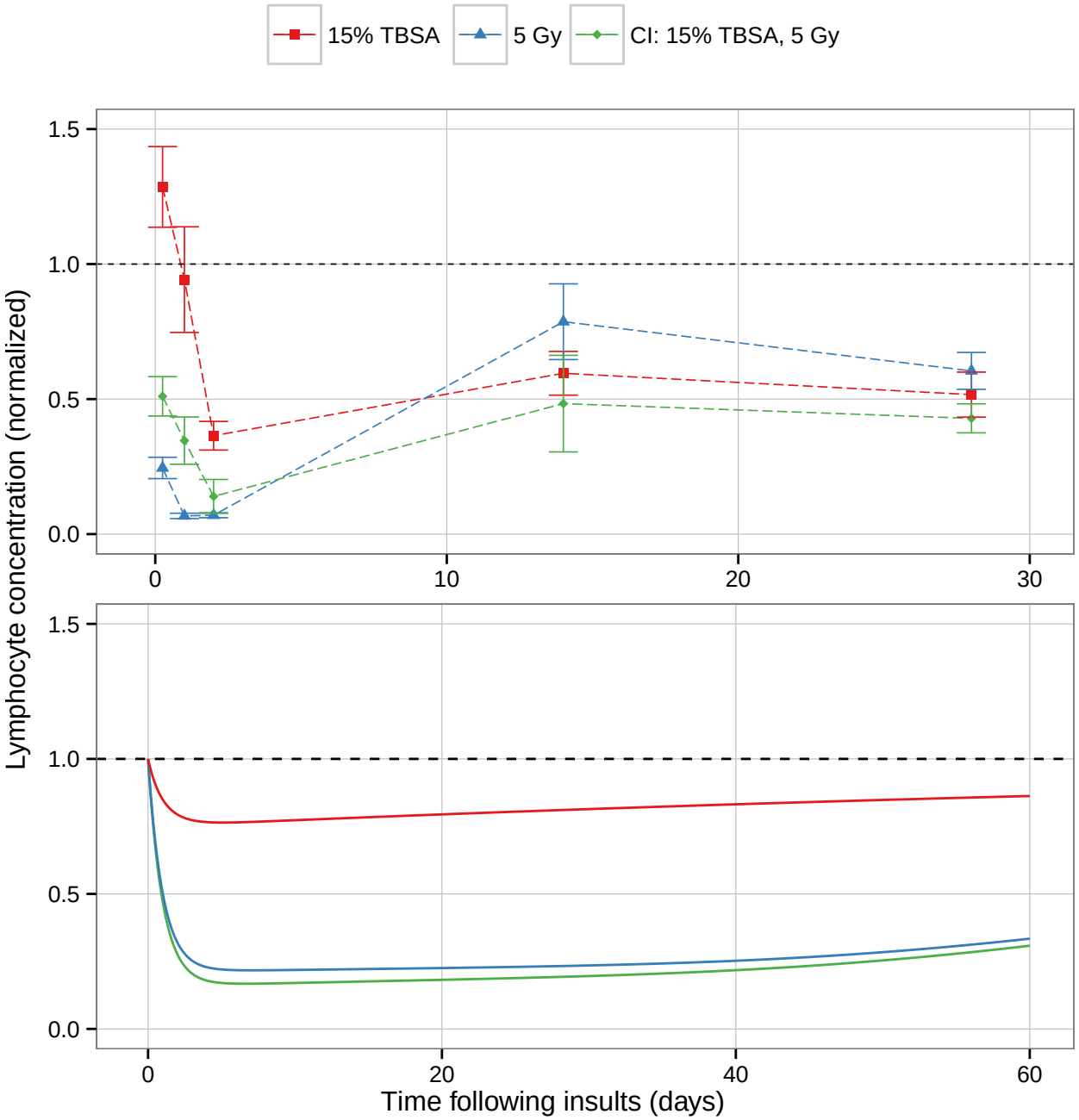

Figure 6.8: Lymphocyte concentration following combined injury in mice (top; Palmer et al. 2011) compared with human model simulations (bottom).

a heterogeneous population of cells (e.g., B cells, T cells, NK cells) which have different dynamic properties. In fact, some lymphocytes are known to proliferate (Macallan et al. 2005), and this dynamic is not currently in the model but may explain the slight increase observed in lymphocyte concentration following burn. This increase may, in turn, contribute to the less severe nadir observed following combined injury. Therefore, a more detailed model of lymphopoiesis that can capture these effects may be warranted in the future.

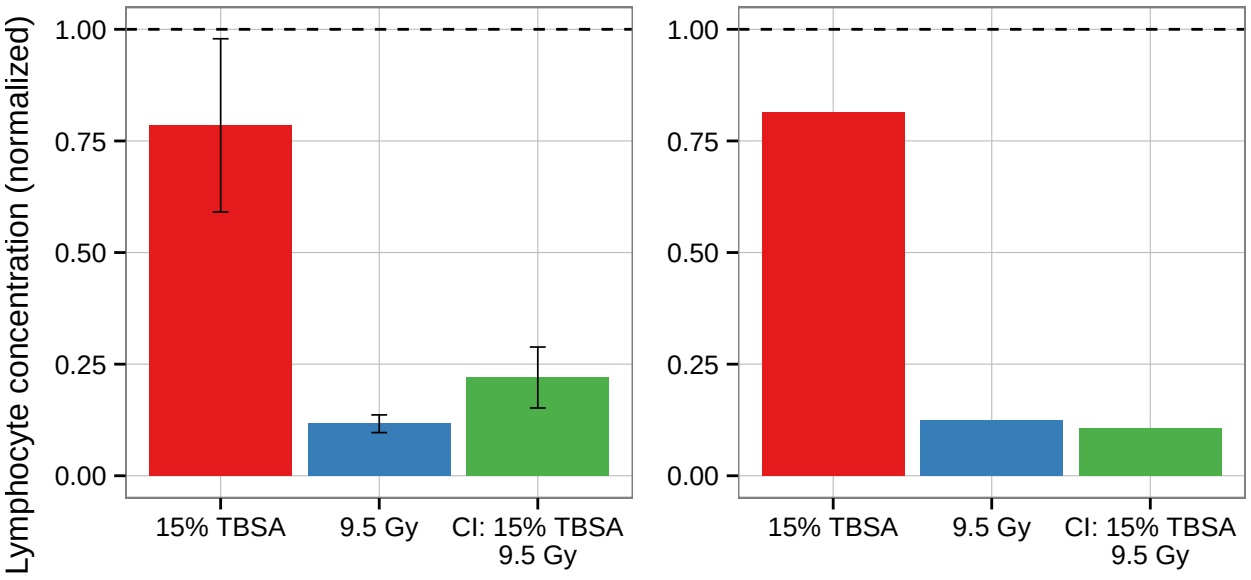

Figure 6.9: Concentration of lymphocytes 30 days following combined injury. Data in mice (left; Kiang et al. 2014) compared with model predictions (right).

Figure 6.10 shows additional lymphocyte combined injury data. This second set of data comes from the same study as the data presented in Figure 6.7 (Tajima et al. 2013). To quantify the lymphocyte population, we pooled flow cytometry data for CD4 T cells, CD8 T cells, NK cells, and B cells. Due to the previously discussed limitations of the study, when examining this data we are mainly interested in the relative differences between combined injury, burn only, and radiation only exposure. At low doses (0.5 and 1 Gy), there is no clear trend between the radiation only, burn only, and CI data. At 2 Gy combined injury leads to a larger decrease in lymphocyte counts. At higher doses ($\geq$ 4 Gy) the radiation only and combined injury response have similar kinetic profiles. Thus, it appears that for higher doses and a TBSA burn of 25%, radiation is the dominant insult. Based on the data shown in Figure 6.8 and 6.9, it appears that burn size has an effect on the early lymphocyte dynamics. Specifically, the decrease in lymphocyte following combined injury is less when the burn size is smaller. This effect of burn is not fully understood and may require a more complex model of lymphopoiesis to accurately simulate the lymphocyte response.

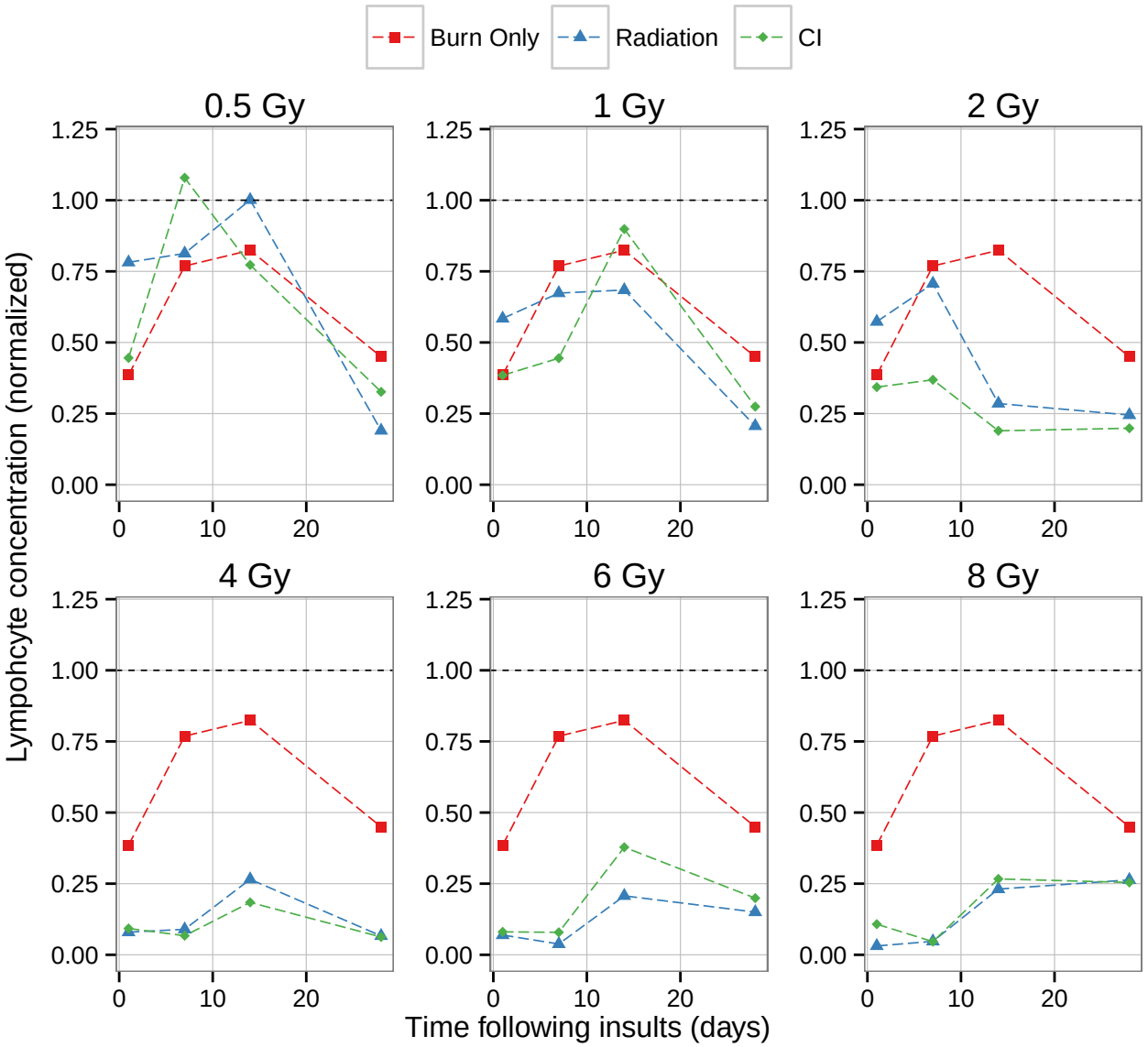

Figure 6.10: Lymphocyte concentration following 25% TBSA burn and irradiation in mice (Tajima et al. 2013).

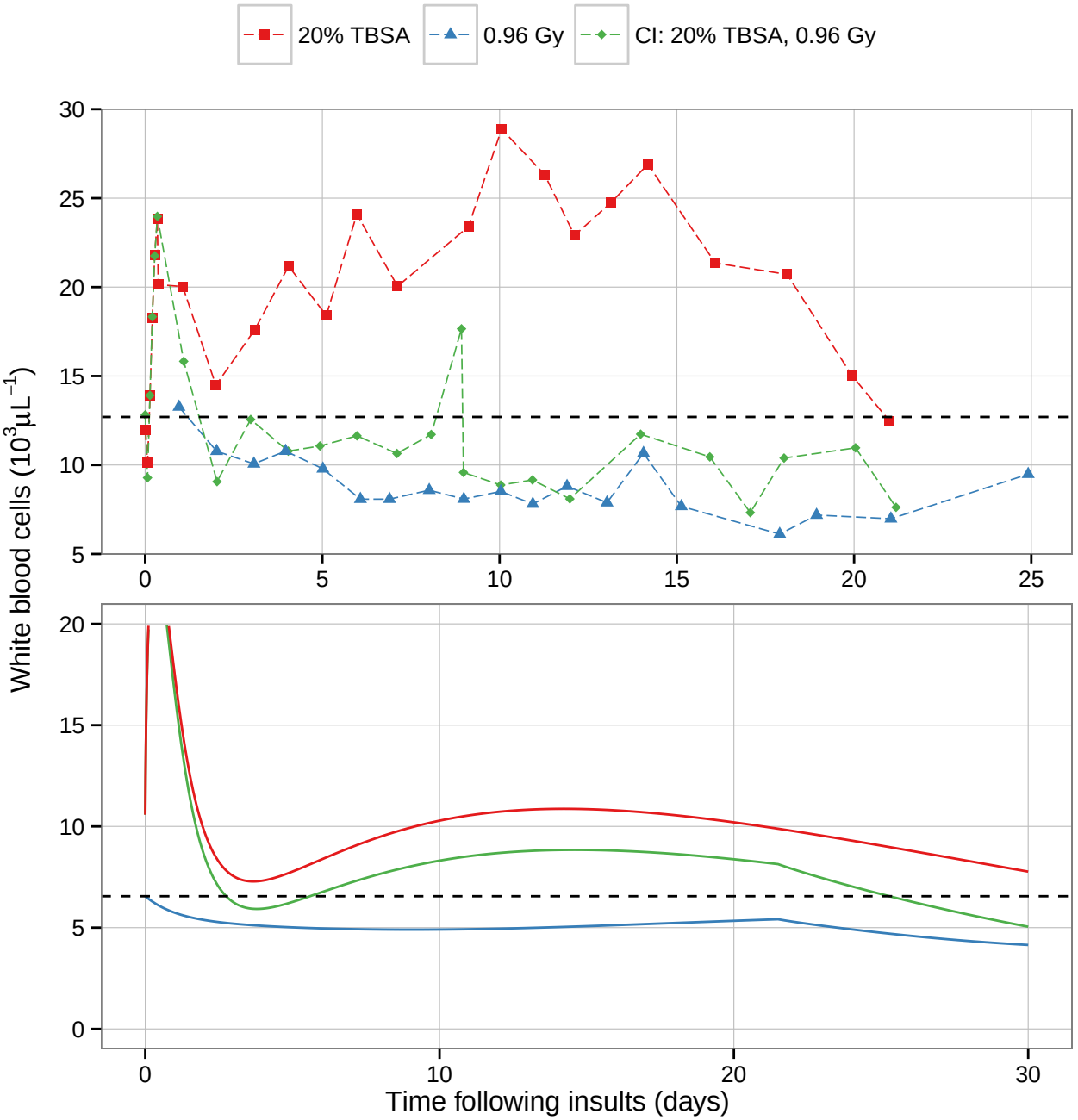

Figure 6.11: White blood cell dynamics following combined injury in dogs (top; Reid et al. 1955) compared with human model simulations (bottom).

6.4 White Blood Cells

Figure 6.11 shows a comparison of the human model's prediction of white blood cell counts with canine data. For this comparison the granulocyte and lymphocyte human model predictions were added together using 4.102 and $2.45 \cdot 10^3 \mu L^{-1}$ as the baseline granulocyte and lymphocyte concentrations, respectively. The model successfully predicts that combined

injury leads to an early ameliorated response in the white blood cell concentration.

6.5 Combined Injury Analysis Summary

Based on the combined injury predictions of the three different blood cell lines, the effects of combined injury are not simply exacerbated from what is observed with single injuries. In some instances combined injury leads to a more severe nadir and/or a delayed recovery. On the other hand, the models suggests that combined injury could accelerate recovery relative to radiation injury alone. The mathematical models help to delineate the potential interactions or contradictory effects of each injury when observed in combination. To fully understand the impact of radiation and burn combined injury, the next step will be to correlate features of the curves (e.g., nadir and duration of cytopenia) with risk of infection, hemorrhage, and/or mortality.

7 Future Work

Hematopoietic models describing the effects of combined radiation and burn injury on blood cell kinetics have been developed. Additional steps will be taken so that the models have direct operational use for nuclear disaster scenario analysis and preparedness planning.

7.1 Validating Combined Injury Model

As mentioned previously, validation of the human combined injury model with data on victims who received both radiation and thermal injury is ultimately needed. This is a necessary step in verifying that we are correctly accounting for the combined effects of radiation and burn. Literature on radiation incidents will be re-examined in an effort to identify human case studies involving thermal burns and radiation exposure that have blood cell kinetics data. Some patients from Nagasaki and Hiroshima were known to have suffered combined injury. However, detailed information on blood cells kinetics from this population has not yet been identified. Another mechanism for adding credibility to our model predictions would be to test these predictions in animal experiments. This would involve a collaborative efforts with experimentalists actively involved in combined injury research and will be dependent on the flexibility of their ongoing research.

7.2 Correlating Model Outputs with Mortality

Efforts are underway to correlate model outputs (i.e., blood cell population nadirs, the duration of cytopenias) with the probability of and time to mortality. If needed, a weighted combination of model outputs may be used to assist in this prediction. Again, correlation of mortality risk with clinical endpoints as provided by the models can be guided and verified to some extent by experimental animal data.

Although we plan to link physiological outputs from the models presented here to mortality predictions, other hematopoietic properties not predicted by the models may contribute to mortality. Potential future modeling endeavors that may assist in mortality predictions are discussed below. However, these efforts would only be considered if a satisfactory mortality prediction model cannot be developed using the models as they stand now.

Thermal injury leads to a variety of changes to the granulopoietic system that are not predicted by our model as it currently stands. Studies have suggested that, following burn, there is a shift of granulocyte-monocyte progenitors towards the monocyte lineage (Santangelo et al. 2001; Noel et al. 2007; Silva et al. 2002). Monocyte concentrations have been correlated with survival following thermal injury (Peterson et al. 1983). Thus, monocytes may prove to be a predictor of mortality risk. Future work may explore the feasibility of developing a model that can predict monocyte dynamics after burn and radiation if adequate data exists.

Also, neutrophil function has been shown to decrease following burn (Arturson 1985). Although this does not affect the kinetics, it may play a large role in determining an individual's susceptibility to infection following burn and subsequent risk of mortality. Thus, future work might involve developing a model to quantify granulocyte dysfunction following

burn. This could be done by creating an injured granulocyte compartment and determining the proportion of granulocytes that are injured. Another approach might be to allow granulocytes to have a range of injury levels that follows a distribution scheme. In turn, the distribution of injury levels could be correlated with the likelihood of infection. These alternate effects of thermal injury provide other areas of exploration which may help predict survivability following combined injury.

As mentioned previously, lymphocyte subsets show a variety of responses after thermal injury. However, our current lymphopoiesis model only predicts the net effect on these subsets. The ratios of different lymphocyte subsets (i.e., the number of T cells compared to the number of B cells) may be of importance for understanding the capabilities of the immune system and whether it is fully functional. Thus, potential model developments may involve dividing the peripheral lymphocyte populations into various sub-populations so that the concentration of each subset and, in turn, the ratio between subsets can be predicted.

7.3 Predicting Combined Injury in an Urban Environment

To improve operational utility of the hematopoietic models, the suite of models will eventually be linked to other tools which provide environment inputs for modern scenarios that include urban environments. Current tools, such as HPAC and NucFast calculate free-in-air radiation dose as well as the incident thermal fluence at specific locations in urban environments. Future work will involve correlating the direct thermal fluence from the blast and secondary fires with %TBSA burn. BURNSIM, a tool which models thermal injury based on the heat flux, may be useful in this task (Knox 2007). This tool provides information on the burn-depth using heat flux and various types of clothing as inputs. By setting a threshold burn-depth level and taking into account the fraction of exposed/covered skin, it may be possible to use this tool to relate thermal fluence to %TBSA burned. With the integration of these models with geospatial population data, more detailed and precise combined injury calculations in urban scenarios will be possible.

8 Conclusion

Models of thrombopoiesis, granulopoiesis, and lymphopoiesis have been developed to simulate the effects of burn injury on hematopoietic cell kinetics and integrated with radiation effects models to make combined injury predictions. The model uses acute radiation exposure and percent surface area burned as inputs and provides predictions of blood cell and progenitor cell counts over time. Each model has been optimized and validated against human data for burn and radiation exposure separately. Model outputs were compared to combined injury data from animals to verify that trends were accurately predicted. Further validation will be required if new data from patients with combined injury becomes available. Outputs from these models (e.g., length of cytopenia or depth of nadirs) will be correlated with mortality to establish a predictive model of mortality risk. This information will assist in disaster preparedness and medical resource planning.

9 References

Andreeff, M., Goodrich, D. W., and Pardee, A. B., 2000. "Cell proliferation, differentiation, and apoptosis," *Holland-Frei Cancer Medicine, 5th edition*. Ed. by R. C. Bast, D. W. Kufe, R. E. Pollock, R. R. Weichselbaum, J. F. Holland, and E. Frei. BC Decker, Ontario, Canada.

Ardia, D., Mullen, K. M., Peterson, B. G., and Ulrich, J., 2015. *'DEoptim': Differential Evolution in 'R'. version 2.2-3*.

Arturson, G., 1985. "Neutrophil granulocyte functions in severely burned patients," *Burns*, 11(5), 309–19.

Asano, S., Okano, A., Ozawa, K., Nakahata, T., Ishibashi, T., Koike, K., Kimura, H., Tanioka, Y., Shibuya, A., and Hirano, T., 1990. "In vivo effects of recombinant human interleukin-6 in primates: stimulated production of platelets," *Blood*, 75(8), 1602–1605.

Asko-Seljavaara, S., 1974. "Granulocyte kinetics in burned mice. Inhibition of granulocyte studied in vivo and in vitro," *Scandinavian Journal of Plastic and Reconstructive Surgery*, 8(3), 185–191.

Baker, G. R., Sullam, P. M., and Levin, J., 1997. "A simple, fluorescent method to internally label platelets suitable for physiological measurements." *American Journal of Hematology*, 56(1), 17–25.

Balch, H. H., 1963. "Resistance to infection in burned patients," *Annals of Surgery*, 157(1), 1–19.

Baxter, C. R., 1974. "Fluid volume and electrolyte changes of the early postburn period," *Clinics in Plastic Surgery*, 1(4), 693–703.

Boudagov, R. S., Oulianova, L. P., and Tsyb, A. F., 2006. *The pathogenesis and therapy of combined radiation injury*. DTRA-TR-06-24, Defense Threat Reduction Agency, Fort Belvoir, VA.

Brecher, G., Endicott, K. M., Gump, H., and Brawner, H. P., 1948. "Effects of X-ray on lymphoid and hemopoietic tissues of albino mice," *Blood*, 3(11), 1259–1274.

Broudy, V. C., Lin, N. L., Sabath, D. F., Papayannopoulou, T., and Kaushansky, K., 1997. "Human platelets display high-affinity receptors for thrombopoietin," *Blood*, 89(6), 1896–904.

Carsin, H., Assicot, M., Feger, F., Roy, O., Pennacino, I., Le Bever, H., Ainaud, P., and Bohuon, C., 1997. "Evolution and significance of circulating procalcitonin levels compared with IL-6, TNF alpha and endotoxin levels early after thermal injury," *Burns*, 23(3), 218–224.

Cavender, D. E., Haskard, D. O., Joseph, B., and Ziff, M., 1986. "Interleukin 1 increases the binding of human B and T lymphocytes to endothelial cell monolayers," *The Journal of Immunology*, 136(1), 203–7.

Chitnis, D., Dickerson, C., Munster, A. M., and Winchurch, R. A., 1996. "Inhibition of apoptosis in polymorphonuclear neutrophils from burn patients," *Journal of Leukocyte Biology*, 59(6), 835–9.

Cohn, S. H., and Milne, W. L., 1956. *The effects of combined administration of strontium-90 and external radiation*. USNRDL-TR-89, Naval Radiological Defense Lab., San Francisco.

D'Arpa, N., Accardo-Palumbo, A., Amato, G., D'Amelio, L., Pileri, D., Cataldo, V., Mogavero, R., Lombardo, C., Napoli, B., and Conte, F., 2009. "Circulating dendritic cells following burn," *Burns*, 35(4), 513–8.

Davis, T. A., Landauer, M. R., Mog, S. R., Barshishat-Kupper, M., Zins, S. R., Amare, M. F., and Day, R. M., 2010. "Timing of captopril administration determines radiation protection or radiation sensitization in a murine model of total body irradiation." *Experimental Hematology*, 38(4), 270–81.

Davis, W. M., Davis, A. K., Lee, W., and Alpen, E. L., 1955. "The combined effects of thermal burns and whole-body x-irradiation. III. Study of blood coagulation," *Annals of Surgery*, 142(1), 66–75.

Deutsch, V. R., and Tomer, A., 2013. "Advances in megakaryocytopoiesis and thrombopoiesis: From bench to bedside," *British Journal of Haematology*, 161(6), 778–793.

Dinarello, C. A., 1984. "Interleukin-1," *Review of Infectious Diseases*, 6(1), 51–95.

Drost, A., Burleson, D., Cioffi, W. G., Jordan, B. S., Mason, A. D., and Pruitt, B. A., 1993. "Plasma cytokines following thermal injury and their relationship with patient mortality, burn size, and time postburn," *The Journal of Trauma*, 35(3), 335–339.

Ebbe, S., 1971. "The megakaryocyte: Maturation and self-renewal," *The Platelet*. The Williams & Wilkins Company, 1–12.

Ebbe, S., and Stohlman, F., 1970. "Stimulation of thrombocytopoiesis in irradiated mice," *Blood*, 35(6), 783–92.

Entezami, K. Z., Khosravi, A., Mousavi, T., and Bahar, M. A., 2010. "Immunophenotype of peripheral blood lymphocytes following thermal injury in patients," *Medical Journal of the Islamic Republic of Iran*, 24(2), 96–102.

Eurenius, K., and Brouse, R. O., 1973. "Granulocyte kinetics after thermal injury," *American Journal of Clinical Pathology*, 60(3), 337–342.

Eurenius, K., Mortensen, R. F., Meserol, P. M., and Curreri, P. W., 1972. "Platelet and megakaryocyte kinetics following thermal injury," *The Journal of Laboratory and Clinical Medicine*, 79(2), 247–257.

Faltynek, C. R., Wang, S., Miller, D., Young, E., Tiberio, L., Kross, K., Kelley, M., and Kloszewski, E., 1992. "Administration of human recombinant IL-7 to normal and irradiated mice increases the numbers of lymphocytes and some immature cells of the myeloid lineage." *The Journal of Immunology*, 149(4), 1276–1282.

Fujimi, S., MacConmara, M. P., Maung, A. A., Zang, Y., Mannick, J. A., Lederer, J. A., and Lapchak, P. H., 2006. "Platelet depletion in mice increases mortality after thermal injury," *Blood*, 107(11), 4399–406.

Ghosh, S. P., Kulkarni, S., Perkins, M. W., Hieber, K., Pessu, R. L., Gambles, K., Maniar, M., Kao, T.-C., Seed, T. M., and Kumar, K. S., 2012. "Amelioration of radiation-induced hematopoietic and gastrointestinal damage by Ex-RAD(R) in mice." *Journal of Radiation Research*, 53(4), 526–36.

Gruber, D. F., and Farese, A. M., 1989. "Bone marrow myelopoiesis in rats after 10% , 20%, or 30% thermal injury," *The Journal of Burn Care and Rehabilitation*, 10(5), 410–417.

Haario, H., Saksman, E., and Tamminen, J., 2001. "An adaptive Metropolis algorithm," *Bernoulli*, 7(2), 223–242.

Hansbrough, J. F., Wikstrom, T., Braide, M., Ph, D., Tenenhaus, M., Rennekampff, O. H., Kiessig, V., and Bjursten, L. M., 1996. "Neutrophil activation and tissue neutrophil

sequestration model of thermal injury in a rat," *Journal of Surgical Research*, 61(1), 17–22.

Hotchkiss, R. S., Tinsley, K. W., Swanson, P. E., Schmieg, R. E., Hui, J. J., Chang, K. C., Osborne, D. F., Freeman, B. D., Cobb, J. P., Buchman, T. G., and Karl, I. E., 2001. "Sepsis-induced apoptosis causes progressive profound depletion of B and CD4+ T lymphocytes in humans," *Journal of Immunology*, 166, 6952–63.

Ishibashi, T., Kimura, H., Shikama, Y., Uchida, T., Kariyone, S., Hirano, T., Kishimoto, T., Takatsuki, F., and Akiyama, Y., 1989. "Interleukin-6 is a potent thrombopoietic factor in vivo in mice," *Blood*, 74(4), 1241–1244.

Johnson, R. C., Mayadas, T. N., Frenette, P. S., Mebius, R. E., Subramaniam, M., Lacasce, A., Hynes, R. O., and Wagner, D. D., 1995. "Blood cell dynamics in P-selectin-deficient mice," *Blood*, 86(3), 1106–14.

Kagan, R. J., Bratescu, A., Jonasson, O., Matsuda, T., and Teodorescu, M., 1989. "The relationship between the percentage of circulating B cells, corticosteroid levels, and other immunologic parameters in thermally injured patients," *The Journal of Trauma*, 29(2), 208–13.

Kalmaz, G. D., and Guest, M. M., 1991. "Burn trauma: role of thrombocytopenia in inhibition of megakaryocytopoiesis," *Annals of the New York Academy of Sciences*, 628, 396–398.

Kaser, A., Brandacher, G., Steurer, W., Kaser, S., Offner, F. A., Zoller, H., Theurl, I., Widder, W., Molnar, C., Ludwiczek, O., Atkins, M. B., Mier, J. W., and Tilg, H., 2001. "Interleukin-6 stimulates thrombopoiesis through thrombopoietin: role in inflammatory thrombocytosis," *Blood*, 98(9), 2720–5.

Kaushansky, K., 2005. "The molecular mechanisms that control thrombopoiesis," *The Journal of Clinical Investigation*, 115(12), 3339–47.

Kiang, J. G., Zhai, M., Liao, P.-J., Bolduc, D. L., Elliott, T. B., and Gorbunov, N. V., 2014. "Pegylated G-CSF inhibits blood cell depletion, increases platelets, blocks splenomegaly, and improves survival after whole-body ionizing irradiation but not after irradiation combined with burn." *Oxidative medicine and cellular longevity*, 2014, 481392.

Knox, T., 2007. *BURNSIM. Version 3.0.2. A model for predicting thermal pain/burn injury. User Guide*. Wright-Patterson Air Force Base, OH.

Kowal-Vern, A., Walenga, J. M., Hoppensteadt, D., Sharp-Pucci, M., and Gamelli, R. L., 1994. "Interleukin-2 and interleukin-6 in relation to burn wound size in the acute phase of thermal injury," *Journal of the American College of Surgeons*, 178(4), 357–362.

Kulkarni, S., Chakraborty, K., Kumar, K. S., Kao, T.-C., Hauer-Jensen, M., and Ghosh, S. P., 2013. "Synergistic radioprotection by gamma-tocotrienol and pentoxifylline: role of cAMP signaling," *ISRN Radiology*, 2013, 1–11.

Kuwaki, T., Hagiwara, T., Yuki, C., Kodama, I., Kato, T., and Miyazaki, H., 1998. "Quantitative analysis of thrombopoietin receptors on human megakaryocytes," *FEBS letters*, 427(1), 46–50.

Laine, M., 2008. *Adaptive MCMC Methods with Applications in Environmental and Geophysical Models*. Finish Meteorological Institute.

Lebedev, M. J., Krizhanova, M. A., Vilkov, S. A., Sholkina, M. N., Vyasmina, E. S., Baryshnikov, A. J., and Novikov, V. V., 2003. "Peripheral blood lymphocytes immunophenotype and serum concentration of soluble HLA class I in burn patients," *Burns*, 29(2), 123–8.

Lupia, E., Bosco, O., Mariano, F., Dondi, A. E., Goffi, A., Spatola, T., Cuccurullo, A., Tizzani, P., Brondino, G., Stella, M., and Montrucchio, G., 2009. "Elevated thrombopoietin in plasma of burned patients without and with sepsis enhances platelet activation," *Journal of Thrombosis and Haemostasis*, 7(6), 1000–1008.

Macallan, D. C., Wallace, D. L., Zhang, Y., Ghattas, H., Asquith, B., Lara, C., Worth, A., Panayiotakopoulos, G., Griffin, G. E., Tough, D. F., and Beverley, P. C. L., 2005. "B-cell kinetics in humans: Rapid turnover of peripheral blood memory cells," *Blood*, 105(9), 3633–3640.

Maldonado, M. D., Venturoli, A., Franco, A., and Nunez-Roldan, A., 1991. "Specific changes in peripheral blood lymphocyte phenotype from burn patients. Probable origin of the thermal injury-related lymphocytopenia," *Burns*, 17(3), 188–92.

Manning, K. L., and McDonald, T. P., 1997. "C3H mice have larger spleens, lower platelet counts, and shorter platelet lifespans than C57BL mice: an animal model for the study of hypersplenism." *Experimental Hematology*, 25(10), 1019–24.

Marck, R. E., Montagne, H. L., Tuinebreijer, W. E., and Breederveld, R. S., 2013. "Time course of thrombocytes in burn patients and its predictive value for outcome," *Burns*, 39(4), 714–22.

McManus, A. T., 1983. "Examination of neutrophil function in a rat model of decreased host resistance following burn trauma," *Reviews of Infectious Diseases*, 5(Supplement 5), S898–S907.

Mirsaeidi, M., Peyrani, P., Aliberti, S., Filardo, G., Bordon, J., Blasi, F., and Ramirez, J. a., 2010. "Thrombocytopenia and thrombocytosis at time of hospitalization predict mortality in patients with community-acquired pneumonia," *CHEST Journal*, 137(2), 416–20.

Moré, J. J., 1978. "The Levenberg-Marquardt algorithm: Implementation and theory," *Numerical Analysis*. Springer Berlin Heidelberg, 105–116.

Mullen, K., Ardia, D., Gil, D., Windover, D., and Cline, J., 2011. "'DEoptim': An R package for global optimization by differential evolution," *Journal of Statistical Software*, 40(6), 1–26.

Neilan, B. A., Taddeini, L., and Strate, R. G., 1977. "T lymphocyte rosette formation after major burns," *JAMA*, 238(6), 493–496.

Nijsten, M. W., Hack, C. E., Helle, M., Ten Duis, H. J., Klasen, J. H., Aarden, L. A., and Klasen, H. J., 1991. "Interleukin-6 and its relation to the humoral immune response and clinical parameters in burned patients," *Surgery*, 109(6), 761–767.

Noel, J. G., Valente, J. F., Ogle, J. D., Cornelius, J., Custer, D. A., Li, B. G., Alexander, J. W., and Ogle, C. K., 2002. "Changes in bone marrow-derived myeloid cells from thermally injured rats reflect changes in the progenitor cell population," *Journal of Burn Care & Rehabilitation*, 23(2), 75–86.

Noel, J. G., Osterburg, A., Wang, Q., Guo, X., Byrum, D., Schwemberger, S., Goetzman, H., Caldwell, C. C., and Ogle, C. K., 2007. "Thermal injury elevates the inflammatory monocyte subpopulation in multiple compartments," *Shock*, 28(6), 684–93.

Palmer, J. L., Deburghgraeve, C. R., Bird, M. D., Hauer-Jensen, M., and Kovacs, E. J., 2011. "Development of a combined radiation and burn injury model," *Journal of Burn Care & Research*, 32(2), 317–23.

Pavić, M., and Milevoj, L., 2007. "Platelet count monitoring in burn patients," *Biochemia Medica*, 17(2), 212–19.

Peterson, V., Hansbrough, J., Buerk, C., Rundus, C., Wallner, S., Smith, H., and Robinson, W. A., 1983. "Regulation of granulopoiesis following severe thermal injury," *The Journal of Trauma*, 23(1), 19–24.

Pillay, J., Braber, I., Vrisekoop, N., Kwast, L. M., Boer, R. J., Borghans, J. A. M., Tesselaar, K., and Koenderman, L., 2010. "In vivo labeling with 2H2O reveals a human neutrophil lifespan of 5.4 days." *Blood*, 116(4), 625–7.

R Core Team, 2013. *R: A Language and Environment for Statistical Computing*. R Foundation for Statistical Computing, Vienna, Austria.

R Core Team, 2015. *R: A Language for Statistical Computing*. Vienna, Austria.

Reid, J. D., Brooks, J. W., Ham, W. T., and Evans, E. I., 1955. "The influence of x-radiation on mortality following thermal flash burns: the site of tissue injury as a factor determining the type of invading bacteria," *Annals of Surgery*, 142(5), 844–50.

Romero-Weaver, A. L., Wan, X. S., Diffenderfer, E. S., Lin, L., and Kennedy, A. R., 2013. "Kinetics of neutrophils in mice exposed to radiation and/or granulocyte colony-stimulating factor treatment." *Radiation Research*, 180(2), 177–88.

Romero-Weaver, A. L., and Kennedy, A. R., 2012. "Comparison of two methods for the determination of the effects of ionizing radiation on blood cell counts in mice," *International Journal of Biomedical Science*, 8(1), 7–15.

Santangelo, S., Gamelli, R. L., and Shankar, R., 2001. "Myeloid commitment shifts toward monocytopoiesis after thermal injury and sepsis," *Annals of Surgery*, 233(1), 97–106.

Satyamitra, M., Ney, P., Graves, J., Mullaney, C., and Srinivasan, V., 2012. "Mechanism of radioprotection by δ-tocotrienol: pharmacokinetics, pharmacodynamics and modulation of signalling pathways," *The British Journal of Radiology*, 85(1019), e1093–e1103.

Satyamitra, M., Lombardini, E., Graves, J., Mullaney, C., Ney, P., Hunter, J., Johnson, K., Tamburini, P., Wang, Y., Springhorn, J. P., and Srinivasan, V., 2011. "A TPO receptor agonist, ALXN4100TPO, mitigates radiation-induced lethality and stimulates hematopoiesis in CD2F1 mice." *Radiation Research*, 175(6), 746–58.

Schluter, B., Konig, B., Bergmann, U., Muller, F. E., and Konig, W., 1991. "Interleukin-6. A potential mediator of lethal sepsis after major thermal trauma: evidence for increased IL-6 production by peripheral blood mononuclear cells," *The Journal of Trauma*, 31(12), 1663–1670.

Shinjo, K., Takeshita, A., Ohnishi, K., and Ohno, R., 1995. "Expression of granulocyte colony-stimulating factor receptor increases with differentiation in myeloid cells by a newly-devised quantitative flow-cytometric assay," *British Journal of Haematology*, 91(4), 783–794.

Shoup, M., Weisenberger, J. M., Wang, J. L., Pyle, J. M., Gamelli, R. L., and Shankar, R., 1998. "Mechanisms of neutropenia involving myeloid maturation arrest in burn sepsis," *Annals of Surgery*, 228(1), 112–122.

Silva, K. D., Gamelli, R. L., and Shankar, R., 2002. "Bone marrow stem cell and progenitor response to injury," *Would Repair and Regeneration*, 9(6), 495–500.

Simon, T. T. L., Curreri, P. W., Seattle, L. A. H., and Harker, L., 1977. "Kinetic characterization of hemostasis in thermal injury," *The Journal of Laboratory and Clinical Medicine*, 89(4), 702–711.

Singh, V. K., Brown, D. S., and Kao, T.-C., 2009. "Tocopherol succinate: a promising radiation countermeasure." *International Immunopharmacology*, 9(12), 1423–30.

Smirnova, O. A., 2010. *Environmental Radiation Effects on Mammals*. Springer New York, New York, NY.

Smith, F., Smith, W. W., Gonshery, L., and Grenan, M. M., 1954. "Effect of immunity on resistance to infection in irradiated mice and rats." *Experimental Biology and Medicine*, 87(1), 23–26.

Soetaert, K., and Petzoldt, T., 2010a. "Inverse modelling, sensitivity and Monte Carlo analysis in R using package FME," *Journal of Statistical Software*, 33(3), 1–28.

Soetaert, K., Petzoldt, T., and Setzer, R. W., 2010b. "Solving differential equations in R: Package deSolve," *Journal of Statistical Software*, 33(9), 1–25.

Summers, C., Rankin, S. M., Condliffe, A. M., Singh, N., Peters, a. M., and Chilvers, E. R., 2010. "Neutrophil kinetics in health and disease," *Trends in Immunology*, 31(8), 318–24.

Tajima, G., Delisle, A. J., Hoang, K., O'Leary, F. M., Ikeda, K., Hanschen, M., Stoecklein, V. M., and Lederer, J. A., 2013. "Immune system phenotyping of radiation and radiation combined injury in outbred mice," *Radiation Research*, 179(1), 101–12.

Tan, W., Huang, W., Zhong, Q., and Schwarzenberger, P., 2006. "IL-17 receptor knockout mice have enhanced myelotoxicity and impaired hemopoietic recovery following gamma irradiation," *The Journal of Immunology*, 176(10), 6186–6193.

Teodorczyk-Injeyan, J. A., Cembrzynska-Nowak, M., Lalani, S., Peters, W. J., and Mills, G. B., 1995. "Immune deficiency following thermal trauma is associated with apoptotic cell death," *Journal of Clinical Immunology*, 15(6), 318–28.

Uchida, T., and Yamagiwa, A., 1992. "Kinetics of rG-CSF-induced neutrophilia in mice." *Experimental Hematology*, 20(2), 152–155.

Valentin, J., 2002. "Basic anatomical and physiological data for use in radiological protection: reference values. ICRP Publication 89," *Annals of ICRP*, 32(3-4), 1–277.

Van Furth, R., and Sluiter, W., 1986. "Distribution of blood monocytes between a marginating and a circulating pool," *The Journal of Experimental Medicine*, 163(2), 474–9.

Van Hinsbergh, V. W. M., 2012. "Endothelium–role in regulation of coagulation and inflammation," *Seminars in Immunopathology*, 34(1), 93–106.

Vindenes, H., Ulvestad, E., and Bjerknes, R., 1995. "Increased levels of circulating Interleukin-8 in patients with large burns," *The Journal of Trauma*, 39(4), 635–40.

Volenec, F. J., Wood, G. W., Mani, M. M., Robinson, D. W., and Humphrey, L. J., 1979. "Mononuclear cell analysis of peripheral blood from burn patients," *The Journal of Trauma*, 19(2), 86–93.

Wallner, S., Vautrin, R., Murphy, J., Anderson, S., Peterson, V., and Walker, S., 1984. "The haematopoietic response to burning: studies in an animal model," *Burns*, 10(4), 236–251.

Wentz, J., Oldson, D., and Stricklin, D., 2014a. *Mathematical Models of Human Hematopoiesis Following Acute Radiation Exposure*. DTRA-TR-14-31, Defense Threat Reduction Agency, Fort Belvoir, VA.

Wentz, J., Oldson, D., and Stricklin, D., 2014b. "Modeling the thrombopoietic effects of burn," *Letters in Biomathematics*, 1(1).

Wentz, J., 2014a. *Modeling Effects of Burn on Thrombopoiesis*. ARA/HS-TN-14-006-B, Applied Research Associates, Inc., Arlington VA.

Wentz, J., 2014b. *Modeling the Effects of Burn on Granulopoiesis*. ARA/HS-TN-14-009-A, Applied Research Associates, Inc., Arlington VA.
Wickrema, A., and Kee, B., eds. 2009. *Molecular Basis of Hematopoiesis*. Springer.

Appendix A Equations for Hematopoietic Models

A.1 Equations for Thrombopoiesis Model

Below is the complete list of equations for the human model of thrombopoiesis.

Cell concentrations after acute radiation exposure (dose D) at time $t = 0$:

$$x_1^{ud} = \bar{x}_1^{ud}\left(1 - (1 - e^{-D/D_1^0})^{n_1}\right) \tag{20}$$

$$x_{2I,i}^{ud} = \frac{\bar{x}_2^{ud}}{n}\left(1 - (1 - e^{-D/D_2^0})^{n_2}\right) \quad (i = 1, 2, ..., n/2) \tag{21}$$

$$x_{2M,i}^{ud} = \frac{\bar{x}_2^{ud}}{n}\left(1 - (1 - e^{-D/D_2^0})^{n_2}\right) \quad (i = 1, 2, ..., n/2) \tag{22}$$

$$x_{3,i} = \frac{\bar{x}_3}{m} \quad (i = 1, 2, ..., m) \tag{23}$$

$$x_1^d = \bar{x}_1^{ud}\left(1 - e^{-D/D_1^0}\right)^{n_1} \tag{24}$$

$$x_2^d = \bar{x}_2^{ud}\left(1 - e^{-D/D_2^0}\right)^{n_2} \tag{25}$$

Change in cell concentrations with time:

$$\dot{x}_1^{ud} = Bx_1^{ud} - \gamma x_1^{ud} \tag{26}$$

$$\dot{x}_{2I,1}^{ud} = \gamma x_1^{ud} - n\delta x_{2I,1}^{ud} \tag{27}$$

$$\dot{x}_{2I,i}^{ud} = n\delta x_{2I,i-1}^{ud} - n\delta x_{2I,i}^{ud} \quad (i = 2, 3, ..., n/2) \tag{28}$$

$$\dot{x}_{2M,1}^{ud} = n\delta x_{2I,n/2}^{ud} - n\delta_0 x_{2M,1}^{ud} \tag{29}$$

$$\dot{x}_{2M,i}^{ud} = n\delta_0 x_{2M,i-1}^{ud} - n\delta_0 x_{2M,i}^{ud} \quad (i = 2, 3, ..., n/2) \tag{30}$$

$$\dot{x}_{3,1} = \sigma n\delta_0 x_{2M,n/2}^{ud} - m\psi x_{3,1} \tag{31}$$

$$\dot{x}_{3,i} = m\psi x_{3,i-1} - m\psi x_{3,i} \quad (i = 2, 3, ..., m) \tag{32}$$

$$\dot{x}_i^d = -\mu x_i^d \quad (i = 1, 2) \tag{33}$$

where

$$B = \frac{\alpha}{1 + \beta\left(x_1^{ud} + x_1^d + \theta_2(x_2^{ud} + x_2^d) + \theta_3 x_3\right)/(1 + b_0 S^{c_0} e^{-a_0 t})} \tag{34}$$

$$x_2^{ud} = \sum_{i=1}^{n/2} x_{2I,i}^{ud} + x_{2M,i}^{ud} \tag{35}$$

$$x_3 = \sum_{i=1}^{m} x_{3,i} \tag{36}$$

$$\delta = \frac{1}{2} Z(2\delta_0, \frac{\delta_{min}}{1 - \frac{\delta_{min}}{2\delta_0}}, \frac{\delta_{max}}{1 - \frac{\delta_{max}}{2\delta_0}})(1 + b_f S^{c_f} e^{-a_f t}) \tag{37}$$

$$\psi = \psi_0(1 + \frac{S}{d_0 + d_1 t}) \tag{38}$$

$$Z(x, x_{min}, x_{max}) = x_{min} + (x_{max} - x_{min})^{1-\left(\frac{x_3}{\bar{x}_3}\right)^\lambda}(x - x_{min})^{\left(\frac{x_3}{\bar{x}_3}\right)^\lambda} \tag{39}$$

A.2 Equations for Granulopoiesis Model

Below is the complete list of equations for the human model of granulopoiesis.

Cell concentrations after acute radiation exposure (dose D) at time $t = 0$:

$$x_i^{ud} = \bar{x}_i^{ud}\left(1 - (1 - e^{-D/D_i^0})^{n_i}\right) \quad (i = 1, 2, 3, 4) \tag{40}$$

$$x_1^{wd} = \bar{x}_1^{ud}\frac{\vartheta}{1 + \vartheta}\left(1 - e^{-D/D_1^0}\right)^{n_1} \tag{41}$$

$$x_i^{wd} = 0 \quad (i = 2, 3, 4) \tag{42}$$

$$x_1^{d} = \bar{x}_1^{ud}\frac{1}{1 + \vartheta}\left(1 - e^{-D/D_1^0}\right)^{n_1} \tag{43}$$

$$x_i^{d} = \bar{x}_i^{ud}\left(1 - e^{-D/D_i^0}\right)^{n_i} \quad (i = 2, 3, 4) \tag{44}$$

where

$$\vartheta = \frac{(1 - e^{-D/D_1^0})^{n_1} - (1 - e^{-D/D_1^{000}})^{n_1}}{(1 - e^{-D/D_1^{000}})^{n_1}}$$

Change in cell concentrations with time:

$$\dot{x}_1^{ud} = Bx_1^{ud} - \gamma x_1^{ud} \tag{45}$$

$$\dot{x}_2^{ud} = \gamma x_1^{ud} - \delta x_2^{ud} \tag{46}$$

$$\dot{x}_3^{ud} = \delta x_2^{ud} - \kappa x_3^{ud} \tag{47}$$

$$\dot{x}_4^{ud} = \kappa x_3^{ud} - \psi x_4^{ud} \tag{48}$$

$$\dot{x}_1^{wd} = \begin{cases} Bx_1^{wd} - \gamma x_1^{wd} & 0 \le t < \Delta t_{ae} \\ -\eta x_1^{wd} & t \ge \Delta t_{ae} \end{cases} \tag{49}$$

$$\dot{x}_2^{wd} = \begin{cases} \gamma x_1^{wd} - \delta x_2^{wd} & 0 \le t < \Delta t_{ae} \\ -\eta x_2^{wd} & t \ge \Delta t_{ae} \end{cases} \tag{50}$$

$$\dot{x}_3^{wd} = \begin{cases} \delta x_2^{wd} - \kappa x_3^{wd} & 0 \le t < \Delta t_{ae} \\ -\eta x_3^{wd} & t \ge \Delta t_{ae} \end{cases} \tag{51}$$

$$\dot{x}_4^{wd} = \begin{cases} \kappa x_3^{wd} - \psi x_4^{wd} & 0 \le t < \Delta t_{ae} \\ -\eta x_4^{wd} & t \ge \Delta t_{ae} \end{cases} \tag{52}$$

$$\dot{x}_i^d = -\mu x_i^d \quad (i = 1, 2, 3, 4) \tag{53}$$

where

$$B = \frac{\alpha}{1 + \beta(x_1^{ud} + x_1^{wd} + x_1^d + \sum_{i=2}^4 \theta_i(x_i^{ud} + x_i^{wd} + x_i^d))} + f_{TBSA}(S) b_0 e^{-a_0 t} \tag{54}$$

$$\delta = \delta_0 \frac{1 + M(x_3^{ud} + x_3^{wd} + x_3^d)^2}{1 + L(x_3^{ud} + x_3^{wd} + x_3^d)^2} \left(1 + f_{TBSA}(S) b_2 e^{-a_2 t}\right) \tag{55}$$

$$\kappa = \kappa_0 \left(1 + f_{TBSA}(S) b_3 e^{-a_3 t}\right) \tag{56}$$

$$\Delta t_{ae} = \tau - vD \tag{57}$$

$$f_{TBSA}(S) = \frac{(A+1)S^k}{A + S^k} \tag{58}$$

S is the fraction of skin surface area affected by burn ($0 \leq S \leq 1$), and

$$x_{3,c}^{ud} = x_3^{ud} \bar{r} \left(1 + f_{TBSA}(S) b_r e^{-a_r t}\right) \tag{59}$$

$$x_{3,c}^{wd} = x_3^{wd} \bar{r} \left(1 + f_{TBSA}(S) b_r e^{-a_r t}\right) \tag{60}$$

$$x_{3,c}^{d} = x_3^{d} \bar{r} \left(1 + f_{TBSA}(S) b_r e^{-a_r t}\right) \tag{61}$$

A.3 Equations for Lymphopoiesis Model

Below is the complete list of equations for the human model of lymphopoiesis.

Cell concentrations after acute radiation exposure (dose D) at time $t = 0$:

$$x_i^{ud} = \bar{x}_i^{ud} \left(1 - (1 - e^{-D/D_i^0})^{n_i}\right) \quad (i = 1, 2, 3) \tag{62}$$

$$x_i^{d} = \bar{x}_i^{ud} \left(1 - e^{-D/D_i^0}\right)^{n_i} \quad (i = 1, 2, 3) \tag{63}$$

Change in cell concentrations with time:

$$\dot{x}_1^{ud} = B x_1^{ud} - \gamma x_1^{ud} \tag{64}$$

$$\dot{x}_2^{ud} = \gamma x_1^{ud} - \delta x_2^{ud} \tag{65}$$

$$\dot{x}_3^{ud} = \delta x_2^{ud} - \psi x_3^{ud} \tag{66}$$

$$\dot{x}_i^{d} = -\mu x_i^{d} \quad (i = 1, 2, 3) \tag{67}$$

where

$$B = \frac{\alpha}{1 + \beta(x_1 + x_1^d + \theta_2(x_2 + x_2^d) + \theta_3(x_3 + x_3^d))} \tag{68}$$

$$\psi = \psi_0 (1 + b_3 S^{c_3} e^{-a_3 t}) \tag{69}$$

and S is the fraction of skin surface area affected by burn ($0 \leq S \leq 1$).

Appendix B Murine Thrombopoiesis and Granulopoiesis Models

In this section the development of the murine thrombopoiesis and granulopoiesis models is discussed. The equations for the models are the same as those given in Appendix A. However, the parameter values in the models were changed using data from rodent studies.

B.1 Methods

Parameter values were optimized using differential evolution optimization with the DEoptim library in R (R Core Team 2015; Mullen et al. 2011; Ardia et al. 2015). To run the optimization, an upper and lower bound for each parameter to be optimized were specified along with a cost value. For our purposes, we set this cost value equal to the sum of the squared residuals. The optimization was run using normalized versions of the data (i.e., data points were divided by a constant baseline value). For doses given in roentgen, a 0.0096 Gy per roentgen conversion factor was used. The optimized parameters and the bounds imposed are given in Table B.1 and B.2 for the thrombopoiesis and granulopoiesis models, respectively. The models were first optimized to murine radiation data. Next, burn-dependent parameters were determined by optimizing the models to murine burn data.

Table B.1: Parameter bounds used during the murine thrombopoiesis model optimizations.

Parameter	Lower Bound	Upper Bound
γ (d^{-1})	0.5	1.9
θ_2	0.001	1
λ	0	6
D_1^0 (Gy)	0.5	3
D_2^0 (Gy)	0	30
b_0	0	20
a_0 (d^{-1})	0.001	10
c_0	0.1	20
b_f	0	20
a_f (d^{-1})	0	10
c_f	0.1	20

Table B.2: Parameter bounds used during the murine granulopoiesis model optimizations.

Parameter	Lower Bound	Upper Bound
η (d^{-1})	0	2
ψ (d^{-1})	0	15
m	0	1000
D_1^0 (Gy)	0	0.899
D_1^{000} (Gy)	0.9	10
D_2^0 (Gy)	0	15
b_0	0	10
a_0 (d^{-1})	0.0001	0.1
b_2	5	100
a_2 (d^{-1})	0.05	10
b_3	0	20
a_3 (d^{-1})	0	10
A	0	1000
k	0	10

B.2 Thrombopoiesis Murine Model Results

Table B.3 provides the finalized parameter values for the murine thrombopoiesis model. Of the optimized parameter values, θ_2 approached the lower bound of 0.001, λ approached the upper bound of 6.0, and b_f approached the upper bound of 20. No other optimized parameters approached the bounds specified. Sources for parameters that were not optimized are given in Table B.3. The derivations of many of these parameter values are described elsewhere (Wentz 2014a; Wentz et al. 2014a), while the derivations of δ_0 and ψ for the murine thrombopoiesis model are given below.

There are three stages of megakaryocyte maturation: megakaryoblast, promegakaryocyte, and granular megakaryocyte. The maturation time through all three compartments in mice is approximately 68 h (Ebbe 1971). However, rodent platelet counts following radiation exposure at low doses typically do not decline until 4 days post irradiation (Ebbe et al. 1970). This suggests that there is a fourth sub-compartment in the post-mitotic compartment which represents non-mitotic megakaryocyte progenitors. Using 4 days as the maturation time leads to a normal maturation rate, δ_0, of 0.25 d^{-1}.

Platelet lifespans vary between mice strain; one experiment noted the platelets in C3H mice have a shorter lifespan (4.8 d) than platelets in C57BL mice (5.7 d) (Manning et al. 1997). Other experiments reported platelet lifespans between 3.1 and 3.3 d (Baker et al. 1997). In the model here, the expected platelet lifespan is 4 d, a generally accepted value (Wickrema et al. 2009). Thus, ψ is 1/4 or 0.25 d^{-1}.

Table B.3: Biological parameter values for murine thrombopoiesis model.

Parameter	Description	Value	Section (References)
α	Maximum rate of mitotic progenitor cell repopulation	2.0 d^{-1}	Andreeff et al. 2000*
γ	Rate of mitotic progenitor cell maturation	1.60 d^{-1}	Optimized
δ_0	Rate of MK maturation	0.25 d^{-1}	Ebbe 1971
ψ	Rate of platelet decay	0.25 d^{-1}	Wickrema et al. 2009
n	Number of MK subcompartments	10	Same as human model*
m	Number of platelet subcompartments	9	Same as human model*
θ_2	Decay rate of mediator due to x_2 cells relative to decay rate due to x_1 cells	0.001	Optimized
θ_3	Decay rate of mediator due to x_3 cells relative by decay rate due to x_1 cells	0.03 θ_2	Kuwaki et al. 1998; Broudy et al. 1997*
δ_{min}	Minimum rate of MK maturation	$(4/3)\delta$	Same as human model*
δ_{max}	Maximum rate of MK maturation	4δ	Same as human model*
λ	Strength of x_3 feedback on immature MK maturation	6.0	Optimized
σ	Number of platelets per MK	3000	Smirnova 2010; Deutsch et al. 2013
D_1^0	Determines fraction of x_1 targets that are hit by radiation at dose D	1.37 Gy	Optimized
n_1	Number of targets per x_1 cell	1	Same as human model*
D_2^0	Determines fraction of x_2 targets that are hit by radiation at dose D	4.65 Gy	Optimized
n_2	Number of targets per x_2 cell	4	Same as human model*
μ	Rate of moderately damaged cell death	1.0 d^{-1}	Smirnova 2010*
b_0	Determines max burn effect on repopulation rate	5.13	Optimized
a_0	Determines duration of burn effect on repopulation rate	0.043 d^{-1}	Optimized
c_0	Determines how run size affects repopulation rate change	1.3	Optimized
b_f	Determines max burn effect on MK maturation	20	Optimized
a_f	Determines duration of burn effect on MK maturation	0.00017	Optimized
c_f	Determines how burn size affects MK maturation rate change	1.6	Optimized
d_0	Determines max effect of burn on platelet decay	0.476	Wentz 2014a
d_1	Determines duration of effect of burn on platelet decay	0.143 d^{-1}	Wentz 2014a

*See Wentz et al. 2014a for description of how parameter value was derived.

Radiation Optimization Results

Figure B.1 shows comparisons of the murine thrombopoiesis model with data used for optimization of the baseline and radiation portion of the model.

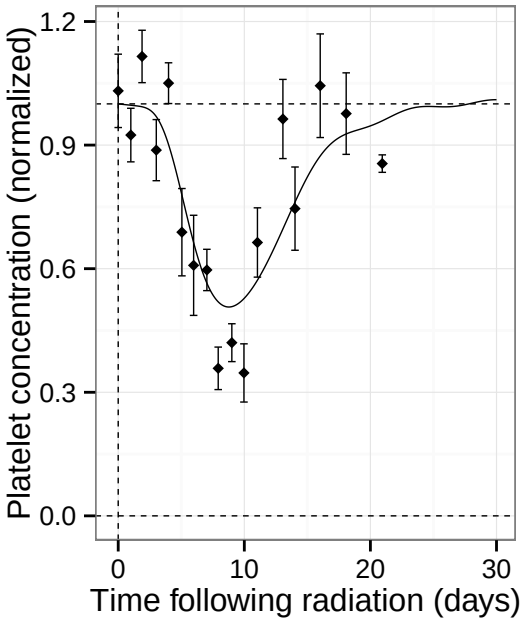

(a) 1.92 Gy (Ebbe et al. 1970)

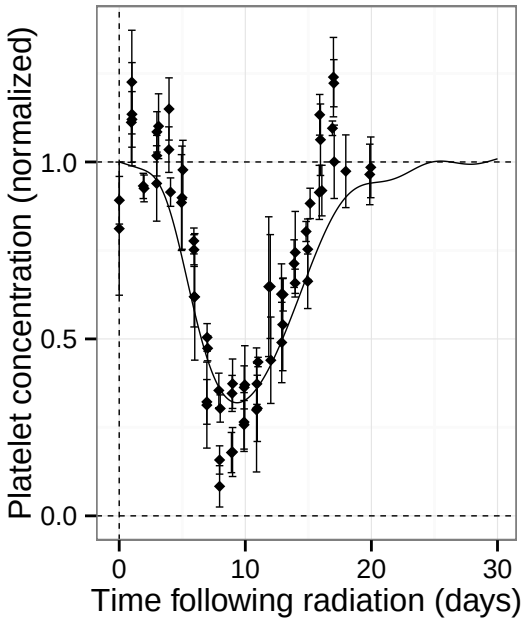

(b) 2.88 Gy (Ebbe et al. 1970)

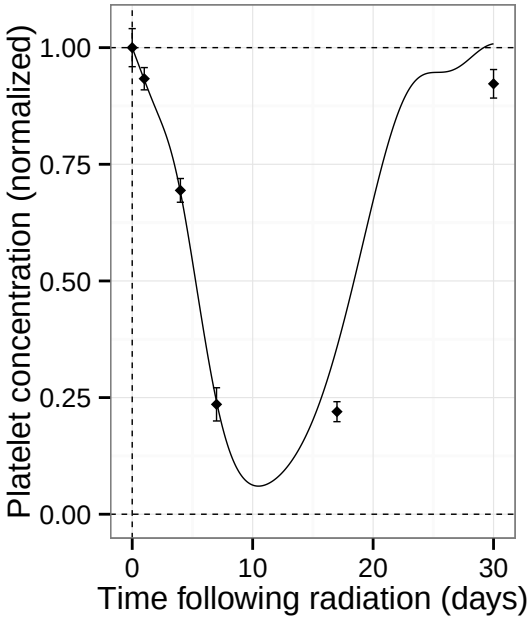

(c) 6 Gy (Ghosh et al. 2012)

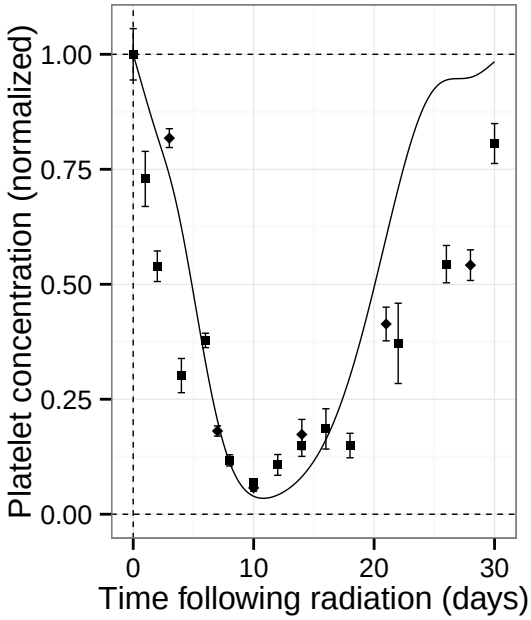

(d) 7 Gy (Satyamitra et al. 2012; Neumedicines, Inc.)

Figure B.1: Murine thrombopoiesis model compared with radiation optimization data (mean ± standard error).

Radiation Validation Results

Figure B.2 show comparisons of the murine thrombopoiesis model with validation data.

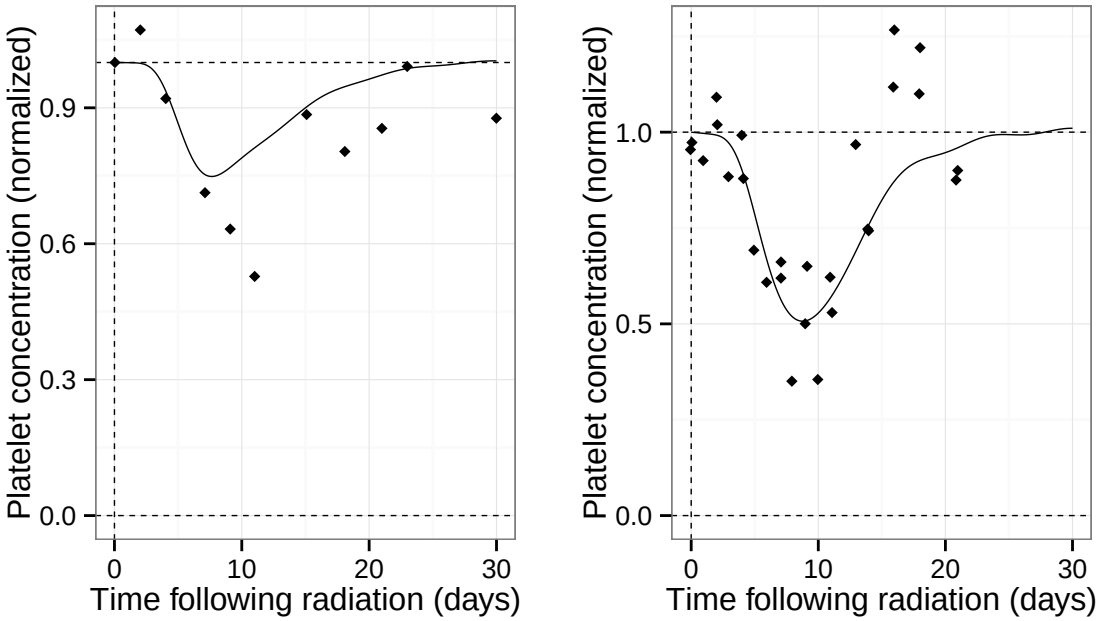

(a) 0.96 Gy (Cohn et al. 1956)

(b) 1.92 Gy (Ebbe et al. 1970)

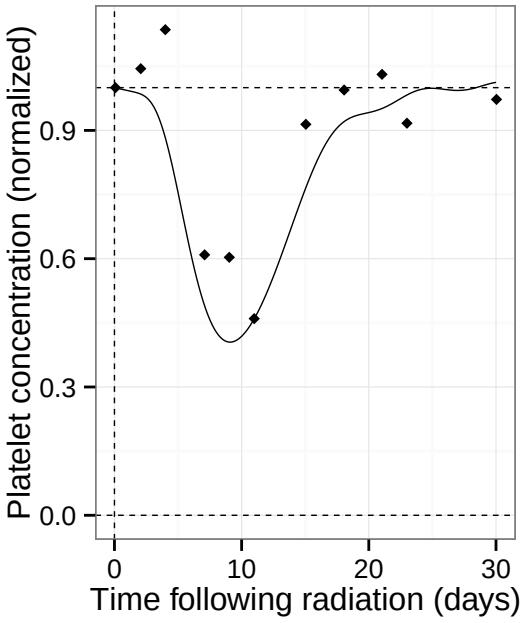

(c) 2.4 Gy (Cohn et al. 1956)

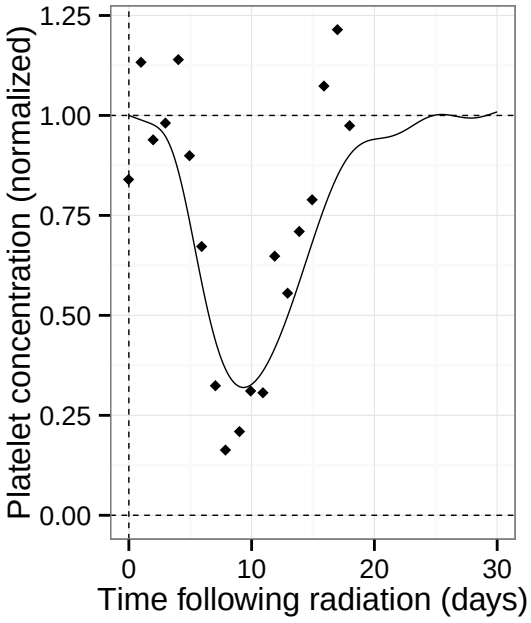

(d) 2.88 Gy (Ebbe et al. 1970)

Figure B.2: (1 of 4) Murine thrombopoiesis model compared with validation data (mean).

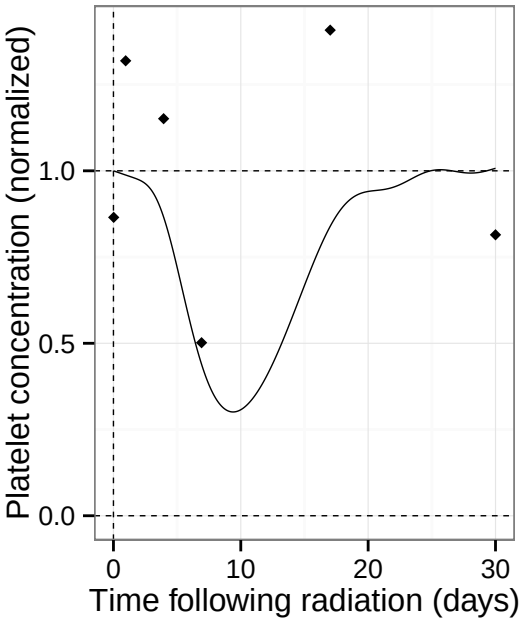

(e) 3 Gy (Singh et al. 2009)

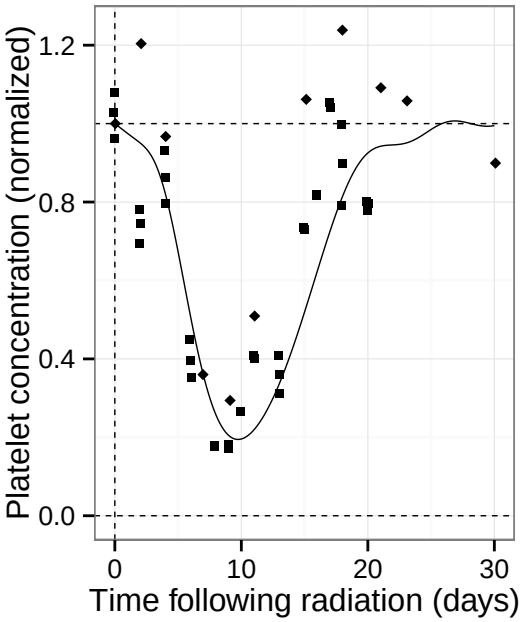

(f) 3.84 Gy (Cohn et al. 1956; Ebbe et al. 1970)

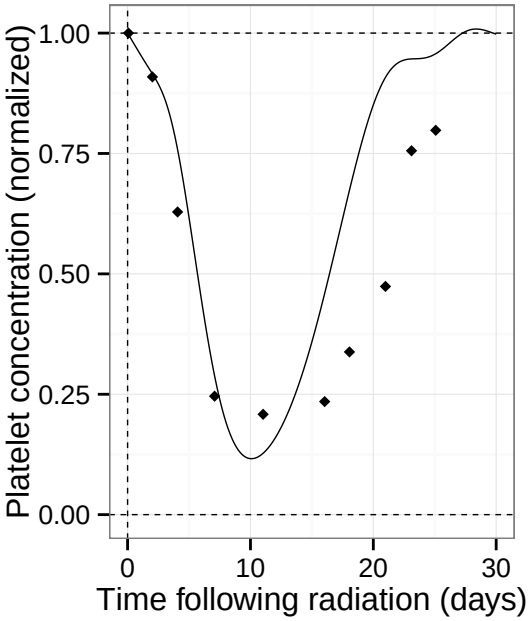

(g) 4.8 Gy (Cohn et al. 1956)

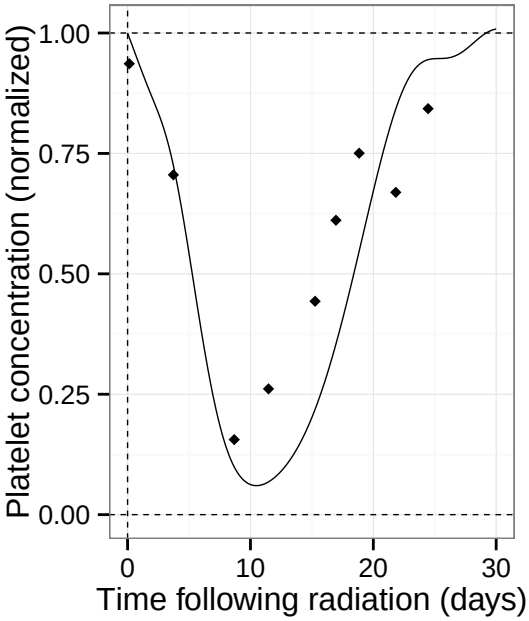

(h) 6 Gy (Faltynek et al. 1992)

Figure B.2: (2 of 4) Murine thrombopoiesis model compared with validation data (mean).

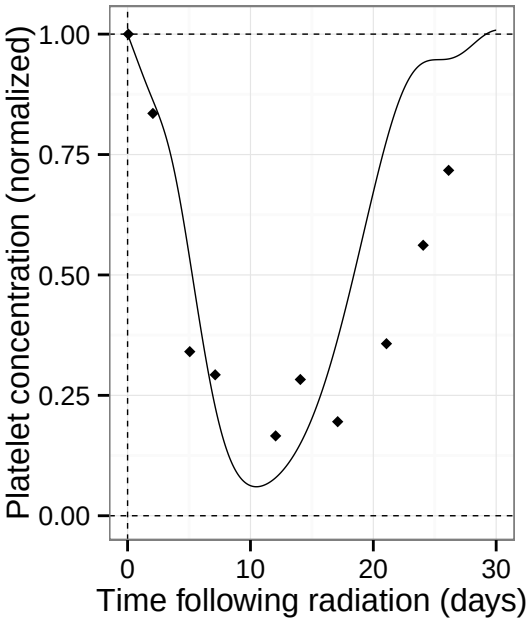

(i) 6 Gy (Cohn et al. 1956)

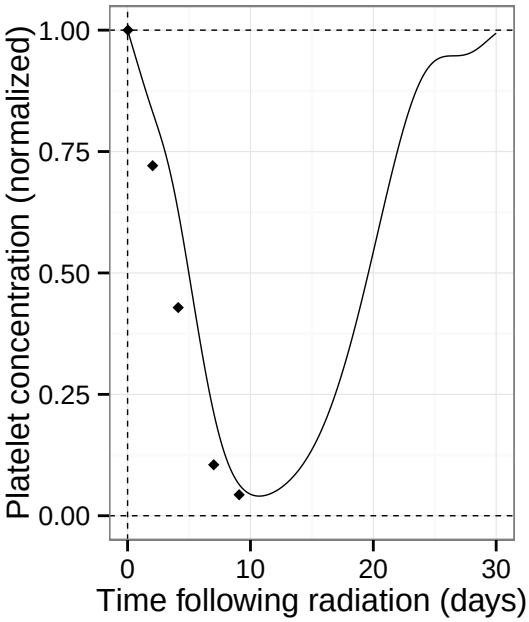

(j) 6.72 Gy (Cohn et al. 1956)

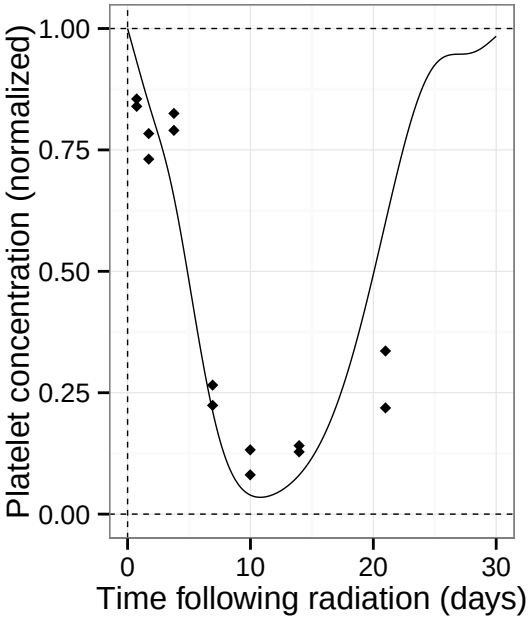

(k) 7 Gy (Satyamitra et al. 2011; Singh et al. 2009)

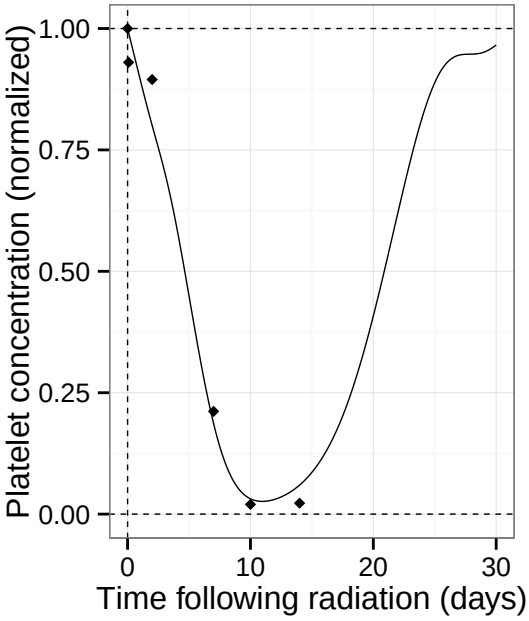

(l) 7.5 Gy (Davis et al. 2010)

Figure B.2: (3 of 4) Murine thrombopoiesis model compared with validation data (mean).

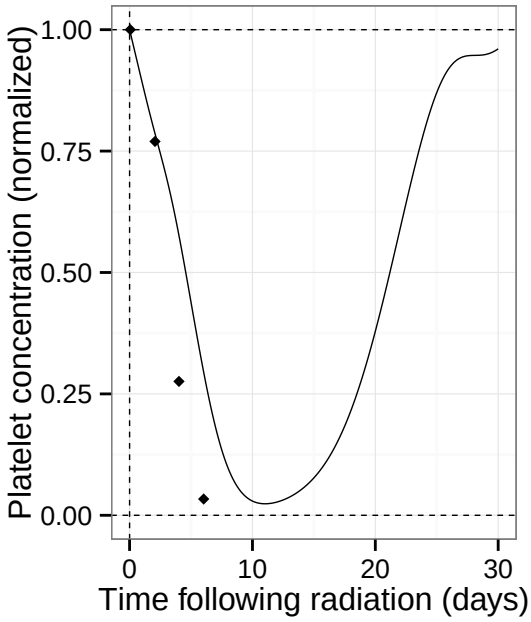

(m) 7.68 Gy (Cohn et al. 1956)

Figure B.2: (4 of 4) Murine thrombopoiesis model compared with validation data (mean).

Burn Optimization Results

Figure B.3 shows comparisons of the thrombopoiesis model with data used to optimize the burn-dependent parameters in the model.

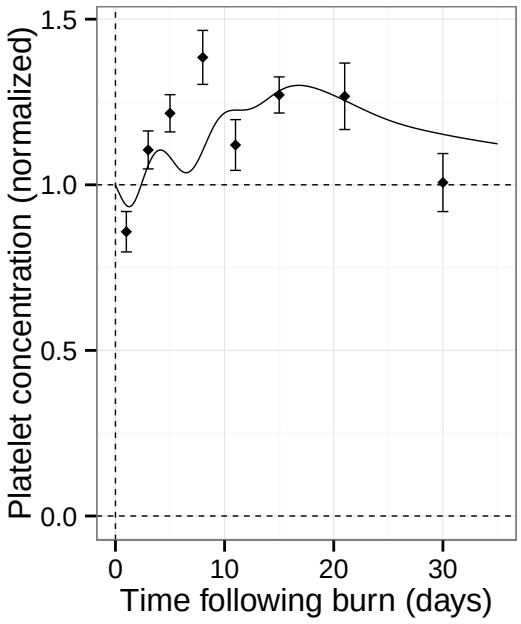

(a) 15% TBSA (Davis et al. 1955)

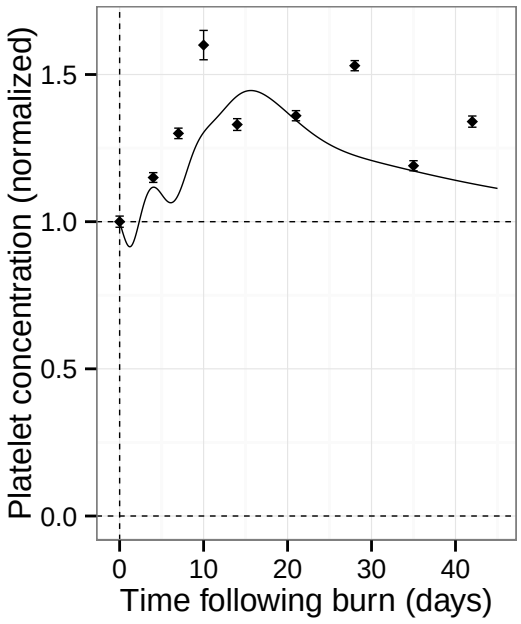

(b) 20% TBSA (Wallner et al. 1984)

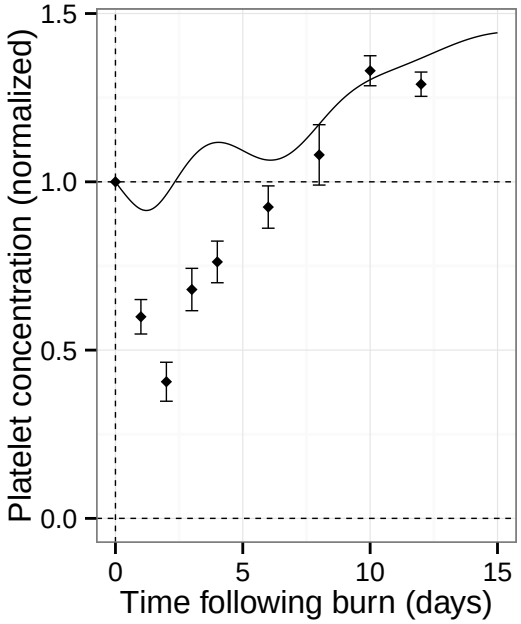

(c) 20% TBSA (Kalmaz et al. 1991)

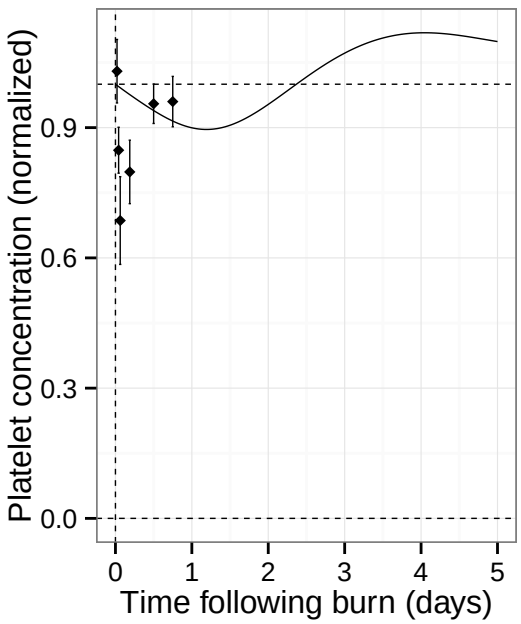

(d) 25% TBSA (Fujimi et al. 2006)

Figure B.3: (1 of 2) Murine thrombopoiesis model compared with burn optimization data (mean ± standard error).

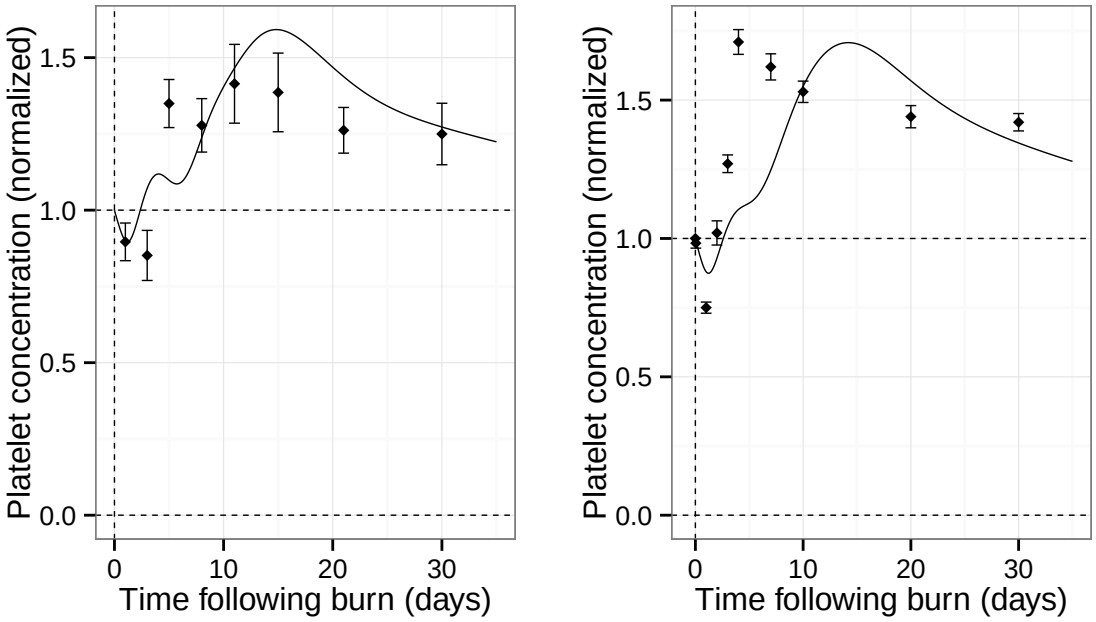

(e) 25% TBSA (Davis et al. 1955) (f) 30% TBSA (Eurenius et al. 1972)

Figure B.3: (2 of 2) Murine thrombopoiesis model compared with burn optimization data (mean ± standard error).

B.3 Granulopoiesis Murine Model Results

Table B.4 provides the finalized parameter values for the murine granulopoiesis model. Of the optimized parameter values, ψ approached the upper bound of 15 d^{-1}, a_0 approached the lower bound of 0.0001 d^{-1}, and a_2 approached the lower bound of 0.05 d^{-1}. All other parameter values were optimized to a value within the bounds specified. Sources for parameter values that were not optimized are given in Table B.4. The derivations of many of these parameter values are described elsewhere (Wentz 2014b; Wentz et al. 2014a), while the derivations of γ, κ, δ, l, τ, and v for the murine granulopoiesis model are model are given below.

Compartment transition rates were estimated using experimental data in mice. The values for γ and κ were taken directly from the literature (Pillay et al. 2010). The transit time through the mitotic compartment was 0.7 d, while the circulating lifespan of the neutrophils was 0.75 d. This leads to rates of 1.43 d^{-1} and 1.33 d^{-1} for γ and κ, respectively. The transit time through the post-mitotic compartment was measured as 1.6 d (Pillay et al. 2010). In the model, this rate is determined by δ, m, and l where the rate of transition F is

$$F = \delta \frac{1 + m x_3^2/\bar{x}_3^2}{1 + l x_3^2/\bar{x}_3^2} \tag{70}$$

Where δ is the maximum rate of transition, and $\delta m/l$ is the minimum. Assuming the data was obtained at equilibrium ($x_3 = \bar{x}_3$) and F_e is the transition rate at equilibrium:

$$F_e = \delta \frac{1 + m}{1 + l} \tag{71}$$

Since the post-mitotic transition time was measured as 1.6 d, $F_e = 0.625$ d^{-1} and

$$\delta = 0.625 \frac{1 + l}{1 + m} \tag{72}$$

A study in mice examined how injected G-CSF altered the post-mitotic transition time. The transition time was found to be reduced by 55% (Uchida et al. 1992). Assuming this represents the minimum transition time or maximum rate (δ), we can derive a relationship between m and l:

$$\frac{1}{\delta} = 0.45 \frac{1}{F_e} \tag{73}$$

$$\rightarrow \delta = \frac{1}{.45} F_e = 2.22\delta \frac{1 + m}{1 + l} \tag{74}$$

$$\rightarrow 1 + l = 2.22(1 + m) \tag{75}$$

$$\rightarrow l = 1.22 + 2.22m \tag{76}$$

The time of abortive elevation Δt_{ae} is determined using the following equation:

$$\Delta t_{ae} = \tau - vD \tag{77}$$

where D is the radiation dose. τ and v were determined through examination of the time of abortive rise in experimental data. At D=2 Gy, the abortive rise occurred approximately on day 10 ($\Delta t_{ae} = 10$) (Romero-Weaver et al. 2012; Romero-Weaver et al. 2013). At D=7 Gy, the abortive rise occurred approximately on day 7 (Neumedicines, Inc.). Using these two time points, values of 11.2 for τ and 0.6 for v were determined.

Table B.4: Biological parameter values for murine granulopoiesis model.

Parameter	Description	Value	Source/Reference
α	Maximum rate of mitotic progenitor cell repopulation	2.0 d^{-1}	Andreeff et al. 2000*
γ	Rate of mitotic progenitor cell maturation	1.43 d^{-1}	Pillay et al. 2010
δ	Determines post-mitotic maturation rate	0.63 $\frac{1+l}{1+m}$ d^{-1}	Pillay et al. 2010
m	Determines post-mitotic maturation rate	11.54	Optimized
l	Determines post-mitotic maturation rate	$1.22 + 2.22m$	Uchida et al. 1992
κ	Rate of transition from blood to tissue	1.33 d^{-1}	Pillay et al. 2010
ψ	Rate of granulocyte decay from tissue	15.0 d^{-1}	Optimized
η	Rate of weakly damaged cell death (when $t > \Delta t_{ae}$)	0.28 d^{-1}	Optimized
θ_2	Decay rate of mediator due to x_2 cells relative to decay rate due to x_1 cells	2.24	Shinjo et al. 1995*
θ_3	Decay rate of mediator due to x_3 cells relative to decay rate due to x_1 cells	8.45	Shinjo et al. 1995*
θ_4	Decay rate of mediator due to x_4 cells relative to decay rate due to x_1 cells	θ_3	Assumed
D_1^0	Determines fraction of damaged x_1 cells	0.67 Gy	Optimized
D_1^{000}	Determines ratio of weakly damaged to damaged x_1 cells	1.14 Gy	Optimized
D_2^0	Determines fraction of damaged x_2 cells	8.12 Gy	Optimized
D_3^0	Determines fraction of damaged x_3 cells	D_2^0	Assumed
D_4^0	Determines fraction of damaged x_4 cells	D_2^0	Assumed
τ	Determines time of abortive rise: $\Delta t_{ae} = \tau - vD$	11.2 d	See text
v	Determines time of abortive rise: $\Delta t_{ae} = \tau - vD$	0.6 d Gy^{-1}	See text
n_i	Number of targets per cell x_i $(i = 1, 2, 3, 4)$	1	Assumed
μ	Rate of damaged cell death	1.0 d^{-1}	Smirnova 2010*
b_0	Determines max burn effect on repopulation rate	0.381	Optimized
a_0	Determines duration of burn effect on repopulation rate	0.0001 d^{-1}	Optimized
b_2	Max relative burn effect on bone marrow release	6.373	Optimized
a_2	Determines duration of burn effect on bone marrow release	0.050 d^{-1}	Optimized
b_3	Max relative burn effect on transition to tissue	0.055	Optimized
a_3	Determines duration of burn effect on transition to tissue	0.036 d^{-1}	Optimized
b_r	Determines max burn effect on marginated ratio	3	Wentz 2014b
a_r	Determines duration of burn effect on marginated ratio	0.106 d^{-1}	Wentz 2014b
A	Determines how changing burn size affects the system	962	Optimized
k	Determines how changing burn size affects the system	0.336	Optimized

*See Wentz et al. 2014a for description of how parameter value was derived from source.

Radiation Optimization Results

Figure B.4 shows comparisons of the murine granulopoiesis model with data used for optimization of the baseline and radiation portion of the model.

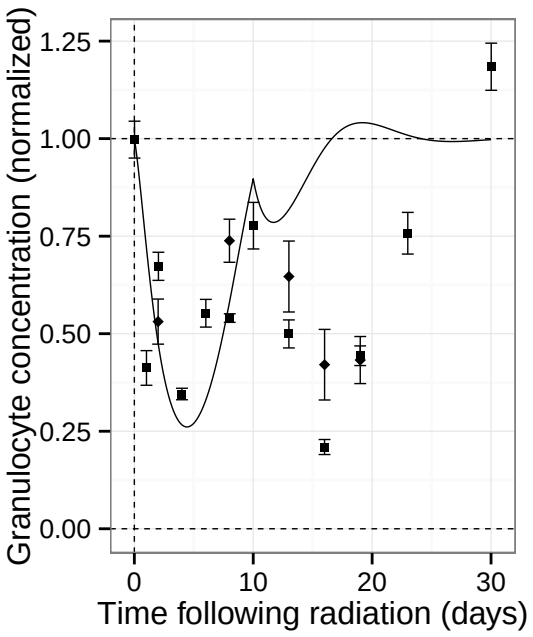

(a) 2 Gy (Diamonds: Romero-Weaver et al. 2012; Squares: Romero-Weaver et al. 2013)

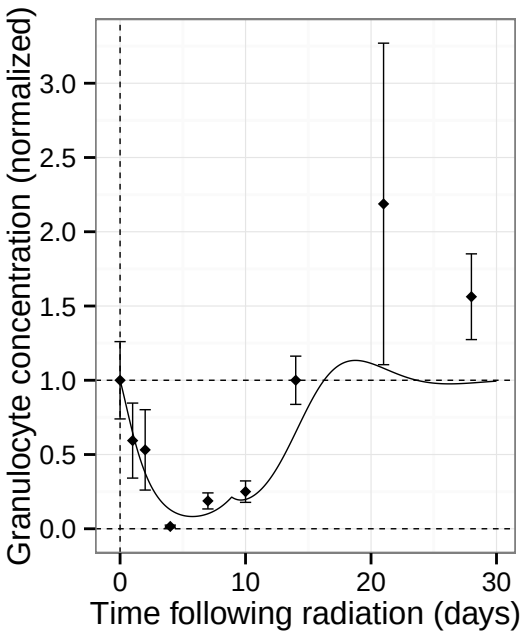

(b) 3.84 Gy (Brecher et al. 1948)

Figure B.4: (1 of 2) Murine granulopoiesis model compared with radiation optimization data (mean ± standard error).

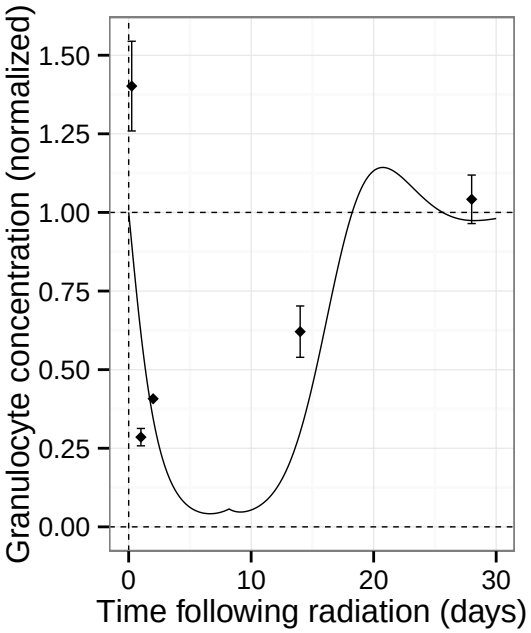

(c) 5 Gy (Palmer et al. 2011)

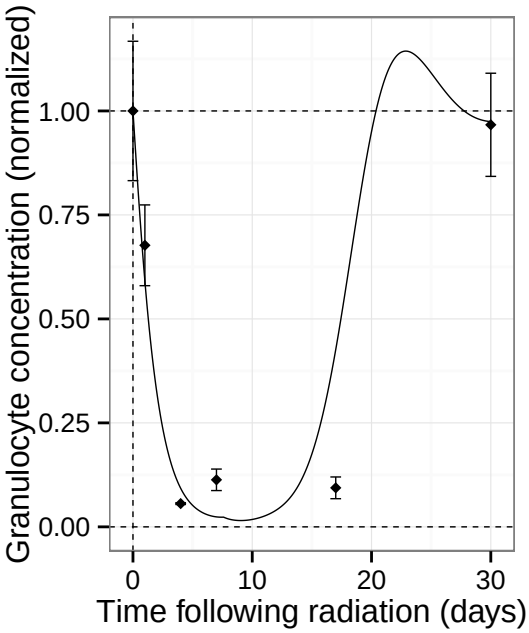

(d) 6 Gy (Ghosh et al. 2012)

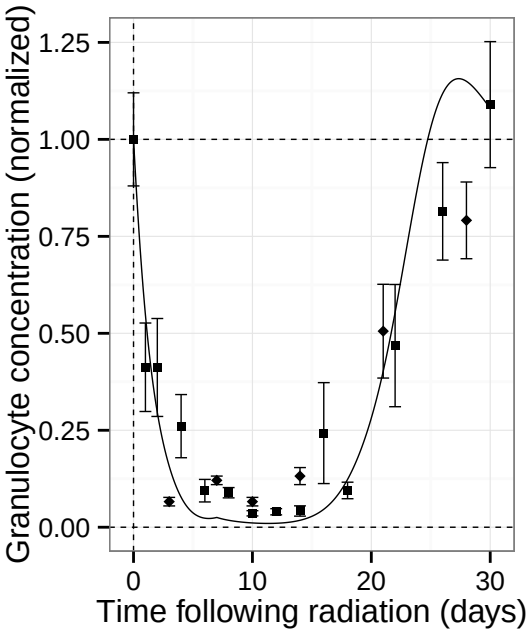

(e) 7 Gy (Diamonds: Satyamitra et al. 2012; Squares: Neumedicines, Inc.)

Figure B.4: (2 of 2) Murine granulopoiesis model compared with optimization data (mean ± standard error).

Radiation Validation Results

Figure B.5 show comparisons of the murine granulopoiesis model with validation data.

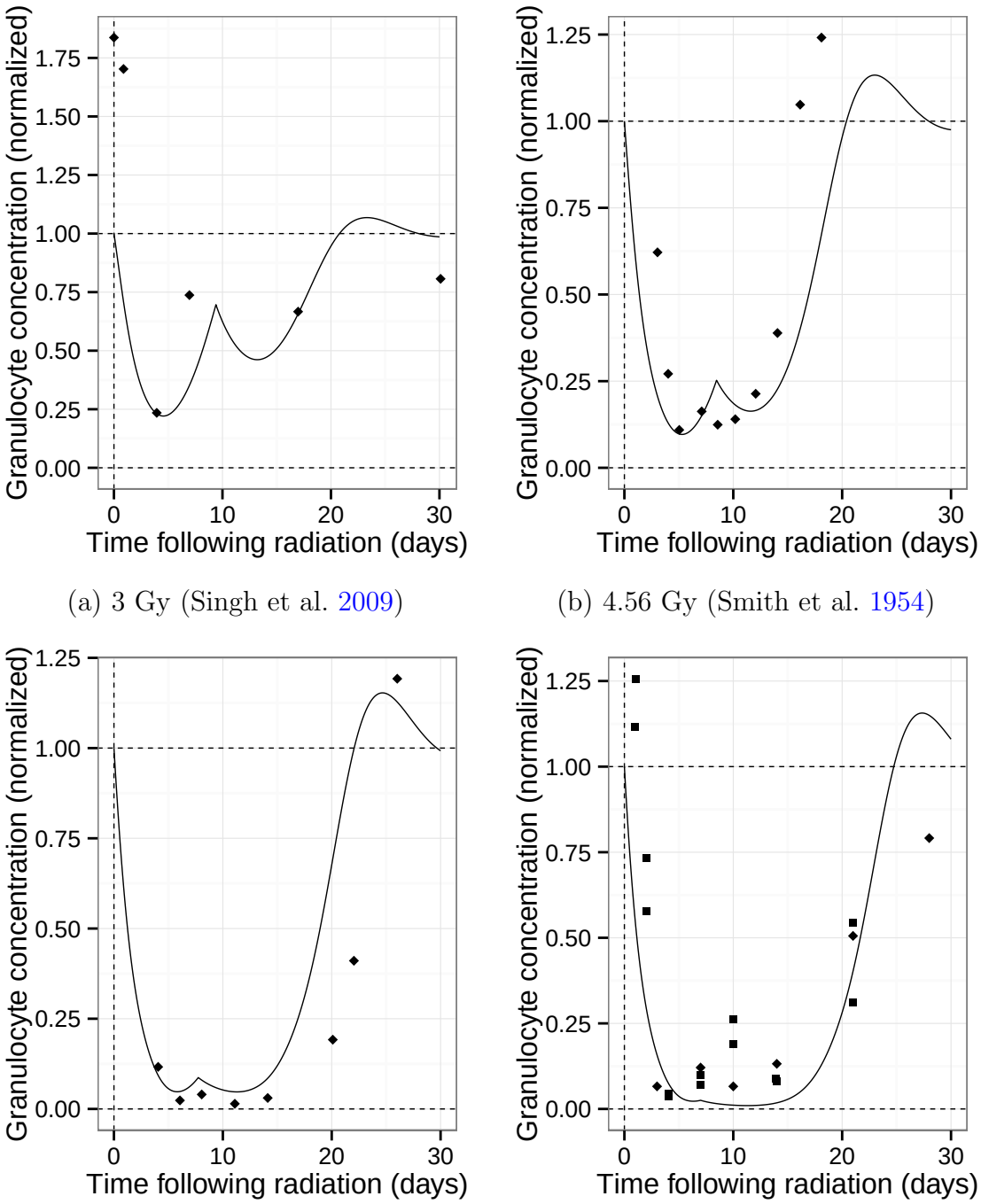

(a) 3 Gy (Singh et al. 2009)

(b) 4.56 Gy (Smith et al. 1954)

(c) 5.76 Gy (Smith et al. 1954)

(d) 7 Gy (Diamonds: Singh et al. 2009; Squares: Satyamitra et al. 2011)

Figure B.5: (1 of 2) Murine granulopoiesis model compared with validation data (mean).

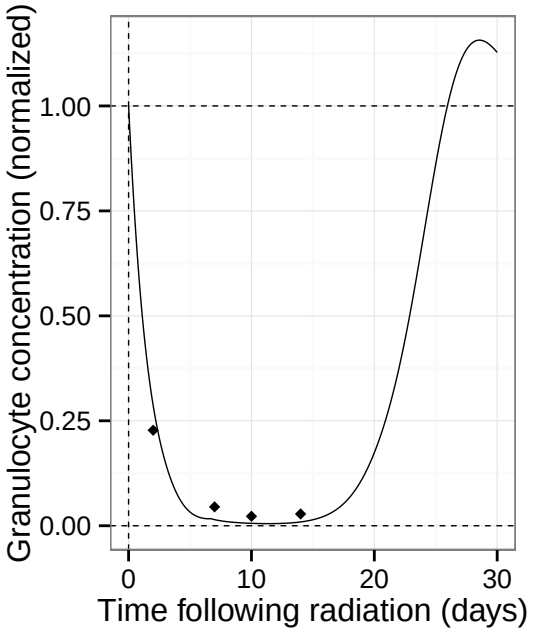

(e) 7.5 Gy (Davis et al. 2010)

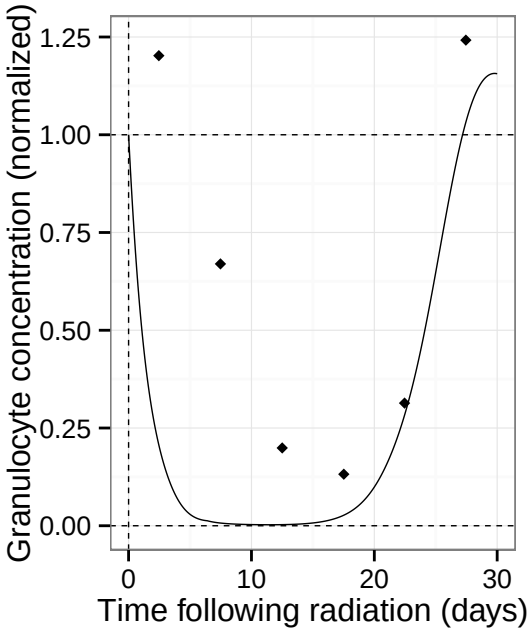

(f) 8 Gy (Kulkarni et al. 2013)

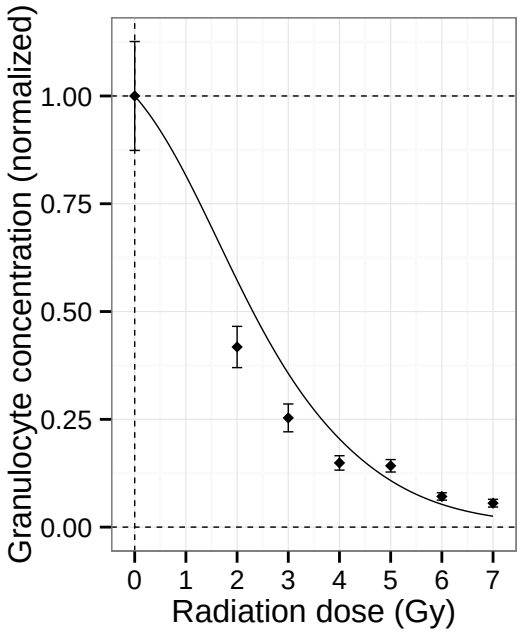

(g) 7 days post exposure (Tan et al. 2006;
errors bars represent standard error)

Figure B.5: (2 of 2) Murine granulopoiesis model compared with validation data (mean).

Burn Optimization Results

Figure B.6 shows comparisons of the granulopoiesis model with data used to optimize the burn-dependent parameters in the model.

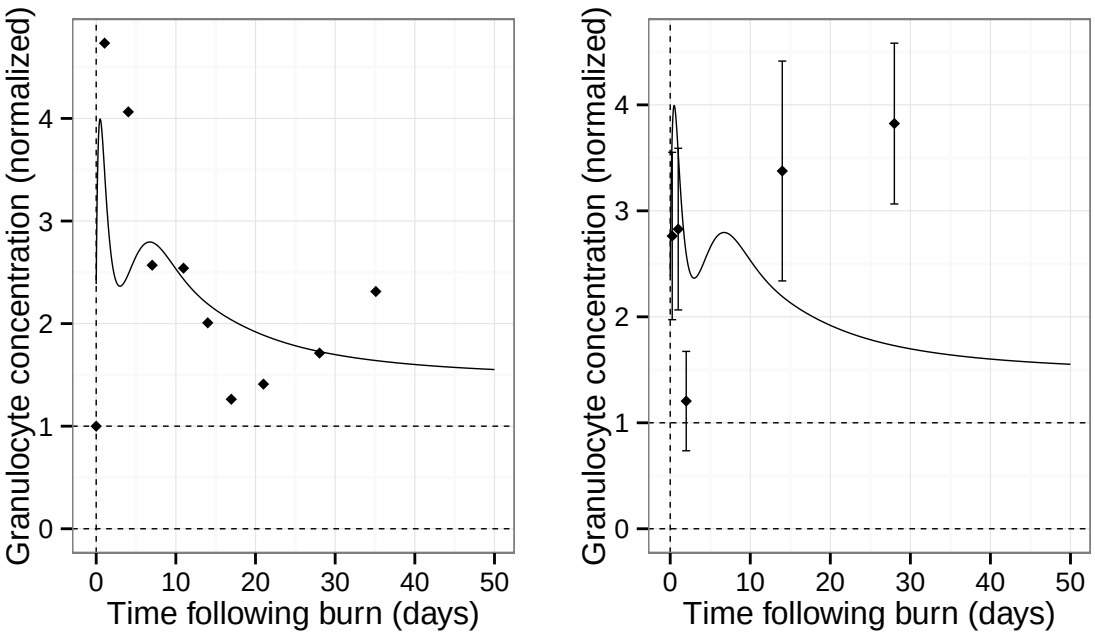

(a) 10% TBSA (Gruber et al. 1989) (b) 15% TBSA (Palmer et al. 2011)

Figure B.6: (1 of 2) Murine granulopoiesis model compared with burn optimization data (mean ± standard error).

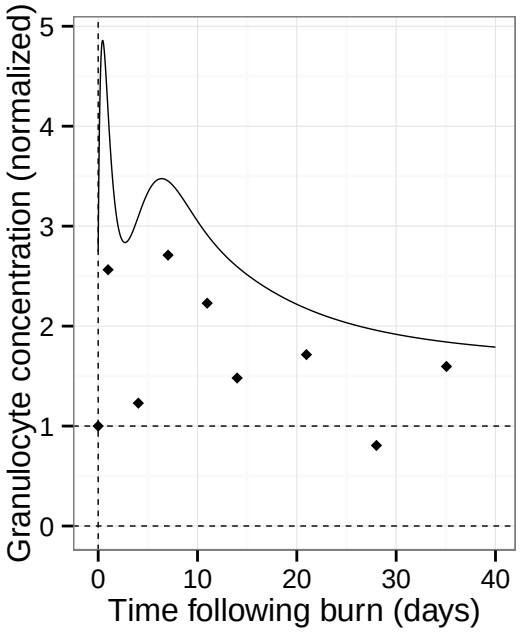

(c) 20% TBSA (Gruber et al. 1989)

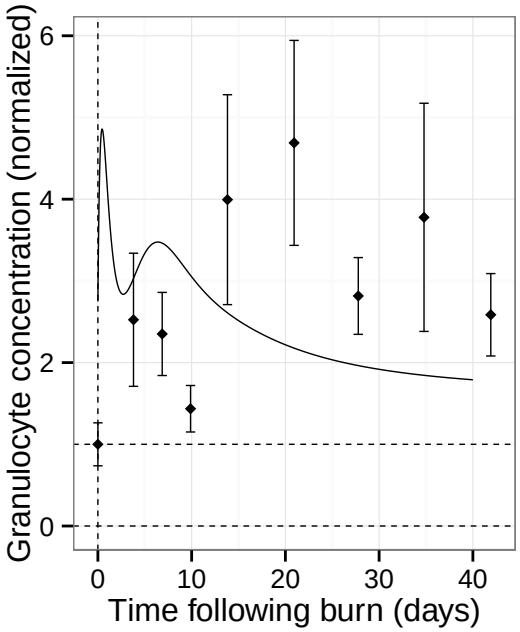

(d) 20% TBSA (Wallner et al. 1984)

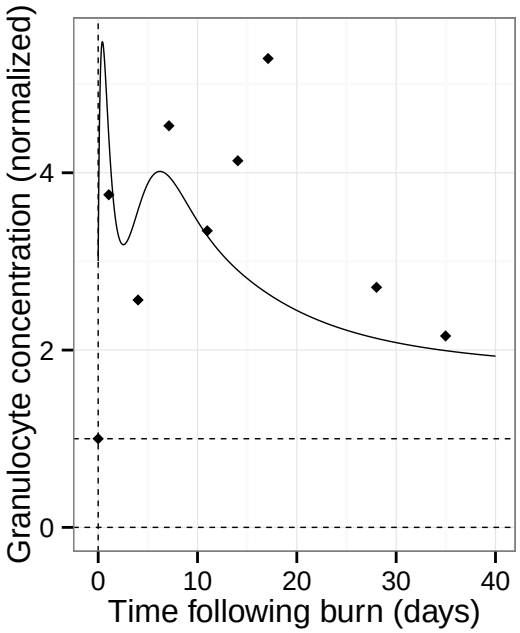

(e) 30% TBSA (Gruber et al. 1989)

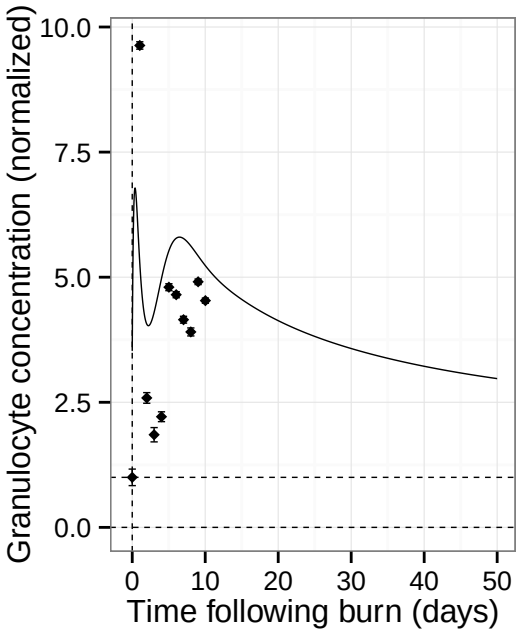

(f) 60% TBSA (McManus 1983)

Figure B.6: (2 of 2) Murine granulopoiesis model compared with burn optimization data (mean ± standard error).

Abbreviations, Acronyms, and Symbols

ARA	Applied Research Associates, Inc.
d	day
DTRA	Defense Threat Reduction Agency
FME	flexible modeling environment for modeling, sensitivity, and Monte Carlo analysis (R plug-in)
G-CSF	Granulocyte colony stimulating factor
Gy	gray
h	hour
HENRE	Health Effects from Nuclear and Radiation Environments (HENRE)
HPAC	Hazard Prediction and Assessment Capability
IL-1	interleukin 1
IL-6	interleukin 6
MCMC	Markov Chain Monte Carlo
MK	megakaryocyte
NA	not available
μL	microliter
NK	natural killer
ODE	ordinary differential equation
R	software programming language for statistical computing
S	surface area burn size fraction
SSR	sum of squared residuals
TBSA	total body surface area
TPO	thrombopoietin